Universidade de Aveiro Departamento de Electrónica, Telecomunicações e Informática
2010

Carlos Miguel Nogueira Gaspar Ribeiro

Esquemas de Estimação de Canal e Desvio de Frequência em Sistemas Multiportadora

Channel and Frequency Offset Estimation Schemes for Multicarrier Systems

Universidade de Aveiro
2010

Departamento de Electrónica, Telecomunicações e Informática

Carlos Miguel Nogueira Gaspar Ribeiro

Esquemas de Estimação de Canal e Desvio de Frequência em Sistemas Multiportadora

Channel and Frequency Offset Estimation Schemes for Multicarrier Systems

Tese apresentada à Universidade de Aveiro para cumprimento dos requisitos necessários à obtenção do grau de Doutor em Engenharia Electrotécnica, realizada sob a orientação científica do Doutor Atílio Manuel da Silva Gameiro, Professor Associado do Departamento de Electrónica, Telecomunicações e Informática da Universidade de Aveiro.

Apoio financeiro da FCT e do FSE no âmbito do Quadro de Referência Estratégico Nacional.

o júri

presidente

Prof. Doutor Amadeu Mortágua Velho da Maia Soares
Professor Catedrático do Departamento de Biologia da Universidade de Aveiro

Prof. Doutor Américo Manuel Carapeto Correia
Professor Catedrático do Departamento de Ciências e Tecnologias da Informação do Instituto Superior de Ciências do Trabalho e da Empresa de Lisboa

Prof. Doutora Ana García Armada
Professora Titular do Departamento de Teoría de la Señal y Comunicaciones da Universidad Carlos III de Madrid

Prof. Doutor Atílio Manuel da Silva Gameiro
Professor Associado do Departamento de Electrónica, Telecomunicações e Informática da Universidade de Aveiro

Prof. Doutor Adão Paulo Soares Silva
Professor Auxiliar do Departamento de Electrónica, Telecomunicações e Informática da Universidade de Aveiro

Prof. Doutor Vitor Manuel Mendes da Silva
Professor Auxiliar do Departamento de Engenharia Electrotécnica e de Computadores da Faculdade de Ciências e Tecnologia da Universidade de Coimbra

agradecimentos

O caminho percorrido para chegar aqui não se faz sem auxílio.
Sem o suporte financeiro dado pelo Instituto Politécnico de Leiria esta aventura não teria sido possível.
O percurso seria muito mais longo sem a orientação do Professor Doutor Atílio Gameiro.
A viagem tem custos que foram parcialmente suportados pela Fundação para a Ciência e a Tecnologia.
Para a viagem usei meios disponibilizados pelo Instituto de Telecomunicações.
A todos humildemente agradeço.

O caminho é solitário.
Nas pausas tenho sorte.
A Mónica abriga-me.
A minha família suporta-me.
Os meus amigos rodeiam-me.

“A perseverança é a mãe da boa sorte.”
Miguel de Cervantes Saavedra
(1547-1616)

“Great works are performed not by strength,
but perseverance.”
Samuel Johnson
(1709-1784)

Em memória da minha mãe Regina
Para o meu pai Celestino

“Perseverance is the hard work you do after
you get tired of doing the hard work you already did.”
Newt Gingrich

“Try and fail, but don't fail to try.”
Stephen Kaggwa

“Perseverança não é uma corrida longa,
são muitas corridas curtas, uma após a outra.”
Walter Elliot
(1842-1928)

palavras-chave

OFDM, MIMO, sub-portadoras piloto, desenho de sequências de pilotos, estimação de canal, estimação de desvio de frequência.

resumo

O presente trabalho aborda o problema da estimação de canal e da estimação de desvio de frequência em sistemas OFDM com múltiplas configurações de antenas no transmissor e no receptor.

Nesta tese é apresentado o estudo teórico sobre o impacto da densidade de pilotos no desempenho da estimação de canal em sistemas OFDM e são propostos diversos algoritmos para estimação de canal e estimação de desvio de frequência em sistemas OFDM com antenas únicas no transmissor e receptor, com diversidade de transmissão e MIMO.

O estudo teórico culmina com a formulação analítica do erro quadrático médio de um estimador de canal genérico num sistema OFDM que utilize pilotos dedicados, distribuidos no quadro transmitido em padrões bi-dimensionais. A formulação genérica é concretizada para o estimador bi-dimensional LS-DFT, permitindo aferir da exactidão da formulação analítica quando comparada com os valores obtidos por simulação do sistema abordado.

Os algoritmos de estimação investigados tiram partido da presença de pilotos dedicados presentes nos quadros transmitidos para estimar com precisão os parâmetros pretendidos. Pela sua baixa complexidade, estes algoritmos revelam-se especialmente adequados para implementação em terminais móveis com capacidade computacional e consumo limitados.

O desempenho dos algoritmos propostos foi avaliado por meio de simulação do sistema utilizado, recorrendo a modelos aceites de caracterização do canal móvel multipercurso. A comparação do seu desempenho com algoritmos de referência permitir aferir da sua validade.

keywords

OFDM, MIMO, pilot sub-carriers, pilot sequence design, channel estimation, frequency offset estimation.

abstract

The present work focus on the problem of channel estimation and frequency offset estimation in OFDM systems, with different antenna configurations at both the transmitter and the receiver.

This thesis presents the theoretical study of the impact of the pilot density in the performance of the channel estimation in OFDM systems and proposes several channel and frequency offset algorithms for OFDM systems with single antenna at both transmitter and receiver, with transmitter diversity and MIMO.

The theoretical study results in the analytical formulation of the mean square error of a generic channel estimator for an OFDM system using dedicated pilots, distributed in the transmitted frame in two-dimensional patterns. The generic formulation is implemented for the two-dimensional LS-DFT estimator to verify the accuracy of the analytical formulation when compared with the values obtained by simulation of the discussed system.

The investigated estimation algorithms take advantage of the presence of dedicated pilots present in the transmitted frames to accurately estimate the required parameters. Due to its low complexity, these algorithms are especially suited for implementation in mobile terminals with limited processing power and consumption.

The performance of the proposed algorithms was evaluated by simulation of the used system, using accepted multipath mobile channel models. The comparison of its performance with the one of reference algorithms measures its validity.

TABLE OF CONTENTS

LIST OF FIGURES

LIST OF TABLES

LIST OF ACRONYMS

0G	Generation Zero mobile cellular systems
1-D	One-dimensional
1G	First Generation mobile cellular systems
2-D	Two-dimensional
2.5G	Generation 2.5 mobile cellular systems
2G	Second Generation mobile cellular systems
3G	Third Generation mobile cellular systems
3GPP	3rd Generation Partnership Project
4G	Fourth Generation mobile cellular systems
ADC	Analog-to-Digital Converter
AMC	Adaptive Modulation and Coding
AMPS	Advanced Mobile Phone System
ARIB/TTC	Japanese Association of Radio Industries and Businesses / Telecommunication Technology Committee
ATIS	Alliance for Telecommunications Industry Solutions

AWGN	Additive White Gaussian Noise
BER	Bit Error Rate
BIC	Bit-Interleaved Coded
BS	Base Station
BWA	Broadband Wireless Access
CCSA	China Communications Standards Association
CDMA	Code Division Multiple Access
CFO	Carrier Frequency Offset
CFR	Channel Frequency Response
CIR	Channel Impulse Response
CP	Cyclic Prefix
CSD	Circuit Switched Data
CSI	Channel State Information
DA	Data Aided
DAB	Digital Audio Broadcasting
DAC	Digital-to-Analog Converter
DCS1800	Digital Cellular System 1800
DFT	Discrete Fourier Transform
DSSS	Direct Sequence Spread Spectrum
DTFT	Discrete-Time Fourier Transform
DVB	Digital Video Broadcasting
EDGE	Enhanced Data Rates for GSM Evolution
EM	Expectation-Maximization
ETSI	European Telecommunications Standards Institute
E-UTRA	Evolved Universal Terrestrial Radio Access
FD	Frequency-Domain
FDMA	Frequency Division Multiple Access
FFT	Fast Fourier Transform

GPRS	General Packet Radio Service
GSM	Global System for Mobile communications
HSCSD	High Speed CSD
HSDPA	High Speed Downlink Packet Access
HSPA	High Speed Packet Access
HSUPA	High Speed Uplink Packet Access
ICI	Inter-Carrier Interference
IDFT	Inverse Discrete Fourier Transform
IFFT	Inverse Fast Fourier Transform
iid	Independent and Identically Distributed
IMT-2000	International Mobile Telecommunications-2000
IMTS	Improved MTS
IS	Interim Standard
ISI	Inter-Symbol Interference
ITU	International Telecommunication Union
JTACS	Japan Total Access Communications System
LAN	Local Area Network
LMS	Least Mean Square
LMMSE	Linear Minimum Mean Square Error
LoS	Line-of-Sight
LS	Least Square
LS-DFT	Least Square – Discrete Fourier Transform
LTE	Long Term Evolution
LTE-Advanced	Advancements for Evolved Universal Terrestrial Radio Access
MAC	Medium Access Control
MAI	Multi-Antenna Interference
MAN	Metropolitan Area Networks
MAP	Maximum-a-Posteriori

MC-CDMA	Multicarrier-CDMA
MIMO	Multiple-Input Multiple-Output
ML	Maximum Likelihood
MMSE	Minimum Mean Square Error
MRC	Maximum Ratio Combining
MSE	Mean Square Error
MT	Mobile Terminal
MTA	Mobile Telephone system A
MTS	Mobile Telephone System
MVU	Minimum Variance Unbiased
NDA	Non-Data Aided
NMT	Nordic Mobile Telephone
NTT	Nippon Telephone and Telegraph
OFDM	Orthogonal Frequency Division Multiplexing
OFDMA	Orthogonal Frequency Division Multiple Access
PAN	Personal Area Network
PAPR	Peak-to-Average Power Ratio
PDC	Personal Digital Cellular
PDF	Probability Distribution Function
PDP	Power Delay Profile
PHY	Physical Layer
PSD	Power Spectral Density
QAM	Quadrature-Amplitude Modulation
QoS	Quality of Service
PSK	Phase-Shift Keying
RF	Radio-Frequency
RLS	Recursive Least Square
SC-FDMA	Single Carrier Frequency Division Multiple Access

SISO	Single-Input Single-Output
SMS	Short Message Service
SNR	Signal-to-Noise Ratio
STC	Significant Tap Catching
TD	Time-Domain
TDMA	Time Division Multiple Access
TS-SCDMA	Time-Division Synchronous CDMA
TTA	Telecommunications Technology Association
UE	User Equipment
UMTS	Universal Mobile Telecommunications System
UTRA	UMTS Terrestrial Radio Access
WAN	Wide Area Network
W-CDMA	Wideband CDMA
WSS	Wide-Sense Stationery
WSSUS	Wide-Sense Stationary Uncorrelated Scattering

LIST OF SYMBOLS

$(.)_i$	Symbol index subscript
$(.)^{(r)}$	Receive antenna index superscript
$(.)^{(r,s)}$	Transmit antenna index to receive antenna index superscript
$(.)^{(s)}$	Transmit antenna index superscript
$(.)^H$	Hermitian transpose operator
$(.)^T$	Transpose operator
$E\{.\}$	Expectation operator
b_{data}	Number of data bits sent per symbol
c	Speed of light
d	Complex symbol
$\hat{f}$	Candidate CFO
f_c	Carrier frequency

f_d	Doppler frequency
f_k	Sub-carriers baseband frequencies
f_o	Frequency offset due to the frequency mismatch of the oscillators of the transmitter and the receiver
f_D	Largest magnitude Doppler frequency shift
h	Channel frequency response
$\tilde{h}$	Channel impulse response
i	Symbol index
k	FD sub-carrier index
k_{ini}	Position of the first pilot sub-carrier
l	Channel path index
m	Size of the constellation
n	TD sample index
n_R	Number of receive antennas
n_S	Number of transmit antennas
r	Receive antenna index
r_b	Input data rate
r_s	Baud rate
s	Transmit antenna index
$s(f)$	OFDM signal frequency response
$\tilde{s}(t)$	Complex envelope of the OFDM signal
t_{CP}	Duration of the CP
t_S	Symbol duration (without CP)
v	Mobile terminal speed
$\tilde{x}$	TD transmitted signal sample
$\tilde{y}$	TD received signal sample

$\hat{w}$	Candidate angular CFO
w_o	Normalized angular CFO
$\hat{w}_o$	Estimate of the normalized angular CFO
B	System's bandwidth
B_c	Coherence bandwidth
D_P	Pilot pattern density
E_b	System's energy per bit
E_b / N_O	System's power efficiency
G_{Div}	Diversity gain
H	Channel frequency response (time, frequency)
$J(\hat{w})$	CFO cost function
$J_0(.)$	Zero-order Bessel function of the first kind
L	Length of guard interval
L_p	Number of channel paths
L_{sp}	Number of sub-paths in a channel path
M	Number of bits per symbol
N_C	Total number of sub-carriers of OFDM system (FFT size)
N_f	Number of sub-carriers between consecutive pilots
N_i	Number of symbols between consecutive pilots
N_O	One-sided noise PSD
N_P	Number of pilot sub-carriers in an OFDM symbol
N_S	Number of symbols in an OFDM frame
N_t	TD CIR replica separation
$S(f)$	OFDM signal's PSD

$S(f_d)$	Doppler PSD
S_h	Channel normalized power
S_r	Received signal power
S_τ	Channel power delay profile
$\overline{S}_{symbol}$	Average symbol power
T_c	Coherence time
T_F	OFDM frame duration
T_S	Symbol duration (with CP)
α_l	Complex value of path l
ϕ_f	Channel frequency correlation function
ϕ_t	Channel time correlation function
ϕ_{α_l}	Time correlation of the multipath channel for the l-th path
φ	Angle of arrival
κ	Free-space phase constant
λ	Carrier frequency wavelength
θ_{ini}	Common phase that affects all samples of the symbol
σ^2_{Ch}	Channel power
σ^2_e	Channel estimation mean square error
σ_{f_D}	Spread of the Doppler PSD
$\sigma^2_h[l]$	Average power of path l
$\hat{\sigma}^2_h[l]$	Estimate of average power of path l
σ^2_n	Noise variance
$\hat{\sigma}^2_n$	Estimate of noise variance
$\sigma^2_{N_S}$	Sampled noise variance

σ_τ	Delay spread
τ_l	Delay of path l
$\hat{\tau}_l$	Estimate of delay of path l
$\tau_{\max}$	Channel's maximum delay
$\overline{\tau}$	Average delay
Δf	Sub-carrier separation
Δt	System's sampling interval
$\Delta\tau$	Delay variation
Φ_H	CFR correlation function
$\wp$	Set of sub-carriers that convey the pilot sequences
$\mathbf{a}$	Set of pattern points
$\mathbf{b}$	Input data vector
$\hat{\mathbf{b}}$	FD column vector with estimate of the transmitted data
$\mathbf{d}$	FD N_C-complex column vector with M-ary PSK or QAM coded data
$\tilde{\mathbf{d}}$	TD N_C-complex column vector with the data symbols' components present in $\tilde{\mathbf{s}}$
$\hat{\mathbf{d}}$	FD N_C-complex column vector with values received on the data sub-carriers
$\tilde{\mathbf{g}}$	TD N_t-complex column vector with the filtered received symbol samples
$\tilde{\mathbf{g}}_d$	TD N_t-complex column vector with the data-dependent component in $\tilde{\mathbf{g}}$
$\tilde{\mathbf{g}}_p$	TD N_t-complex column vector with the pilot-dependent component in $\tilde{\mathbf{g}}$
$\mathbf{h}$	FD N_C-complex column vector with the CFR
$\tilde{\mathbf{h}}$	TD N_C-complex column vector with the CIR
$\hat{\mathbf{h}}$	FD N_C-complex column vector with the channel's estimate
$\hat{\tilde{\mathbf{h}}}$	TD N_C-complex column vector with the channel's estimate

$\hat{\tilde{\mathbf{h}}}_{LS}$	TD N_t-complex column vector with the LS channel's estimate
$\mathbf{j}$	$\left(N_t - n_S L_p\right)$–complex column vector with the samples of $\tilde{\mathbf{g}}$ with no CIR energy (only data-dependent and noise)
$\mathbf{n}$	FD N_C-complex column vector with noise values
$\tilde{\mathbf{n}}$	TD N_C-complex column vector with noise samples
$\bar{\tilde{\mathbf{n}}}$	TD $\left(N_C + L\right)$-complex column vector with noise samples
$\mathbf{p}$	FD N_C-complex column vector with pilot values
$\tilde{\mathbf{p}}$	TD N_C-complex column vector with pilot symbols' components present in $\tilde{\mathbf{s}}$
$\mathbf{r}$	FD N_C-complex column vector with the received symbol values
$\tilde{\mathbf{r}}$	TD N_C-complex column vector with the received symbol samples (without CP)
$\tilde{\mathbf{r}}_c$	TD N_C-complex column vector with the received symbol samples after CFO correction
$\tilde{\mathbf{r}}_d$	TD N_C-complex column vector with the data-dependent component in $\tilde{\mathbf{r}}$
$\tilde{\mathbf{r}}_p$	TD N_C-complex column vector with the pilot-dependent component in $\tilde{\mathbf{r}}$
$\mathbf{s}$	FD N_C-complex column vector with transmitted signal
$\tilde{\mathbf{s}}$	TD N_C-complex column vector with transmitted signal (without CP)
$\tilde{\mathbf{t}}$	TD rectangular low-pass window vector
$\mathbf{u}_i$	Channel's PSD replicas placement (symbol dimension) basis column vector
$\mathbf{u}_k$	Channel's PSD replicas placement (frequency dimension) basis column vector
$\mathbf{v}$	FD N_t-complex column vector with filtered noise samples
$\tilde{\mathbf{v}}$	TD N_t-complex column vector with filtered noise samples
$\mathbf{v}_i$	Symbol dimension pilot pattern basis column vector
$\mathbf{v}_k$	Frequency dimension pilot pattern basis column vector

$\tilde{\mathbf{x}}$	TD $(N_C + L)$-complex column vector with transmitted signal (with CP)
$\tilde{\mathbf{y}}$	TD $(N_C + L)$-complex column vector with the symbol samples (with CP)
$\tilde{\mathbf{z}}$	TD $(N_C + L)$-complex column vector with the ISI samples that affect the symbol
$\mathbf{A}_{CP}$	$(N_C + L) \times N_C$ CP adding matrix
$\mathbf{C}_{N_C}(\nu_o)$	$N_C \times N_C$ diagonal matrix with the phase rotations that affects the symbol samples
$\mathbf{F}$	$N_C \times N_C$ DFT matrix
$\mathbf{H}$	FD $N_C \times N_S$ channel frequency response matrix (frame)
$\tilde{\mathbf{H}}_{circ}$	TD $N_C \times N_C$ circulant matrix with circulant vector $\tilde{\mathbf{h}}$
$\tilde{\mathbf{H}}_{lin}$	TD $(N_C + L) \times (N_C + L)$ lower triangular Toeplitz channel convolution matrix with first column $\tilde{\mathbf{h}}$
$\hat{\mathbf{H}}_{LS}$	FD $N_C \times N_S$ matrix with sampled LS channel's estimate
$\hat{\mathbf{H}}'_{LS}$	FD $\frac{N_C}{N_f} \times \frac{N_S}{N_i}$ matrix with LS channel's estimate
$\mathbf{I}_{N_C}$	$N_C \times N_C$ identity matrix
$\mathbf{I}_{N_C,L}$	$N_C \times L$ matrix with the L last columns of $\mathbf{I}_{N_C}$
$\mathbf{N}$	FD $N_C \times N_S$ matrix with noise values
$\mathbf{N}_S$	FD $N_C \times N_S$ matrix with sampled noise values
$\mathbf{Q}$	FD $N_C \times N_C$ channel frequency response diagonal matrix
$\mathbf{R}_{CP}$	$N_C \times (N_C + L)$ CP removing matrix
$\mathbf{R}_{\tilde{b}\tilde{b}}$	TD $(N_t \times N_t)$ channel correlation matrix
$\mathbf{R}_{\tilde{b}\hat{\tilde{b}}}$	TD $(N_t \times N_t)$ filter input–output cross-correlation matrix
$\mathbf{R}_{\hat{\tilde{b}}\hat{\tilde{b}}}$	TD $(N_t \times N_t)$ filter input correlation matrix

$\mathbf{S}$	FD $N_C \times N_S$ matrix with transmitted signal
$\mathbf{T}$	$N_t \times N_C$ matrix with TD pilot sub-carriers selection (multi-band) filter
$\mathbf{U}$	2×2 channel's PSD replicas placement basis matrix
$\mathbf{V}$	2×2 pilot pattern basis matrix
$\mathbf{W}$	2-D estimation filter matrix
$\mathbf{W}_e$	Error filter matrix
$\tilde{\mathbf{W}}_{MMSE}$	TD $N_C \times N_C$ LMMSE filter
$\mathbf{W}_P$	Ideal 2-D *sinc* filter matrix
$\mathbf{0}_{N_C \times L}$	$N_C \times L$ null matrix
$d[k]$	FD data vector $\mathbf{d}$ k-th element
$\tilde{d}[n]$	TD data vector $\tilde{\mathbf{d}}$ n-th element
$\tilde{g}[n]$	TD filtered vector $\tilde{\mathbf{g}}$ n-th sample
$\tilde{g}_d[n]$	TD data-dependent filtered vector $\tilde{\mathbf{g}}_d$ n-th sample
$\tilde{g}_p[n]$	TD pilot-dependent filtered vector $\tilde{\mathbf{g}}_p$ n-th sample
$h[k]$	Channel frequency response vector $\mathbf{h}$ k-th element
$\tilde{h}[n]$	Discrete-time channel impulse response vector $\tilde{\mathbf{h}}$ n-th element
$\tilde{n}[n]$	TD noise vector $\tilde{\mathbf{n}}$ n-th sample of *iid* zero mean AWGN with variance σ_n^2
$\overline{\tilde{n}}[n]$	TD noise vector $\overline{\tilde{\mathbf{n}}}$ n-th sample of *iid* zero mean AWGN with variance σ_n^2
$p[k]$	FD pilot vector $\mathbf{p}$ k-th element
$\tilde{p}[n]$	TD pilot vector $\tilde{\mathbf{p}}$ n-th element
$\tilde{r}[n]$	TD received vector $\tilde{\mathbf{r}}$ n-th signal sample
$\tilde{r}_p[n]$	TD received pilot-dependent vector $\tilde{\mathbf{r}}_p$ n-th signal sample
$s[k]$	FD transmitted signal vector $\mathbf{s}$ k-th element
$\tilde{s}[n]$	TD transmitted signal vector $\tilde{\mathbf{s}}$ n-th element

$\tilde{t}[n]$	TD rectangular low-pass window $\tilde{\mathbf{t}}$ n-th element
$u[n]$	Unit-step function
$v[k]$	FD filtered noise vector $\mathbf{v}$ k-th sample
$\tilde{v}[n]$	TD filtered noise vector $\tilde{\mathbf{v}}$ n-th sample
$\tilde{y}[n]$	TD received vector $\tilde{\mathbf{y}}$ n-th signal sample
$E[k,i]$	Estimation error of the k-th sub-carrier of the i-th symbol
$H[k,i]$	FD channel frequency response matrix (k,i)-th element
$\hat{H}[k,i]$	FD channel frequency response estimate (k,i)-th element
$\hat{H}_{LS}[k,i]$	FD LS channel's estimate matrix (k,i)-th element
$\hat{H}'_{LS}[k,i]$	FD sampled LS channel's estimate matrix (k,i)-th element
$H_S[k,i]$	FD sampled channel frequency response (k,i)-th element
$N[k,i]$	FD noise matrix (k,i)-th element
$N_S[k,i]$	FD sampled noise matrix (k,i)-th element
$S[k,i]$	FD transmitted signal matrix (k,i)-th element
$S_H(w_k,w_i)$	Channel's power spectral density (w_k,w_i)-th element
$S_{H_S}(w_k,w_i)$	Sampled channel's power spectral density (w_k,w_i)-th element
$W[k,i]$	2-D estimation filter (k,i)-th element
$W_e[k,i]$	Error filter (k,i)-th element
$W_P[k,i]$	Ideal 2-D *sinc* filter (k,i)-th element

CHAPTER 1

INTRODUCTION

In this chapter we present a brief historic evolution of the wireless cellular systems leading to the adoption of multicarrier modulations schemes in the most recent standards. We then emphasize the importance of the multicarrier wireless system's operations addressed in this thesis: channel estimation and carrier frequency offset estimation, as a motivation to this work and present the thesis statement. The main contributions resulting of this thesis are identified, followed by an overview of the structure of this document.

1.1. Evolution of Cellular Systems

The appearance of wireless communications over a century ago changed the society we live in. Its origin can be traced back to 1886, when Hertz generated for the first time electromagnetic waves, thus proving the equations by Maxwell that predicted its existence two decades before [Mah03]. The work of Marconi in the following years showed the world the potential of this new discovery, culminating in 1901 with first transatlantic radio communication. The 1920s witness the beginning of regular radio broadcasting services. In 1940 the first two-way radio, the "Handie-Talkie" SCR536, was presented by Motorola [Mot09] and in 1946 the Bell System introduced in St. Louis one of the earliest mobile telephone standards in the USA, the Mobile Telephone System (MTS). It was a half-duplex system, where the operator assisted the user to place or route the call in both directions. An improved full-duplex version of this system, the Improved MTS (IMTS), offering direct-dial and caller identification, was only released in 1964. Meanwhile, Ericsson developed the first fully automatic phone system, the Mobile Telephone system A (MTA) [Bil06], and made the first trials in Sweden in 1956. The base stations were fully automatic and the client's equipment weighed around 40Kg.

In the context of mobile cellular systems, each generation of systems is characterized by a concept and/or technologic leap from the previous. Some authors consider these early pre-cellular systems to constitute the generation zero (0G) of the mobile cellular systems. The first generation (1G) of mobile cellular systems breakthrough was the use of the concept of cellular network. The cellular concept for mobile wireless systems was proposed by Bell Labs engineer D. H. Ring in his 1947 technical memorandum [Rin47]. The main idea behind this concept is the reuse of the available spectrum, by dividing the geographical area to be covered by the system in adjacent non-overlapping hexagonal-shaped cells. Unlike 0G system, where a single powerful transmitter covered all area and used all available frequency channels, the new generation systems would have low-power transceivers, the Base Station (BS), in each cell, using only a subset of all available channels. By doing so, BSs in non-adjacent cells could reuse the channels with little interference and greatly increase the overall number of channels available for the system's users.

The cellular technology and the required electronics were mainly developed at Bell Labs until the 1970s [CEUC97], and the first commercial systems saw the light of day in the early 80s. A wealth of systems rapidly spread in different countries. Ericsson claims that its Nordic Mobile Telephone (NMT) was the first truly mobile cellular system to be deployed in Scandinavian countries in 1981. This system was also adopted by Switzerland, Netherlands and some Eastern Europe countries. Shortly afterward, in 1984, the Bell Labs' Advanced

Mobile Phone System (AMPS) initiated its operation in the USA and was later adopted in Australia. In 1985, the Total Access Communication System was inaugurated in Great Britain. Germany and Portugal adopted the C-450 system. In Japan, multiple systems were developed and deployed. The Nippon Telephone and Telegraph (NTT) developed and deployed three standards: TZ-801, TZ-802, and TZ-803, and the competitor DDI used the Japan Total Access Communications System (JTACS) [Pad95], [Rap96], [Stu96].

The 1G systems shared some important characteristics like analog frequency modulation for voice transmission, digital signalling, handover and the separation of the channels by allocation of different non-overlapping frequency bands, called frequency division multiple access (FDMA) [Pro01]. These systems suffer from the important drawback of being incompatible among each other. Its capacity was quickly exhausted with the rapid increase in the number of users and the quality of service provided was far from satisfying the customers.

The advances in the area of micro-electronics, with an ever increasing rate of integration, leading to the introduction of the microprocessor in the 70's and the development of efficient digital signal processing techniques, like digital speech coders, channel coders for error protection and encryption algorithms for improved security and privacy, supported the birth of the second generation (2G) mobile cellular systems [Pad95], the first fully digital cellular generation. Presenting significant improvements in quality of service and availability for customers, and increased spectral efficiency, smaller, more reliable, less power-hungry BSs and overall cheaper provider structure, the 90's witness the burst of digital personal wireless communications [CEUC97]. The majority of the 2G systems used time division multiple access (TDMA) schemes [Pro01] to separate the channels of the different users. The ubiquitous Global System for Mobile communications (GSM) is one such system, making its debut in Europe and spreading to most continents in over 100 countries. Other examples of successful 2G TDMA systems are the Digital Cellular System 1800 (DCS1800) present in Europe, the Interim Standard (IS) 54 in the USA and the Personal Digital Cellular (PDC) system in Japan, just to name a few [Rap96], [Stu96].

Stemming from the military secure communications systems of the first half on the 20th century [Sch82], commercial 2G systems using code division multiple access (CDMA) with direct sequence spread spectrum (DSSS) [Pro01] were developed and deployed with considerable success [Rap96], [Stu96]. Characterized by using a bandwidth much greater than the minimum required for a single user [Dix94], the information from the users is separated in the code domain, by the use of independent spreading codes. Of this group, the USA IS-95 system stands out as the most successful one.

The 2G systems were developed as cellular systems for the transmission of voice. Services other than voice calls (Facsimile, Short Message Service (SMS) and other low data rate services) were introduced to broaden the range of provided services but the circuit-

switched nature of the system kept unchanged. The extraordinary growth of Internet users in the 90's was seen as a promising new breath for the wireless cellular systems that would provide Internet access anywhere with the plus of adding mobility.

The original 2G systems fell short in handling packet-oriented services required by Internet access. The most severe limitations were the limited bandwidth and its circuit switched nature. To overcome the limited bandwidth, higher data rate evolutions were introduced. Still in 20th century, Circuit Switched Data (CSD) and High Speed CSD (HSCSD) services promise speeds of up to 57,6 kbit/s, when aggregating 4 GSM time slots. In the early 21st century, the General Packet Radio Service (GPRS) offered up to 115 kbit/s and the Enhanced Data Rates for GSM Evolution (EDGE) service claimed the figure of 384 kbit/s.

These added services, that came to be known as generation 2.5 (2.5G), pave the way for the third generation (3G) of wireless cellular systems. The motivation behind the development of this generation was to offer a wireless system that supported a wide range of services, advertised with the slogan "Anywhere, Anything, Anytime". The traditional low bitrate voice calls with be offered along high bandwidth demanding multimedia services like video-calls and video related applications, high speed Internet surfing, online gaming, etc.

These new services should be available in indoor and outdoor scenarios, with high mobility, variable and asymmetric bitrates, different quality of service (QoS) demands, while providing a smooth transition from the previous generation systems.

The development of the 3G systems started in the late 80's under the guidance of several standardization bodies. The European Telecommunications Standards Institute (ETSI) was involved in the collaborative 3rd Generation Partnership Project (3GPP) [3GPP], along with the Japanese Association of Radio Industries and Businesses/Telecommunication Technology Committee (ARIB/TTC), the China Communications Standards Association (CCSA), the North American Alliance for Telecommunications Industry Solutions (ATIS) and South Korean Telecommunications Technology Association (TTA), from what emerged the first Universal Mobile Telecommunications System (UMTS) standard in 1998 [ETS98] defining the Wideband CDMA-based (W-CDMA) UMTS Terrestrial Radio Access (UTRA). This is the 3G standard currently adopted and deployed throughout Europe.

The European UMTS standard together with a number of other 3G standards, like the North American CDMA2000 and the Chinese Time-Division Synchronous CDMA (TS-SCDMA), form the International Mobile Telecommunications-2000 (IMT-2000) family of standards, defined by the International Telecommunication Union (ITU) with the intent of facilitating the growth of 3G systems worldwide. Though several radio interfaces are defined in the several standards making up IMT-2000, the major technological breakthroughs of the

3G systems are the adoption of CDMA, Turbo Coding and Multiple-Input Multiple-Output (MIMO) techniques [Lu02], [Pra01].

The growth of bandwidth demanding multimedia services continued at a fast pace and the 3G systems kept evolving to satisfy the demands of customers. In 2002, the 3GPP Release 5 standard defined the enhanced 3G packet-oriented full-IP radio interface High Speed Downlink Packet Access (HSDPA) [Par06] which allows UMTS-based systems to reach downlink rates of up to 14,0Mbit/s. The 2004 3GPP Release 6 standard defined the uplink counterpart High Speed Uplink Packet Access (HSUPA) for increased uplinks rates of up to 5,8Mbit/s. Collectively these two new radio access schemes form the High Speed Packet Access (HSPA) that is being widely adopted by operators all over the world. The 2008 Release 8 provided a further rate increase with HSPA+, promising speeds of up 42Mbit/s in the downlink and 11Mbit/s in the uplink, with the adoption of MIMO capability and high-order modulations (64 levels Quadrature-Amplitude Modulation (QAM) in the downlink and 16-QAM in the uplink).

The HSPA standards represent a smooth evolution of the deployed UMTS networks, maintaining most of the structure and sometimes implemented as a software upgrade for both customers and providers. Building on the success of Orthogonal Frequency Division Multiplexing (OFDM)-based local area network (LAN) and wide area network (WAN) standards like IEEE 802.11a/g [802.11a], [802.11g] and 802.16 [802.16], the 3GPP has been involved in the parallel development of the OFDM-based Long Term Evolution (LTE) specification, a strong candidate has the underlying technology for the 4th generation (4G) wireless cellular systems, technologically incompatible with the current CDMA-based 3G standards.

The LTE specifications were introduced by the 3GGP Release 8 standard in 2008. The demands on the new standard are remarkable:

- Widest range of services from telephony to real-time high-definition video, mobile TV or high speed Internet surfing, and flexibility to accommodate future bandwidth-demanding applications;
- Interconnection and interoperability with different wireless and wired systems;
- Interaction with users to simplify the introduction of new applications and business models;
- Flexible spectrum utilization;
- High spectral efficiency;
- Variable QoS for different applications and scenarios (indoor, outdoor);

- High mobility scenarios;
- Variable and on-demand bitrates;
- Highly asymmetric bitrates;

To meet the goals, the LTE new radio interface Evolved Universal Terrestrial Radio Access (E-UTRA) is defined [LTE]. Some of its most significant specifications are:

- OFDM-based modulations for both downlink (Orthogonal Frequency Division Multiple Access – OFDMA) and uplink (Single Carrier Frequency Division Multiple Access – SC-FDMA);
- Adaptive Modulation and Coding (AMC) with up to 64-QAM and turbo coding;
- Single user and multi-user MIMO with up to four antennas per station;
- Flexible bandwidth from 1,25 MHz to 20 MHz;
- Peak bitrates of 326,4Mbit/s for MIMO 4x4 and 172,8Mbit/s for MIMO 2x2 for every 20 MHz of bandwidth, increasing the spectral efficiency 2 to 4 times when compared with HSPA;

The current LTE Release 8 still fells short of the ITU targeted peak bitrate of 1Gbit/s to fully support the 4G requirements [ITU1645] and the LTE-Advanced standard is currently in development and it is expected that will represent a backward compatible enhancement of current LTE standard [LTEadv]. The 3GPP Release 10 standard will define its specifications and it should be final in 2010. Some key topics that it should address are the use of wider bandwidths by spectrum aggregation, improved MIMO techniques to increase bitrates, use of relaying techniques to increase throughput and coverage and coordinated multipoint transmission/reception [Par08].

1.2. Thesis Statement

The OFDM-based broadband wireless systems are emerging in distinct services. In broadcasting it can be found in the European standards for Digital Audio Broadcasting (DAB) [DAB] and in the terrestrial Digital Video Broadcasting (DVB) [DVB-T]. In the wireless LAN environment is used daily by millions of people connecting to their networks with IEEE 802.11a [802.11a] and IEEE 802.11g [802.11g] wireless cards. In the wireless metropolitan area networks (MAN), Broadband Wireless Access (BWA) systems, commercially termed "WiMAX" and defined in IEEE 802.16 standard [802.16], are currently being installed all over

the world and the trends for future 4G systems [LTEadv] point for the adoption of OFDM-based radio interfaces.

The transmission over multipath wireless channels has a severe impact on the system's performance. The received signal is attenuated, distorted and delayed. A detailed description of these impairments is introduced in the next chapter. Noise, interference and system's imperfection also negatively impacts the system's performance.

To fully explore the potential of OFDM modulation, the system must mitigate these negative effects. Firstly, the receiver needs to recover the synchronization of the received signal. The use of multiple sub-carriers makes OFDM systems highly susceptible to synchronization errors [Pol95], [Pol95a] and the ability of the receiver to mitigate these errors is of paramount importance for the system's performance [Moo94], [Wan03], [Rug05], [Kro08].

The synchronization entails three distinct tasks: symbol timing synchronization, sampling frequency synchronization and carrier frequency offset (CFO) correction [Ai06]. The symbol timing synchronization is the process of determining the correct symbol starting position. The sampling frequency synchronization goal is to mitigate the misalignment of the samples of the received signal, due to the mismatch of the crystal oscillators of the transmitter digital-to-analog converter (DAC) and the receiver analog-to-digital converter (ADC). The CFO correction aims at reducing the frequency offset present in the received signal, caused by the frequency mismatch between the local oscillators of the transmitter and the receiver.

Once synchronization is achieved, or in a joint process, the effect of the channel on the received signal must be estimated. This operation is also of major relevance for the system. The channel estimate will be used throughout the system for coherent detection [Pro01], AMC [Kee06], MIMO techniques [Ges03], pre-equalization [Sil04], interference cancellation [Ver98], mobile terminal (MT) positioning [TS36.305] and cross-layer design [Lau06].

The importance of channel estimation is well-known and studied. In [Pro01] a closed formula is given for the bit error rate (BER) performance as a function of the correlation between the channel and its estimate, when transmitting over a multipath channel and using 4 Phase-Shift Keying (QPSK) modulation with coherent Maximum Ratio Combining (MRC) detection. This analysis clearly shows the impact of the multipath channel and of the channel estimator in the system's performance.

The recent standards for wireless systems define the use of high order modulations and extended service coverage, thus forcing the receivers to operate at very low signal-to-noise ratio (SNR) regimes. The synchronization algorithms must achieve a near perfect performance and the channel estimation scheme must output a very accurate estimate, while keeping the complexity to a minimum to maintain the MT portability, low cost and battery life.

A considerable body of work can be found in the literature and research actively continues on the topics of synchronization and channel estimated for OFDM-based systems.

This thesis addresses the topics of channel estimation and CFO estimation for OFDM-based systems with multiple antennas at both ends of the link. It aims at contributing with original low complexity algorithms with a performance that meets the requirements of the recent and near future wireless cellular standards.

This thesis states that the careful design and placement of the pilot sequences, together with the exploitation of properties of the DFT, allow the design and implementation of reduced complexity cooperating channel and CFO estimation algorithms that exhibit good performance when compared with the reference algorithms in the literature.

1.3. Contributions of this Thesis

The work developed in this thesis was partially supported by the European projects "WISQUAS - WIreless Systems providing high QUAlity Services" [WIS05], "Network of Excellence ACE - Antenna Centre of Excellence" [ACE06], "CRUISE - CReating Ubiquitous Intelligent Sensing Environments" [CRU06], "CODIV – Enhanced Wireless Communication Systems Employing COoperative DIVersity" [COD08], and the National projects "FFT-XXI – FFT-based solutions for the wireless communications of the XXIst century" [FFT05] and "PHOTON – Distributed and Extendible Heterogeneous Radio Architectures using Fibre Optic Networks" [PHO07] and the original contributions were disseminated in the publications listed in Section 1.3.1. It can be synthesized in the following:

- The analytical formulation of the channel estimation mean square error (MSE) for the single-user OFDM downlink scenario with a generic channel estimation scheme for a given power efficiency;
- A pilot-aided minimum MSE (MMSE) channel estimation scheme for broadband OFDM systems is developed. The careful placement of the pilots in the OFDM symbol leads to the proposal of a simplified time-domain (TD) MMSE estimator that explores the Fourier properties of the pilot and data-carrying symbols to extract the MMSE channel impulse response (CIR) estimate from the TD received symbol samples. Using the knowledge that the CIR energy is mainly limit to a small set of samples, a method to estimate the filter parameters is introduced.
- A pilot-aided channel estimation scheme for broadband MIMO OFDM systems is proposed. By constraining the placement of the orthogonal phase-

shifted pilot sequences and exploring the properties of the DFT, the investigated algorithm extracts the CIRs in the TD for all channels involved in the transmission process. The investigated pilot sequences allow the separation of the CIRs for the different channels from the data components when the symbols are transmitted over Rayleigh fading multipath channels and are robust against co-channel interference.

- A CFO estimation algorithm and associated channel estimation method for broadband OFDM systems with transmitter diversity is proposed. The investigated CFO estimation algorithm explores the TD structure of the transmitted symbols carrying pilots and data. Avoiding additional overhead, like training symbols or null sub-carriers, and relying solely on the data component present on those symbols, the investigated CFO algorithm outputs a highly accurate estimate. An intermediate output of the algorithm is used as input to the TD MMSE filter used in the investigated channel estimation scheme, resulting in a low complexity joint block with no performance trade-off.

1.3.1 Dissemination of original contributions

The original contributions presented in this thesis were disseminated in the following scientific publications.

Scientific Journals with Referees:

[Rib09] C. Ribeiro, A. Gameiro, "Estimation of CFO and Channels in Phase-Shift Orthogonal Pilot-Aided OFDM Systems with Transmitter Diversity," *EURASIP Journal on Wireless Communications and Networking*, vol. 2009, no. 1, pp. 1 – 10, January 2009.

[Rib08a] C. Ribeiro, M. J. Garcia, V. Jiménez, A. Gameiro, A. Armada, "Uplink channel estimation for multi-user OFDM-based systems," *Wireless Personal Communications*, vol. 47, no. 1, pp. 125 – 136, October 2008.

[Rib08b] C. Ribeiro, A. Gameiro, "An OFDM Symbol Design for Reduced Complexity MMSE Channel Estimation," *Journal of Communications*, vol. 3, no. 4, pp. 26 – 33, September 2008.

Scientific Conferences with referees:

[Nev09] D. Neves, C. Ribeiro, A. Silva, A. Gameiro, "Channel Estimation Schemes for OFDM Relay-Assisted Systems," in Proc. *IEEE Vehicular Technology Conference*, Barcelona, Spain, April 2009.

[Rib08c] C. Ribeiro, A. Gameiro, "Mitigating CFO in OFDM systems by exploring the symbol's structure," in Proc. *IEEE International Symposium on Wireless Communication Systems*, Reykjavik, Iceland, October 2008.

[Rib08d] C. Ribeiro, A. Gameiro, "MIMO-OFDM Channel Estimation – a Pilot Sequence Design for Time-domain Processing," in Proc. *International Conference on Wireless Information Networks and Systems*, Oporto, Portugal, July 2008.

[Rib07a] C. Ribeiro, A. Gameiro, "On the impact of the pilot density in the channel estimation of MC-CDMA systems," in Proc. *IEEE International Symposium on Wireless Communication Systems*, Trondheim, Norway, October 2007.

[Rib07b] C. Ribeiro, A. Gameiro, "Direct time-domain channel impulse response estimation for OFDM-based systems," in *Proc. IEEE Vehicular Technology Conference*, Baltimore, USA, September 2007.

[Rib07c] C. Ribeiro, A. Gameiro, "Uplink time-domain MMSE channel estimation for MC-CDMA systems," in Proc. *IEEE International Symposium on Personal, Indoor and Mobile Radio Communications*, Athens, Greece, September 2007.

[Rib07d] C. Ribeiro, A. Gameiro, "2D Wiener channel estimation performance analysis with diamond-shaped pilot-symbol pattern in MC-CDMA systems," in Proc. *Conference on Telecommunications*, Peniche, Portugal, May 2007.

[Rib07e] C. Ribeiro, M. J. Garcia, V. Jiménez, A. Gameiro, A. Armada, "Uplink channel estimation for multi-user OFDM-based systems," in Proc. *COST 289 Workshop on Spectrum and Power Efficient Broadband Communications*, Gothenburg, Sweden, April 2007.

1.4. Thesis Organization

This thesis is made-up of seven chapters with similar structure. With the exception of last chapter, each has its own abstract, state-of-the-art and references section. The rationale beyond this structure is to ease the reading of the document, as the reader can easily identify the chapter(s) of interest to his work.

Chapter 2 presents an overview of the wireless multipath channel and its modelling, and the DFT-based multicarrier transmission systems. The wireless multipath channel review focus on the wide-sense stationary uncorrelated scattering (WSSUS) channel model that will

be used throughout this thesis. The expressions of the multipath channel that are relevant for the following chapters are introduced. Some channel characterization measurements, like coherence bandwidth and coherence time, are given. A brief historical overview of multicarrier systems focusing on OFDM systems follows. The chapter ends with the basic working principles of OFDM and a detailed analysis of the signal flow from origin to destination, with emphasis on the role played by the wireless channel and how the OFDM deals with time dispersive nature of the multipath channel.

The impact of the pilot density in the performance of the channel estimation for OFDM systems is investigated in Chapter 3,. The analytical formulation of the channel estimation MSE for the single-user downlink scenario with a generic channel estimation scheme for a given power efficiency is given. The chapter ends with a set of system simulations that validate the analytical formulation.

Chapter 4 revisits the MMSE pilot-aided channel estimation for broadband OFDM systems. The careful design of the OFDM symbol leads to the proposal of a simplified TD MMSE estimator that explores the Fourier properties of the pilot and data- carrying symbols to extract the CIR from the TD received symbol samples and directly input it to the MMSE filter. Additionally, by using the knowledge that the CIR energy is mainly limit to a small set of samples, a simple, yet efficient, estimation of the filter parameters is introduced. Indoor and outdoor simulation results show that the performance of the investigated channel estimation scheme presents a tolerable degradation when compared with the *a-priori* knowledge of the channel correlation and noise variance, while exhibiting a reduced computational load.

In chapter 5, a channel estimation scheme for broadband MIMO OFDM systems is proposed. The design of the pilot sequences to explore the properties of the DFT opened way to the extraction of the CIRs in the TD for all channels involved in the transmission process. The investigated pilot sequences allow the separation of the CIRs for the different channels from the data components when the symbols are transmitted over Rayleigh fading multipath channels and are robust against co-channel interference. The feasibility of the investigated scheme is substantiated by system simulations.

Chapter 6 presents a CFO estimation algorithm and an associated channel estimation method for broadband OFDM systems with transmitter diversity. The investigated CFO estimation algorithm explores the TD structure of the transmitted symbols carrying pilots and data. Relying solely on the data component present on those symbols, it estimates the CFO with high accuracy, avoiding additional overhead like training symbols or null sub-carriers. An intermediate output of the CFO algorithm provides an easy to get initial CIR estimate that will be improved with the utilization of a TD MMSE filter. Indoor and outdoor system simulations show that the joint algorithms result in a near optimal system's performance.

The last chapter starts with a brief introduction to the demands that the future cellular wireless systems will have to fulfil to fully support the 4G requirements, and to some of the most challenging issues affecting the OFDM-based systems. The topics of research addressed in this thesis are identified and the main conclusions that come out of this work drawn. The major contributions resulting from this thesis are related to the main conclusions and, finally, the directions for future research work are identified.

1.5. References

[3GPP] Third Generation Partnership Project, http://www.3gpp.org.

[802.11a] IEEE Std. 802.11a-1999, "Local and metropolitan area networks – Specific requirements – Part 11: Wireless MAC and PHY specifications – High-speed physical layer in the 5 GHz band," Sept. 1999.

[802.11g] IEEE Std. 802.11g-2003, "Local and metropolitan area networks – Specific requirements – Part 11: Wireless LAN medium access control (MAC) and physical layer (PHY) specifications – Amendment 4: Further higher data rate extension in the 2.4 GHz band," June 2003.

[802.16] IEEE Std. 802.16-2009, "Local and metropolitan area networks – Part 16: Air interface for broadband wireless access systems," May 2009.

[ACE06] Network of Excellence ACE – Antenna Centre of Excellence, http://www.ist-ace.org/, 2006.

[Ai06] B. Ai, C. Pan, J. Ge, Y. Wang, Z. Lu, "On the synchronization techniques for wireless OFDM systems," *IEEE Transactions on Broadcasting*, vol. 52, no. 2, pp. 236 – 244, June 2006.

[Bil06] O. Billström, L. Cederquist, M. Ewerbring, G. Sandegren, J. Uddenfeldt, "Fifty years with mobile phones: From novelty to no. 1 consumer product," www.ericsson.com/ericsson/corpinfo/publications/review/2006_03/files/3_fifty_years.pdf, 2006.

[CEUC97] Committee on Evolution of Untethered Communications, National Research Council, *The Evolution of Untethered Communications*, Washington D.C., USA, National Academy Press, 1997.

[COD08] CODIV – Enhanced Wireless Communication Systems Employing COoperative DIVersity, http://www.ict-codiv.eu/, 2008.

[CRU06] CRUISE - CReating Ubiquitous Intelligent Sensing Environments, http://www.ist-cruise.eu/, 2006.

[DAB] ETSI Std. ETS 300 401 v1.4.1, "Radio broadcasting systems; Digital audio broadcasting (DAB) to mobile, portable and fixed receivers," June 2006.

[Dix94] R. Dixon, *Spread Spectrum Systems with Commercial Applications*, New York, USA, John Wiley & Sons, 1994.

[DVB-T] ETSI Std. ETS 300 744 v1.6.1, "Digital video broadcasting (DVB); Framing structure, channel coding and modulation for digital terrestrial television," Jan. 2009.

[ETS98] ETSI SMG Tdoc 032/98, "Proposal for a Consensus Decision on UTRA," 1998.

[FFT05] FFT-XXI – FFT-based solutions for the wireless communications of the XXIst century, http://www.av.it.pt/motion/projects_4.htm, 2005.

[Ges03] D. Gesbert, M. Shafi, D. Shiu, P. Smith, A. Naguib, "From theory to practice: An overview of MIMO space–time coded wireless systems," *IEEE Journal on Selected Areas in Communications*, vol. 21, no. 3, pp. 281–302, April 2003.

[ITU1645] ITU-R Recommendation M.1645, "Framework and overall objectives of the future development of IMT-2000 and systems beyond IMT-2000," June 2003.

[Kee06] S. Kee-Bong, A. Ekbal, C. Taek, J. Cioffi, "Adaptive modulation and coding (AMC) for bit-interleaved coded OFDM (BIC-OFDM)," *IEEE Transactions on Wireless Communications*, vol. 5, no. 7, pp. 1685 – 1694, July 2006.

[Kro08] M. Krondorf, G. Fettweis, "OFDM Link Performance Analysis under Various Receiver Impairments," *EURASIP Journal on Wireless Communications and Networking*, vol. 2008, pp. 1 – 11, January 2008.

[Lau06] V. Lau, Y. Kwok, *Channel-Adaptive Technologies and Cross-Layer Designs for Wireless Systems with Multiple Antennas: Theory and Applications*, Hoboken, New Jersey, USA, John Wiley & Sons, 2006.

[LTE] ETSI Technical Specification TS 136 201 v8.3.0, "LTE; Evolved universal terrestrial radio access (E-UTRA); Long Term Evolution (LTE) physical layer; General description," April 2009.

[LTEadv] ETSI Technical Report 136 913 V8.0.1, "LTE; Requirements for further advancements for Evolved Universal Terrestrial Radio Access (E-UTRA) (LTE-Advanced)," April 2009.

[Lu02] W. Lu, *Broadband Wireless Mobile: 3G and Beyond*, Chichester, England, John Wiley & Sons, 2002.

[Mah03] B. Mahon, *The Man Who Changed Everything: The Life of James Clerk Maxwell*, Chichester, England, John Wiley & Sons, 2003.

[Moo94] P. Moose, "A technique for orthogonal frequency division multiplexing frequency offset correction," *IEEE Transactions on Communications*, vol. 42, no. 10, pp. 2908 – 2914, October 1994.

[Mot09] Motorola, "A Timeline Overview of Motorola History, 1928-2009*",* www.motorola.com/staticfiles/Business/Corporate/US-EN/history/timeline.html, 2009.

[Pad95] J. Padgett, C. Gunther, T. Hattori, "Overview of wireless personal communications," *IEEE Communications Magazine*, vol. 33, no. 1, pp. 28 – 41, January 1995.

[Par06] S. Parkvall, E. Englund, M. Lundevall, J. Torsner, "Evolving 3G mobile systems: broadband and broadcast services in WCDMA," *IEEE Communications Magazine*, vol. 44, no. 2, pp. 30 – 36, February 2006.

[Par08] S. Parkvall, E. Dahlman, A. Furuskar, Y. Jading, M. Olsson, S. Wanstedt, K. Zangi, "LTE-Advanced - Evolving LTE towards IMT-Advanced," in *Proc. IEEE 68th Vehicular Technology Conference*, pp. 1 – 5, Calgary, Canada, September 2008.

[PHO07] PHOTON – Distributed and Extendible Heterogeneous Radio Architectures using Fibre Optic Networks, http://www.it.pt/project_detail_p.asp?ID=1160, 2007.

[Pol95] T. Pollet, M. Bladel, M. Moeneclaey, "BER sensitivity of OFDM systems to carrier frequency offset and Wiener phase noise," *IEEE Transactions on Communications*, vol. 43, no. 234, pp. 191 – 193, Feb./Mar./Apr. 1995.

[Pol95a] T. Pollet, M. Moeneclaey, "Synchronizability of OFDM signals," in Proc. *IEEE Global Telecommunications Conference*, vol. 3, pp. 2054 – 2058, Singapore, November 1995.

[Pra01] R. Prasad, *Towards a global 3G system: advanced mobile communications in Europe*, Vol. 1, Artech House, 2001

[Pro01] J. Proakis, *Digital Communications*, New York, USA, McGraw-Hill, 2001.

[Rap96] T. Rappaport, *Wireless Communications: Principles and Practice*, Upper Saddle River, New Jersey, USA, Prentice Hall, 1996.

[Rin47] D. Ring, "Mobile Telephony – Wide Area Coverage," *Technical Memorandum*, Bell Telephone Laboratories, USA, December 1947.

[Rug05] L. Rugini, P. Banelli, "BER of OFDM systems impaired by carrier frequency offset in multipath fading channels," *IEEE Transactions on Wireless Communications*, vol. 4, no. 5, pp. 2279 – 2288, September 2005.

[Sch82] R. Scholtz, "The origins of spread-spectrum communications," *IEEE Transactions on Communications*, vol. 30, no. 5, pp. 822 – 854, May 1982.

[Sil04] A. Silva, A. Gameiro, "Downlink Space-Frequency Pre-Equalization Techniques for TDD MC-CDMA Mobile Radio Systems," *EURASIP Journal on Wireless Communications and Networking*, vol. 1, no. 1, pp. 67 – 73, August 2004.

[Stu96] G. Stüber, *Principles of Mobile Communications*, Boston, USA, Kluwer Academic Publishers, 1996.

[TS36.305] 3GPP TS 36.305, "Evolved Universal Terrestrial Radio Access Network (E-UTRAN); Stage 2 functional specification of User Equipment (UE) positioning in E-UTRAN (Release 9)," May 2009.

[Ver98] S. Verdú, *Multiuser Detection*, Cambridge, UK, Cambridge University Press, 1998.

[Wan03] X. Wang, T. Tjhung, Y. Wu, B. Caron, "SER performance evaluation and optimization of OFDM system with residual frequency and timing offsets from imperfect synchronization," *IEEE Transactions on Broadcasting*," vol. 49, no. 2, pp. 170 – 177, June 2003.

[WIS05] WISQUAS - WIreless Systems providing high QUAlity Services, http://www.wisquas.org, 2005.

CHAPTER 2

MULTICARRIER SYSTEMS ON MULTIPATH WIRELESS CHANNELS

In this chapter we present an overview of the wireless multipath channel and its modelling, and the discrete DFT-based multicarrier transmission systems. The wireless multipath channel review focus on the WSSUS channel model that will be used throughout this thesis. We derive the expressions for the channel impulse and frequency responses and the channel correlation functions that will be used in the following chapters. We introduce some channel characterization measurements, like coherence bandwidth and coherence time, that provide an indication of the expected system's performance. We give a brief historical overview of multicarrier systems and then focus on OFDM systems. We'll go through the basic working principles of OFDM and present a detailed analysis of the signal flow from origin to destination, with emphasis on the role played by the wireless channel and how the OFDM deals with time dispersive nature of the multipath channel.

2.1. Introduction

In a cellular scenario, the communication takes place between a BS and a set of MT [Jak74], [Lee89]. The characteristics of the transmission medium have a profound impact in the specification of the multicarrier transmission system. The transmission commonly occurs in dense scenarios, with several obstacles surrounding or obstructing the transmission path. Considering that the transmitted signal travels over an additive white Gaussian noise (AWGN) channel will not be a reasonable assumption and the system's performance will fall short of the simulated one. The obstacles in the vicinity of the transmission path will strongly influence the system's performance. They will reflect the transmitted signal originating multiple signal replicas that will arrive at the receiver in different instants. This phenomenon is referred to as multipath propagation, giving rise to the multipath wireless channel.

In this chapter we will introduce the fundamental concepts of multipath wireless channel and also the basic concepts of the multicarrier wireless transmission systems.

The chapter is organized as follows. Next Section gives provides an introduction to the wireless channels and models used to describe it. In Section 2.3 will make a detailed introduction of the multicarrier transmission system. In Section 2.4, the discrete version of the channel model is derived using the assumptions of the previous section. The final section is devoted to some concluding remarks on the multicarrier systems.

Throughout the thesis, the notation $(\tilde{})$ is used for TD vectors and elements and its absence denotes frequency-domain (FD) vectors and elements. The index *n* denotes TD elements, the index *k* denotes FD elements and the index *i* denotes OFDM symbols. Unless stated otherwise, the vectors involved in the transmission/reception process are column vectors with N_C complex elements, and the matrices are square matrices with $(N_C \times N_C)$ complex values. The superscripts $(.)^T$ and $(.)^H$ denote transpose and Hermitian transpose, respectively.

2.2. The Multipath Wireless Channel and Its Modelling

Let's consider that the BS is transmitting a signal to a MT. The propagation of the signal from the origin to the destination is complex. Three basic physical propagation mechanisms are recognized to affect the transmission of the signal: reflection, diffraction and scattering [Rap96], [Par92], [Pat02], [Ste94].

The reflection occurs when a propagating electromagnetic wave impinges on a smooth surface whose dimension is much larger than the radio-frequency (RF) signal wavelength. The diffraction is the phenomenon that accounts for the transmission when there is no line-of-sight (LoS) between the transmitter and the receiver. It occurs when the transmission path is obstructed by a dense body with large dimensions compared to signal wavelength, causing secondary waves to be formed. The scattering occurs when a propagating wave impinges on a surface whose dimensions are smaller than the signal wavelength, causing the reflected energy to scatter in all directions.

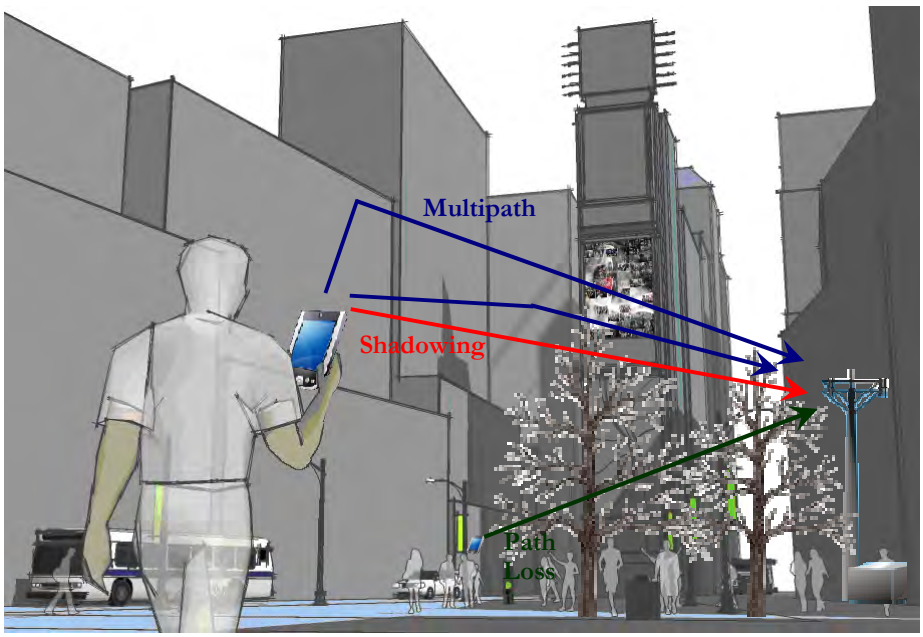

Figure 2.1. Effects of the propagation in wireless channels.

The physical propagation mechanisms are responsible for the effects observed in the received signal (cf. Figure 2.1). The path loss represents the attenuation of the signal caused by the dispersion of its energy as the electromagnetic wave travels from the transmitter to the receiver. The shadowing is caused by obstruction of the LoS by large elements (ex.: hills, forests, buildings), leading to significant fluctuations in the average received signal power. The estimate of the path loss as a function of the distance is commonly performed using a log-normal distribution that simulates the fluctuation of the received signal power. The multipath fading accounts for the existence of multiple reflective paths between the transmitter and the receiver. This effect causes dramatic changes in the received signal's amplitude, phase, and angle of arrival as a result of small changes in the spatial separation between the receiver and transmitter. The multipath propagation causes a time-spreading of the received signal (signal dispersion) and the time-variant behaviour of the channel. Due to the rapidity of the changes this phenomenon is also called fast fading.

Due to the slow speed of variation, the path loss and the shadowing can be compensated [Rap96] either by the MT or the BS (by receiving feedback information from the MT). From this point forward, in this thesis it is considered that power control mechanisms deal with path loss and shadowing and that the only mechanism affecting the transmitted signal is the multipath propagation.

2.2.1 The WSSUS channel model

The WSSUS channel model was introduced in [Bel63] and has since then been almost exclusively used for the description of frequency-selective mobile wireless channels. This model provides a simple statistical model for the multipath fading phenomenon. An example of a typical urban propagation scenario is depicted in Figure 2.2.

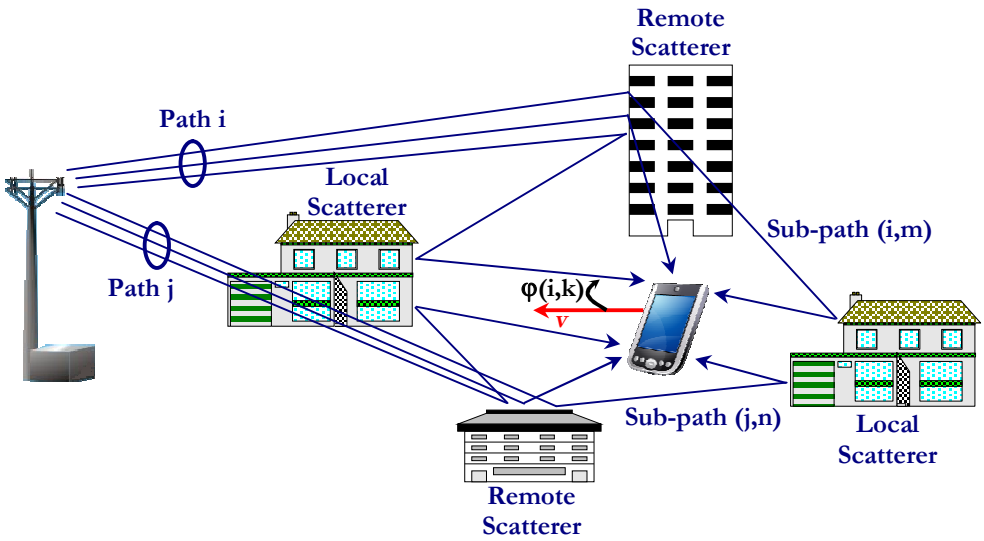

Figure 2.2. Example of a typical urban propagation scenario.

The signal arriving at the receiver is made-up of L_p replicas travelling over different paths. The local scatterers (cf. Figure 2.2) originate L_{sp} sub-paths in each path with delay differences that are considered much smaller than the system's sampling interval. Therefore, this model considers that each signal replica is the vectorial sum of the L_{sp} sub-paths originated in local scatterers arriving simultaneously with delay τ_l.

The replicas arriving from different paths are considered independent. Empirical analysis by Bello [Bel63] and Parsons [Par82] shown that such a channel is effectively wide-sense stationery (WSS) in both the time and frequency domains, for small time intervals or spatial areas.

The characteristics of the time-variant mobile wireless channels are, among others, thoroughly overviewed in [Par82], [Ste87], [Ska97] and the main subject of numerous books, for example [Par92], [Ste94], [Rap96], [Stu96], [Pat02].

When there is a dominant non-fading signal component (such as a LoS propagation path), the envelope of the received signal is described by a Rician probability distribution function (PDF) [Ste94]. If there is no LoS, the envelope of the received signal is described by a Rayleigh PDF. In the typical urban propagation scenario, the LoS is rarely present and this is the scenario considered throughout this thesis.

The complex baseband representation [Ste94] of the CIR can be described by

$$\tilde{h}(t,\tau)=\sum_{l=0}^{L_p-1}\alpha_l(t)\delta(\tau-\tau_l), \tag{2.1}$$

where τ_l is the delay of the l-th path and $\alpha_l(t)$ is the corresponding complex amplitude. Due to the motion of the MT, the complex amplitudes $\alpha_l(t)$ are independent WSS complex Gaussian processes.

The frequency response of the time-varying WSSUS channel at time t is the Fourier transform of the CIR,

$$h(t,f)\triangleq\int_{-\infty}^{+\infty}\tilde{h}(t,\tau)e^{-j2\pi f\tau}d\tau=\sum_{l=0}^{L_p-1}\alpha_l(t)e^{-j2\pi f\tau_l}\ . \tag{2.2}$$

Assuming that all paths have the same time correlation function ϕ_t, the time correlation of the multipath channel for the l-th path is

$$\phi_{\alpha_l}(\Delta t)\triangleq E\left\{\alpha_l(t+\Delta t)\alpha_l^*(t)\right\}=\sigma_h^2[l]\phi_t(\Delta t), \tag{2.3}$$

where $\sigma_h^2[l]$ is the average power of the l-th path.

The correlation function of the channel frequency response (CFR) for different times and frequencies is [Li98]

$$\begin{aligned}\Phi_H(\Delta t,\Delta f)&\triangleq E\left\{H(t+\Delta t,f+\Delta f)H^*(t,f)\right\}\\&=E\left\{\sum_{l=0}^{L_p-1}\alpha_l(t+\Delta t)e^{-j2\pi(f+\Delta f)\tau_l}\sum_{m=0}^{L_p-1}\alpha_m^*(t)e^{j2\pi f\tau_m}\right\},\\&=\sum_{l=0}^{L_p-1}\phi_{\alpha_l}(\Delta t)e^{-j2\pi\Delta f\tau_l}=\phi_t(\Delta t)\sum_{l=0}^{L_p-1}\sigma_h^2[l]e^{-j2\pi\Delta f\tau_l}\\&=\sigma_{Ch}^2\phi_t(\Delta t)\phi_f(\Delta f)\end{aligned} \tag{2.4}$$

where σ_{Ch}^2 is the total average power of the channel defined as

$$\sigma_{Ch}^2 \triangleq \sum_{l=0}^{L_p-1} \sigma_h^2[l]. \tag{2.5}$$

Without loss of generality, in this thesis it is assumed that $\sigma_{Ch}^2 = 1$. The frequency correlation function ϕ_f is defined as

$$\phi_f(\Delta f) = \sum_{l=0}^{L_p-1} \frac{\sigma_h^2[l]}{\sigma_{Ch}^2} e^{-j2\pi\Delta f \tau_l}. \tag{2.6}$$

Equation (2.4) puts in evidence that the correlation function of the CFR can be split in the product of the time and frequency correlation functions.

The frequency correlation function is the Fourier transform of the channel power delay profile (PDP) S_τ, and represents the correlation between the channel's response to two narrowband complex exponential signals as a function of their frequency separation. It can be seen as the channel's frequency transfer function.

The coherence bandwidth B_c is a statistical measure of the range of frequencies where the multipath channel exhibits approximately equal gain and linear phase. It represents a frequency range over which frequency components have a strong potential for amplitude correlation. That is, two complex exponentials transmitted in that range will be similarly affected by the channel, for example, exhibiting fading or no fading.

The coherence bandwidth is related to the channel's maximum delay $\tau_{\max}$, that represents the time interval between the first and last received signal replicas, corresponding to the shortest and longest paths. As an approximation, it can be related by [Ste94]

$$B_c \approx \frac{1}{\tau_{\max}}. \tag{2.7}$$

Figure 2.3 depicts the PDP and respective frequency correlation function for the BRAN-E channel model [Med98], [Med98a], defined in the HIPERLAN/2 standard, resulting from measurements performed in an outdoor scenario.

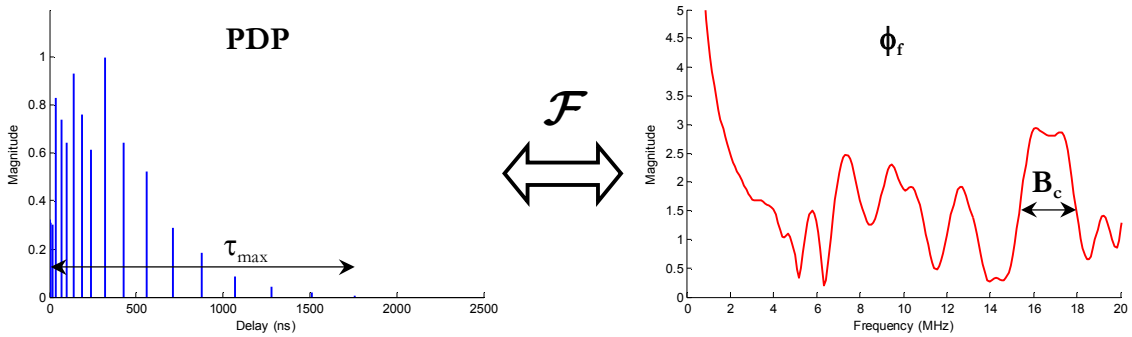

Figure 2.3. Hiperlan/2 BRAN-E PDP and frequency correlation function.

The maximum excess delay may not be the best indicator of the system's performance on a particular channel because different channels with the same maximum delay can exhibit very different profiles of signal intensity over the delay span.

Two important measurements [Pat02] are commonly used for the characterization of the channel: the average delay and the delay spread. The average delay is the first moment of the PDP,

$$\overline{\tau} = \frac{\int_{-\infty}^{+\infty} \tau S_{\tau}(\tau)\, d\tau}{\int_{-\infty}^{+\infty} S_{\tau}(\tau)\, d\tau}. \tag{2.8}$$

The average delay quantifies the statistical mean delay that a signal incurs when travelling over the considered multipath channel.

The delay spread is the squared root of the second moment of the PDP,

$$\sigma_{\tau} = \sqrt{\frac{\int_{-\infty}^{+\infty} (\tau - \overline{\tau})^2 S_{\tau}(\tau)\, d\tau}{\int_{-\infty}^{+\infty} S_{\tau}(\tau)\, d\tau}}. \tag{2.9}$$

The delay spread quantifies the statistical time spread that a signal incurs when travelling over the considered multipath channel. This measurement is the most widely used to characterize the multipath channel.

An exact relationship between coherence bandwidth and delay spread does not exist. A common approximation for the coherence bandwidth corresponding to a frequency range having a correlation of at least 0,5 is [Rap96]

$$B_c \approx \frac{1}{5\sigma_{\tau}}. \tag{2.10}$$

For mobile scenarios, the channel is time-variant because the MT motion (or BS for that matter) results in propagation path changes. As a result of the motion, the receiver sees amplitude and phase variations on a continuous transmitted signal. Assuming that all of the channel's scatterers are stationary, whenever motion ceases, the amplitude and phase of the received signal remains constant: the channel appears to be time-invariant. Whenever motion occurs, the channel becomes time-variant. Time variance can be equivalently treated as spatial variance as the channel characteristics are dependent on the positions of the transmitter and receiver.

The time correlation function is dependent on the Doppler frequency f_d (or equivalently on the MT speed v) and can be obtained by the Fourier transform of Doppler power spectral density (PSD) $S(f_d)$. It represents the correlation between narrowband complex exponential signals as a function of their time separation.

Using the dense-scatterer channel model with constant velocity of motion and an unmodulated continuous wave signal [Cla68], the normalized time correlation function can be described as,

$$\phi_t(\Delta t) = J_0(2\pi f_D \Delta t), \tag{2.11}$$

where $J_0(.)$ is the zero-order Bessel function of the first kind and f_D represents the largest magnitude frequency shift that occurs when the scatterer is directly ahead or directly behind the moving element (MT or BS). It is defined by

$$f_D = \frac{v}{\lambda}. \tag{2.12}$$

The frequency shifts are positive when the distance between the transmitter and the receiver decreases, and negative when they are moving away from each other. For scatterers directly broadside of the moving element the magnitude of the frequency shift is zero.

The coherence time T_c is a statistical measure of the expected time interval over which the channel's response is essentially invariant. It provides the knowledge about the fading rapidity of the channel. In a motionless scenario, the channel's response would be highly correlated for all time intervals and the time correlation function would be a constant value.

Defining the free-space phase constant that transforms distance to phase, $\kappa = 2\pi/\lambda$, where λ is the signal wavelength, coherence time can be measured in either time or distance travelled, assuming the MT travels with a fixed velocity.

In a multipath environment where the received signal arrives via multiple paths with distinct distances and angles of arrival, the Doppler frequency shift incurred by the signal replica arriving from a path is in general different from that arriving by another path. The effect of the sum of the different signal replicas results in a spectral broadening of the transmitted signal carrier frequency, rather than a single frequency shift. Like its frequency-related counterpart coherence bandwidth, the coherence time is related to the maximum Doppler frequency. As an approximation, it can be related by,

$$T_c \approx \frac{1}{f_D}. \tag{2.13}$$

A common approximation for the coherence time correspond to a time interval over which the time correlation function as a value of at least 0,5 is [Ste94]

$$T_c \approx \frac{9}{16\pi f_D}. \tag{2.14}$$

For the case of the dense-scatterer channel model, where the replicas of an unmodulated continuous wave signal impinge in an isotropic receive antenna with an uniform distribution of arriving angles $\varphi(i,k)$ (cf. Figure 2.2), throughout the range $[0, 2\pi[$, the Doppler PSD $S(f_d)$ is [Cla68]

$$S(f_d) = \begin{cases} \dfrac{1}{\pi f_D \sqrt{1-\left(\dfrac{f_d}{f_D}\right)^2}}, & |f_d| \le f_D \\ 0, \quad remaining \end{cases}. \tag{2.15}$$

and is commonly denominated Jakes spectrum [Jak74]. The spread of the Doppler PSD can be defined as,

$$\sigma_{f_D} \le 2|f_D|. \tag{2.16}$$

Figure 2.4 depicts the Doppler PSD and respective time correlation function for a received signal with maximum Doppler frequency shift $f_D = 1000Hz$ and a carrier frequency $f_c = 5GHz$.

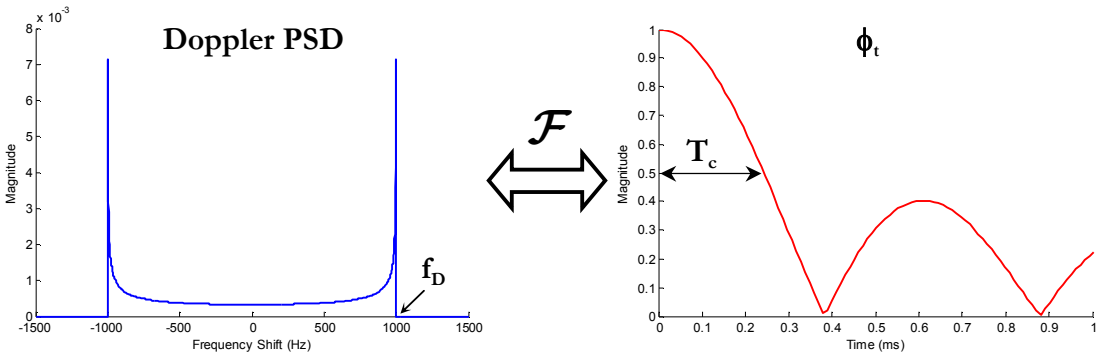

Figure 2.4. Doppler PSD and time correlation function.

2.3. The Discrete DFT-Based Multicarrier Transmission System

This section provides an overview of the multicarrier transmission systems, focusing on the OFDM system, the supporting transmission system for the work developed in this thesis, with emphasis on the topics relevant for the following chapters.

2.3.1 Introduction

The concept of multicarrier transmission has a long history. It can be traced back to the late 1950's, to the initial work of Mosier [Mos58]. The first multicarrier systems appear in the late 1950's and 1960's, for high frequency military communications. Such systems, like the KINEPLEX [Mos58], KATHRYN [Zim67] and ANDEFT [Por68], are best characterized as frequency-division multiplexed systems.

The work of Chang [Cha66] that shows that multicarrier modulation can solve the multipath problem without reducing data rate is commonly considered to be the first official publication on multicarrier modulation. It was followed by the work of Saltzberg [Sal67] that shows that a multicarrier modulation is essentially a Fourier transform of the original stream and the set of coherent demodulators at the receiver is an inverse Fourier transform operation. The use and viability of the concept was questioned until the theoretical viability of the system was confirmed by Chang and Gibby [Cha68]. The first patent on multicarrier systems was filled by Chang and issued in January 1970 [Cha70].

In 1971, the discrete DFT-based multicarrier transmission systems is proposed by Weinstein and Ebert [Wei71], where they show that multicarrier modulation can be accomplished using a discrete Fourier transform (DFT). The currently used concept of the OFDM was established by Peled and Ruiz [Pel80] where they propose the introduction of the cyclic prefix that transforms the effect of the multipath wireless channel to become equivalent

to a cyclic convolution, while mitigating the inter-symbol interference (ISI) caused by the time dispersion of the symbol samples.

The work of Hirosaki [Hir81] investigated the use of *M*-ary QAM in conjunction with the DFT operation. In 1985, Cimini describes the use of OFDM for mobile communications [Cim85], identifying many of the key issues in OFDM transmission and develops a proof-of-concept design.

In recent years, the discrete DFT-based multicarrier transmission systems have been adopted as the air interface of multiple broadband wireless systems. Among others systems, in wireless LAN environment is present in the IEEE 802.11a [802.11a] and IEEE 802.11g [802.11g] standards; in the wireless metropolitan area network (MAN) environment, multicarrier systems can be found in the fixed and mobile IEEE 802.16 (also called BWA and commercially termed "WiMAX") standards [802.16], [802.16d], [802.16e], and on the European LTE standard [LTE]. The current European standards for DAB [DABa], [DABb] and terrestrial DVB [DVB-Ta], [DVB-Tb] are also supported by a multicarrier transmission system. In the near future, the discrete DFT-based multicarrier transmission systems present themselves as the strongest candidate for air interface of the broadband 4 Generation mobile communications systems [LTEadv].

The robustness of these systems to the frequency-selective dispersive nature of the multipath wireless channel and the simple architecture of the air interface when compared to that of single carrier systems, with modulation/demodulation implementation based on efficient FFT operations, have grant this transmission technique a huge commercial success.

2.3.2 Basic principles on multicarrier systems

In a single carrier transmission system, the input data is 2^M-level modulated, originating a high baud rate stream that is up-converted to the system's carrier frequency f_c before transmission. This idea is depicted in Figure 2.5. Each transmitted symbol has the duration $t_S = M/r_b$, where M is the number of bits carried in a symbol and r_b is the input data rate, or equivalently a baud rate $r_s = r_b/M$.

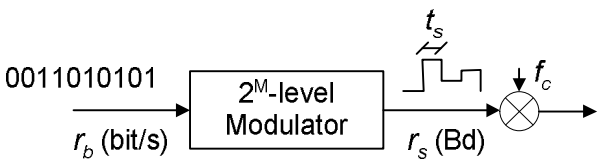

Figure 2.5. Single carrier modulation.

In a classical multicarrier system the input data is divided into N_C parallel data streams with a lower data rate. Each low data rate stream is individually modulated by an independent 2^M-level modulator. Assuming that the individual modulators use the same number of signalling levels, 2^M, at the output of each modulator, the duration of each symbol is $t_S = N_C M / r_b$. Comparing with the previous single carrier example, the duration of each symbol is increased by a factor of N_C.

To simultaneously transmit the N_C low baud rate streams, the total system's bandwidth is divided into N_C frequency sub-channels or sub-carriers, each carrying a low baud rate stream; i.e., the individual streams are frequency multiplexed. This principle is depicted in Figure 2.6.

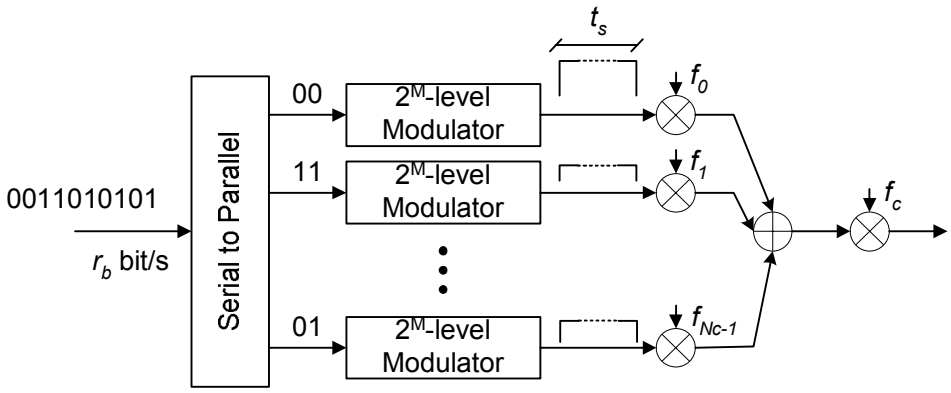

Figure 2.6. Multicarrier modulation.

The splitting of the system's bandwidth in numerous narrowband channels each carrying a low baud rate stream is the main advantage of this transmission system, making it more robust against the frequency-selective time-dispersive fading wireless channel effects. A single fade can cause the single-carrier system to fail. In the multicarrier system, the fade affects only a small percentage of the sub-carriers [Pra04].

To ease the sub-channel separation at the receiver and to avoid the performance degradation caused by inter-channel interference, the frequency band of the individual channels should not overlap. Moreover, guard bands should be introduced in between the different sub-carriers to effectively isolate them, allowing the receiver to separate the sub-channels using a bank of filters of appropriate cut-off frequencies and a bank of coherent demodulators.

The implementation of the multicarrier transmission systems using a bank of parallel modulators, demodulators, filters and oscillators is far from efficient, demanding a large

amount of hardware. The non-overlapping frequency sub-channels result in a low spectral efficiency, worsen by the presence of guard bands.

The OFDM transmission systems proposed by Weinstein and Ebert [Wei71] and Peled and Ruiz [Pel80], has an improved spectral efficiency by allowing the overlap of the frequency bands of the sub-carriers and eliminating the band guards in between them. Figure 2.7 presents an example of the PSD of a set of sub-carriers, where the overlapping of the sub-carriers is visible.

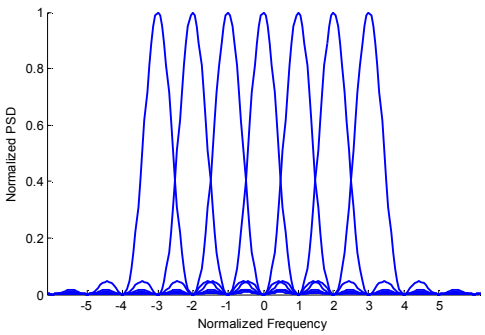

Figure 2.7. PSD of the individual OFDM sub-carriers.

Examining Figure 2.7, it is visible that at the centre frequency of each sub-carrier there is no inter-carrier interference (ICI). The OFDM sub-carriers are arranged in a away such so that the sidelobes of the individual sub-carriers overlap but can be separated by receiver without ICI. This is achieved by exploiting the DFT properties and making the sub-carriers orthogonal to each other, when using a rectangular baseband pulse. The separation of the sub-carriers is inverse of the OFDM symbol duration,

$$\Delta f = \frac{1}{t_S}, \tag{2.17}$$

and the samples of the individual sub-carriers are synchronously transmitted, spaced in time by

$$\Delta t = \frac{t_S}{N_C}. \tag{2.18}$$

With this arrangement, the bank of modulators is replaced by a single IDFT operation as it will be introduced in the next section.

The receiver acts as a bank of demodulators that down convert each carrier to DC and integrates the resulting signal for the duration of the OFDM symbol to recover the transmitted symbol. The contribution of the unwanted (remaining) sub-carriers is null because

they are integrated over an integer number of cycles. Thus, each sub-carrier is orthogonal (independent) to the remaining.

The bank of demodulators is implemented with a single DFT operation. At the output of the DFT operation, the sub-carrier value is recovered without interference and not requiring any filtering. This will be introduced in the next section.

The DFT operations required at both transmitter and receiver sides are implemented using efficient fast Fourier transform (FFT) algorithms that reduce the number of operations from N_C^2 to $N_C \log_2(N_C)$ [Zou95]. This simplification is increasingly important as the number of sub-carriers of the systems increases.

It is worth mentioning that OFDM can be seen as either a modulation technique or a multiplexing technique, where different sub-carriers can be used by different users.

The complex envelope of the OFDM signal, $\tilde{s}(t)$, can be expressed as,

$$\tilde{s}(t) = \frac{1}{\sqrt{N_C}} \sum_{k=0}^{N_C-1} d[k] \exp(j2\pi f_k t), \quad 0 \le t < t_s \tag{2.19}$$

where $d[k]$ is the complex symbol conveyed by the k-th sub-carrier and $f_k = n\Delta f, \quad n = 0, \cdots, N_c - 1$ are the baseband frequencies of the N_C sub-carriers.

The PSD of the OFDM signal is the sum of the PSD of the individual sub-carriers, and can be expressed as,

$$S(f) = E\left\{|s(f)|^2\right\} = \frac{t_S^2}{N_C} \sum_{k=0}^{N_C-1} E\left\{|d[k]|^2\right\} |sinc(ft_S - k)|^2, \tag{2.20}$$

where $s(f)$ is the Fourier transform of $\tilde{s}(t)$. Assuming that the system has a high number of sub-carriers transmitted with equal power, the PSD of the signal tends to be flat, approaching the PSD of a single carrier system with ideal Nyquist filtering [Pro01]. This can be observed in Figure 2.8 that depicts the PSD of 2 OFDM signals with $N_C = 8$ sub-carriers (blue plot) and $N_C = 1024$ sub-carriers (red plot).

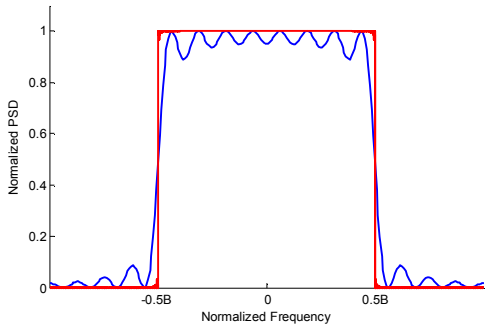

Figure 2.8. PSD of the OFDM signal (red – 1024 sub-carriers; blue – 8 sub-carriers).

For a high number of sub-carriers, the system's bandwidth B is approximately,

$$B \approx N_C \Delta f = \frac{N_C}{t_S}. \tag{2.21}$$

2.3.3 Analysis of the OFDM system

This section provides an analysis of a simplified OFDM baseband system. Figure 2.9 and Figure 2.10 depict, respectively, the considered OFDM baseband transmitter and receiver models.

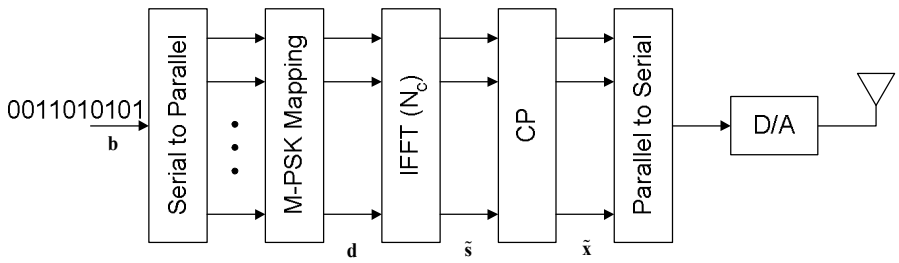

Figure 2.9. OFDM baseband transmitter model.

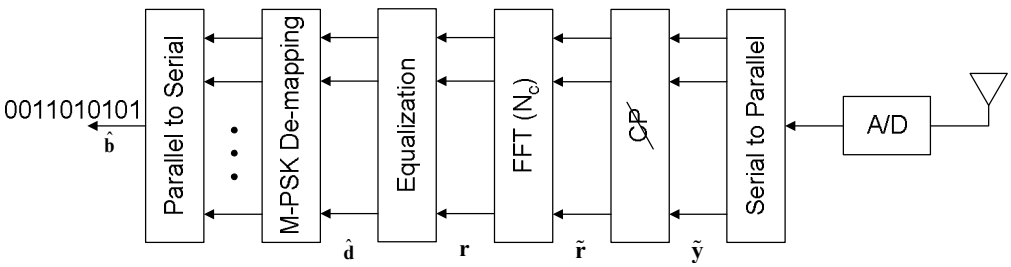

Figure 2.10. OFDM baseband receiver model.

The input data stream (represented by vector $\mathbf{b}$) is divided by the Serial to Parallel block into N_C lower rate data streams. Assuming that all streams are modulated with the

same number of bits per symbol M, each set of M bits from each stream is mapped into a complex value corresponding to a point of a 2^M-points PSK or QAM constellation. The vector $\mathbf{d}$ containing N_c complex constellation points is passed to the IFFT that transforms it to the TD vector $\tilde{\mathbf{s}}$ with the n-th element,

$$\tilde{s}[n] = \frac{1}{\sqrt{N_C}} \sum_{k=0}^{N_C-1} d[k] \exp\left[j \frac{2\pi}{N_C} kn \right], \tag{2.22}$$

where $d[k]$ is the k-th element of $\mathbf{d}$. This vector forms the baseband signal carrying the N_C data symbols on a set of orthogonal sub-carriers.

The constellation mapping and IFFT blocks constitute the modulation block of the OFDM system. These 2 blocks replace the bank of oscillators, modulators and filters that otherwise would be required by the multicarrier system introduced in the previous section.

The value N_C should be a power of 2, so that the IDFT operation can be efficiently implemented using the IFFT algorithm.

Transforming vector $\tilde{\mathbf{s}}$ to the analogue domain for transmission using an digital-to-analogue converter with rectangular pulse shape, would yield the signal defined by (2.19). Prior to this transformation, a second key operation for the performance of the OFDM system is executed – the introduction of the cyclic prefix (CP). The concept of introducing a guard interval in the form of CP was introduced in [Pel80]. The very simple idea of copying the L last samples of each symbol and prefixing it to the beginning of the symbol is of major importance for the analysis and performance of the system. The CP mitigates the ISI, thus leading to the preservation of the sub-carriers' orthogonality, enabling the design of a simple equalizer as it will be introduced. The principle is depicted in Figure 2.11.

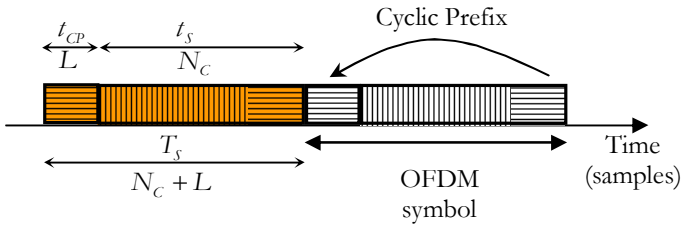

Figure 2.11. Constitution of the OFDM symbol – adding the CP.

The duration of the CP, t_{CP}, is chosen to be larger than the worst case wireless channel maximum delay, so that the ISI can be totally removed and the effect of the multipath channel on the transmitted signal goes from a linear convolution to a circular one. The CP increases the OFDM symbol duration from t_S to $T_S = t_S + t_{CP}$ (or equivalently, from N_C samples to

$N_C + L$). The samples of the CP do not carry any new information, leading to a decrease of the system's spectral efficiency. This loss depends on the length of the CP, but commonly remains below 1dB [Pra04].

The operation of adding the CP can be expressed in matrix form as,

$$\tilde{\mathbf{x}} = \mathbf{A}_{CP}\tilde{\mathbf{s}}, \tag{2.23}$$

where $\mathbf{A}_{CP} = \left[\mathbf{I}_{N_C,L} \quad \mathbf{I}_{N_C}\right]^T$ is the matrix that adds the CP, with $\mathbf{I}_{N_C}$ denoting the $N_C \times N_C$ identity matrix and $\mathbf{I}_{N_C,L}$ denoting the last L columns of $\mathbf{I}_{N_C}$. The resulting vector $\tilde{\mathbf{x}}$ is after serialized and converted to analogue domain by a digital-to-analogue converter, before being sent for transmission.

The addition of cyclic prefix is usually accompanied with the windowing operation. The rectangular baseband pulse presents an infinite bandwidth (with its *sinc* function Fourier transform). In order to reduce the out-of-band emission, especially for systems with lower number of sub-carriers (cf. Figure 2.8), the windowing is commonly used [Pra04]. This operation shapes the samples that make-up the CP, not influencing the useful symbol samples. As the windowing does not affect the purpose of the CP of eliminating the ISI and maintaining the orthogonality of the sub-carriers, this operation is not considered in this analysis, nor in the remaining of this thesis.

The receiver starts by sampling the baseband signal with a sampling rate $1/\Delta t$. Assuming the receiver is perfectly synchronized, the *n*-th received signal sample of the *i*-th symbol can be expressed as

$$\tilde{y}_i[n] = \sum_{l=0}^{L_p-1} \tilde{h}_i[l]\,\tilde{x}_i[n-l], \tag{2.24}$$

where $\tilde{\mathbf{h}}_i$ is discrete-time CIR that will be introduced in the next section. Collecting the $(N_C + L)$ samples of the symbol, the effect of the transmission over the multipath channel can be expressed in matrix form as,

$$\tilde{\mathbf{y}}_i = \tilde{\mathbf{H}}_{i,lin}\tilde{\mathbf{x}}_i + \tilde{\mathbf{z}}_i, \tag{2.25}$$

where the vector $\tilde{\mathbf{z}}_i$ represents the ISI caused by the channel dispersion and the matrix $\tilde{\mathbf{H}}_{i,lin}$ is the $(N_C + L)\times(N_C + L)$ lower triangular Toeplitz channel convolution matrix with first column $\tilde{\mathbf{h}}_i$ padded with zeros.

The next operation is the removing of the CP from the received symbol. The operation can be expressed in matrix form as,

$$\tilde{\mathbf{r}}_i = \mathbf{R}_{CP}\tilde{\mathbf{y}}_i = \mathbf{R}_{CP}\tilde{\mathbf{H}}_{i,lin}\tilde{\mathbf{x}}_i + \mathbf{R}_{CP}\tilde{\mathbf{z}}_i = \mathbf{R}_{CP}\tilde{\mathbf{H}}_{i,lin}\mathbf{A}_{CP}\tilde{\mathbf{s}}_i + \mathbf{R}_{CP}\tilde{\mathbf{z}}_i\,, \tag{2.26}$$

where $\mathbf{R}_{CP} = \left[\mathbf{0}_{N_C \times L} \quad \mathbf{I}_{N_C}\right]$ is the matrix that removes the CP with $\mathbf{0}_{N_C \times L}$ representing the $(N_C \times L)$ null matrix.

With the assumption that the length of the CP is larger than the duration of CIR, the ISI is completely removed and equation (2.26) can be written as,

$$\tilde{\mathbf{r}}_i = \tilde{\mathbf{H}}_{i,circ}\tilde{\mathbf{s}}_i = \mathbf{F}^H\mathbf{Q}_i\mathbf{d}_i\,, \tag{2.27}$$

where $\tilde{\mathbf{H}}_{i,circ} = \mathbf{R}_{CP}\tilde{\mathbf{H}}_{i,lin}\mathbf{A}_{CP}$ is the $(N_C \times N_C)$ circulant matrix with circulant vector $\tilde{\mathbf{h}}_i$ and $\mathbf{F} \triangleq N_C^{-1/2}\exp\left(-j\frac{2\pi}{N_C}kn\right)_{k,n=0,0}^{N_C-1,N_C-1}$ is the $(N_C \times N_C)$ DFT matrix. Due to the properties of the DFT, the CFR matrix is

$$\mathbf{Q}_i = \mathbf{F}\tilde{\mathbf{H}}_{i,circ}\mathbf{F}^H = diag\left(\mathbf{h}_i\right), \tag{2.28}$$

where the vector $\mathbf{h}_i$ holds discrete-time CFR that will be introduced in the next section.

The TD vector with the received samples $\tilde{\mathbf{r}}$ is transformed to FD using a DFT operation. Like the transmitter, the DFT operation is implemented using the efficient FFT algorithm. The resulting vector $\mathbf{r}$ is feed to the equalizer block. Due to (2.28) (and the assumptions that lead to it – no ISI, nor ICI), the optimum MRC equalizer is implemented by a diagonal matrix corresponding to the Hermitian transpose of $\mathbf{Q}_i$. If no noise affects the transmission process, the transmitted symbol vector is recovered with no distortion,

$$\hat{\mathbf{d}}_i = \mathbf{Q}_i^H\mathbf{F}\tilde{\mathbf{r}}_i = \mathbf{Q}_i^H\mathbf{F}\mathbf{F}^H\mathbf{Q}_i\mathbf{d}_i = \mathbf{d}_i\,. \tag{2.29}$$

The de-mapping block maps each complex value in the corresponding M bits that once converted from parallel to serial form the data estimate vector $\hat{\mathbf{b}}$.

The de-mapping, equalizer and FFT blocks replace the bank of oscillators, demodulators and filters that would be required by the receiver of the non DFT-based multicarrier system introduced in the previous section.

2.4. The Discrete-Time WSSUS Channel Model Affecting the Multicarrier System

The wireless digital transmission systems exhibit a finite delay resolution that is defined by the system's sampling interval and reciprocal to the system's bandwidth. In the classical analysis of the channel effects on finite delay resolution systems [Ste94], the effect of the paths that arrive in the interval of two consecutive samples is replaced by the effect of a single path with a delay τ_n, multiple of the sampling interval. The single path represents the effect of all the paths in the denominated delay bin and is obtained by the vector sum of the phasors of the unresolved paths in each delay bin.

With the increase of the systems bandwidth/delay resolution in recent years, with OFDM system's specified with a sampling interval of a few tens of nanoseconds, the local scatterers may be considered themselves as generating new paths and the previous approach was questioned. The results in [Bee95] and [Li98] have shown that for a OFDM system with a CP longer than the channel's maximum delay, the discrete-time CIR can be obtained with tolerable leakage by sampling the analogue CIR at time instants $t = n\Delta t$. It is expressed as

$$\tilde{h}[n] \triangleq \tilde{h}(n\Delta t) = \sum_{l=0}^{L_p-1} \alpha_l(t)\,\delta(\tau - \tau_l), \tag{2.30}$$

where L_p now stands for the number of resolvable paths and the delays τ_l have values multiple of the OFDM system sampling interval. These assumptions were considered in the national and European projects related with this thesis and are assumed is this work. Further assumptions on the channel properties are:

- The CIR is constant for the duration of one OFDM symbol;
- The channel taps are zero mean WSS complex Gaussian random variables;
- The channel taps are assumed to be mutually uncorrelated.

The discrete-time channel frequency response of the time-varying WSSUS channel affecting the sampled received signal is expressed as

$$h[k] \triangleq h(k\Delta f) = \sum_{l=0}^{L_p-1} \alpha_l(t) \exp\left(j\frac{2\pi}{N_C}k\tau_l\right). \tag{2.31}$$

The discrete-time correlation function of the CFR for different sub-carriers and OFDM symbols can be split in the product of the time and frequency discrete-time correlation functions [Li98]

$$\Phi_H[k,i] = \phi_f[k]\phi_t[i], \tag{2.32}$$

where

$$\phi_f[k] = \phi_f(k\Delta f), \tag{2.33}$$

and

$$\phi_t[i] = \phi_t(iT_S). \tag{2.34}$$

The average delay defined in (2.8) for the channel model with L_p resolvable paths can be rewritten as,

$$\bar{\tau} = \frac{\sum_{l=0}^{L_p-1} \tau_l \sigma_b^2[l]}{\sum_{l=0}^{L_p-1} \sigma_b^2[l]} = \sum_{l=0}^{L_p-1} \tau_l \sigma_b^2[l], \tag{2.35}$$

keeping in mind the previous assumption, $\sigma_{Cb}^2 = \sum_{l=0}^{L_p-1} \sigma_b^2[l] = 1$. Similarly, the delay spread defined in (2.9) can be rewritten as,

$$\sigma_\tau = \sqrt{\frac{\sum_{l=0}^{L_p-1} (\tau_l - \bar{\tau})^2 \sigma_b^2[l]}{\sum_{l=0}^{L_p-1} \sigma_b^2[l]}} = \sqrt{\sum_{l=0}^{L_p-1} (\tau_l - \bar{\tau})^2 \sigma_b^2[l]}. \tag{2.36}$$

The relationship between the channel's maximum delay and the OFDM sampling interval is commonly utilized to define two channel categories: frequency-selective and frequency non-selective (or flat fading) channels.

A channel is said to exhibit frequency-selective fading if $\tau_{\max} > \Delta t$, or equivalently $B > B_c$, where B is the system's bandwidth. For current broadband OFDM systems with a sampling interval of a few tens of nanoseconds this is the most usual type of channel that the system has to deal with, with the received multipath replicas extending far beyond a single sampling interval. Frequency-selective fading distortion occurs whenever the signal's spectral components fall outside the coherence bandwidth (cf. Figure 2.3) and are unequally affected by the channel.

A channel is said to exhibit frequency non-selective or flat fading if $\tau_{\max} < \Delta t$, or equivalently $B < B_c$, in which case all received multipath replicas arrive within a single

sampling interval, thus representing a single resolvable path channel. Hence, all of the signal's spectral components will be similarly affected by the channel.

In parallel with the channel selectivity, the relationship between the channel's coherence time and the OFDM symbol duration is commonly used to define the channel as fast fading or slow fading.

A channel is said to be fast fading if $T_S > T_c$. Fast fading describes the situation where the time duration over which is expected that the channel is highly correlated is shorter compared to the OFDM symbol duration. It can be expected that the fading character of the channel will change significantly within the OFDM symbol duration, leading to distortion of the baseband signal shape.

A channel is said to be slow fading if $T_S < T_c$. Opposite to the previous situation, here, the channel is expected to be highly correlated for the duration of the OFDM symbol, causing little distortion in the baseband signal shape. For current broadband OFDM systems with a symbol duration in the order of microseconds, the channel is usually slow fading for the common range of MT speeds.

2.5. Summary

The transmission over multipath wireless channels poses great challenges in the design of the transmission systems, with its time dispersive and time varying nature. The discrete DFT-based multicarrier transmission systems have some key advantages that have grant them a huge commercial success in recent years. These key advantages can be summarized as,

- Multicarrier systems are robust against multipath propagation; if the channel delay spread keeps within the length of the CP, the orthogonality of the sub-carriers is maintained after transmission;
- Lower complexity equalization than that of a conventional single-carrier system[1]; under the proven assumptions that the ISI and ICI are negligible, the optimum equalizer is implemented with a element-wise multiplication of the sub-carriers;
- Simple architecture of the air interface with modulation/demodulation implementation based on efficient FFT operations;

[1] The complexity of the equalizer in the single-carrier systems can however be mitigated by performing this operation in the FD. Such an example can be found in the uplink of LTE systems, SC-FDMA.

- In low mobility scenarios, the system's capacity can be considerably enhanced by adapting the individual sub-carriers' data rate according to its instantaneous SNR, pushing to the channel's capacity limit;
- Simplicity of multiple access schemes, by dividing the available sub-carriers among the different users;
- Data rate flexibility; varying the number of the used sub-carriers and/or the number of bits carried by each sub-carriers, the user's data rate can be easily adapted.
- Simple support for asymmetric services, by using different number of sub-carriers in the downlink and in the uplink.

On the downside, the multicarrier systems have the following important disadvantages when compared with the single-carrier systems:

- High sensitivity to carrier frequency offset. Any residual frequency offset will cause significant ICI that will have a severely negative impact in the performance of the system. A careful design of the receiver's carrier frequency offset estimation and mitigation algorithms is required;
- High sensitivity to Doppler spreads; in the design of the system, the sub-carrier spacing should be chosen much larger than the maximum Doppler spread, $\Delta f \ll 2|f_D|$, to keep the ICI to a minimum;
- High sensitivity to phase noise; the multicarrier system requires high quality oscillators, with very restrict bounds on the generated phase noise;
- High peak-to-average power ratio (PAPR) that tends to increase with the number of sub-carriers; demands high excursion power amplifiers to reduce amplification distortion; this type of amplifier tends to be less efficient/more power consuming.

2.6. References

[802.11a] IEEE Std. 802.11a-1999, "Local and metropolitan area networks – Specific requirements – Part 11: Wireless MAC and PHY specifications – High-speed physical layer in the 5 GHz band," Sept. 1999.

[802.11g] IEEE Std. 802.11g-2003, "Local and metropolitan area networks – Specific requirements – Part 11: Wireless LAN medium access control (MAC) and physical layer (PHY) specifications – Amendment 4: Further higher data rate extension in the 2.4 GHz band," June 2003.

[802.16] IEEE Std. 802.16-2009, "Local and metropolitan area networks – Part 16: Air interface for broadband wireless access systems," May 2009.

[802.16d] IEEE Std. 802.16-2004, "Local and metropolitan area networks – Part 16: Air interface for fixed broadband wireless access systems," Oct. 2004.

[802.16e] IEEE Std. 802.16e-2005, "Local and metropolitan area networks – Part 16: Air interface for fixed and mobile broadband wireless access systems – Amendment 2: Physical and medium access control layers for combined fixed and mobile operation in licensed bands," Feb. 2006.

[Bee95] J.-J. van de Beek, O. Edfors, M. Sandell, S. Wilson, P. Borjesson, "On channel estimation in OFDM systems," in Proc. *IEEE Vehicular Technology Conference*, pp. 815 – 819, Chicago, USA, July 1995.

[Bel63] P. Bello, "Characterization of Randomly Time-Variant Linear Channels," *IEEE Transactions on Communication Systems*, vol. 11, no. 4, pp. 360–393, December 1963.

[Cha66] R. Chang, "Synthesis of band limited orthogonal signals for multichannel data transmission," *Bell System Technical Journal,* vol. 45, pp. 1775 – 1796, Dec. 1966.

[Cha68] R. Chang, R. Gibby, "Theoretical study of performance of an orthogonal multiplexing data transmission scheme," *IEEE Transactions on Communication Technology*, vol. 16, no. 4, pp. 529 – 540, Aug. 1968.

[Cha70] R. Chang, "Orthogonal frequency multiplex data transmission system," U.S. Patent no. 34884555, Jan. 1970.

[Cim85] L. Cimini, "Analysis and simulation of a digital mobile channel using orthogonal frequency division multiplexing," IEEE Transactions on Communications, vol. 33 no. 4, pp. 665 – 675, July 1985.

[Cla68] R. Clarke, "A Statistical Theory of Mobile Radio Reception," *Bell System Technical Journal*, vol. 47, no. 6, pp. 957 – 1000, July 1968.

[DABa] ETSI Std. ETS 300 401 ed.2, "Radio broadcasting systems; Digital audio broadcasting (DAB) to mobile, portable and fixed receivers," May 1997.

[DABb] ETSI Std. ETS 300 401 v1.4.1, "Radio broadcasting systems; Digital audio broadcasting (DAB) to mobile, portable and fixed receivers," June 2006.

[DVB-Ta] ETSI Std. ETS 300 744 ed.1, "Digital video broadcasting (DVB); Framing structure, channel coding and modulation for digital terrestrial television," March 1997.

[DVB-Tb] ETSI Std. ETS 300 744 v1.6.1, "Digital video broadcasting (DVB); Framing structure, channel coding and modulation for digital terrestrial television," Jan. 2009.

[Hir81] B. Hirosaki, "An orthogonally multiplexed QAM system using the discrete Fourier transform," *IEEE Transactions on Communications*, vol. 29, pp. 982 – 989, July 1981.

[Jak74] W. Jakes, *Microwave Mobile Communications*, New York, USA, Wiley, 1974.

[Lee89] W. Lee, *Mobile Cellular Communications*, New York, USA, McGraw-Hill, 1989.

[Li98] Y. Li, L. J. Cimini, N. R. Sollenberger, "Robust channel estimation for OFDM systems with rapid dispersive fading," *IEEE Transactions on Communications*, vol. 46, pp. 902 – 915, July 1998.

[LTE] ETSI Technical Specification TS 136 201 v8.3.0, "LTE; Evolved universal terrestrial radio access (E-UTRA); Long Term Evolution (LTE) physical layer; General description," April 2009.

[LTEadv] ETSI Technical Report 136 913 V8.0.1, "LTE; Requirements for further advancements for Evolved Universal Terrestrial Radio Access (E-UTRA) (LTE-Advanced)," April 2009.

[Med98] J. Medbo, J.-E. Berg, "Measured Radiowave Propagation Characteristics at 5GHz for typical HIPERLAN/2 Scenarios," ETSI BRAN doc. 3ERI074b, Jan. 1998.

[Med98a] J. Medbo, "Radio Wave Propagation Characteristics at 5 GHz with Modelling Suggestions for HIPERLAN/2," ETSI BRAN doc. 3ERI074a, Jan. 1998.

[Mos58] R. Mosier, R. Clabaugh, "Kineplex, a bandwidth efficient binary transmission system," *AIEE Transactions*, vol. 76, pp. 723 – 728, Jan. 1958.

[Par82] J. Parsons, A. Bajwa, "Wideband characterisation of fading mobile radio channels," *IEEE Proceedings*, vol. 129, no. 2, pp. 95 – 10, April 1982.

[Par92] D. Parsons, *The Mobile Radio Propagation Channel*, New York, USA, Wiley, 1992.

[Pat02] M. Patzold, *Mobile Fading Channels*, Chichester, West Sussex, England, Wiley, 2002.

[Pel80] A. Peled, A. Ruiz, "Frequency domain data transmission using reduced computational complexity algorithms," in Proc. *International Conference on Acoustics, Speech, and Signal Processing*, pp. 964 – 967, Denver, USA, Apr. 1980.

[Por68] G. Porter, "Error distribution and diversity performance of a frequency differential PSK HF modem," *IEEE Transactions on Communications*, vol. 16, pp. 567 – 575, Aug. 1968.

[Pra04] R. Prasad, *OFDM for Wireless Communications Systems*, Artech House, Boston, USA, 2004.

[Pro01] J. Proakis, *Digital Communications*, New York, USA, McGraw-Hill, 2001.

[Rap96] T. Rappaport, *Wireless Communications: Principles and Practice*, Upper Saddle River, New Jersey, USA, Prentice Hall, 1996.

[Sal67] B. Saltzberg, "Performance of an efficient parallel data transmission system," *IEEE Transactions on Communication Technology*, vol. 15, no. 6, pp. 805 – 811, Dec. 1967.

[Ska97] B. Sklar, "Rayleigh Fading Channels in Mobile Digital Communication Systems, Part I: Characterization," *IEEE Communications Magazine*, vol. 35, no. 7, pp. 90 – 100, July 1997.

[Ste87] S. Stein, "Fading channel issues in system engineering," *IEEE Journal on Selected Areas in Communications*, vol. 5, no. 2, pp. 68 – 89, Feb. 1987.

[Ste94] R. Steele, *Mobile Radio Communication*s, Chichester, West Sussex, England, Wiley, 1996.

[Stu96] G. Stüber, *Principles of Mobile Communications*, Boston, USA, Kluwer Academic Publishers, 1996.

[Wei71] S. Weinstein, P. Ebert, "Data Transmission by Frequency Division Multiplexing Using the Discrete Fourier Transform," *IEEE Transactions on Communication Technology* , Vol. 19, no. 5, pp. 628 – 634, Oct. 1971.

[Zim67] M. Zimmerman, A. Kirsch, "The AN/GSC-10 (KATHRYN) variable rate data modem for HF radio," *IEEE Transactions on Communications*, vol. 15, pp. 197 – 205, April 1967.

[Zou95] W. Zou, Y. Wu, "COFDM: an overview," *IEEE Transactions on Broadcasting*, vol. 41, no. 1, pp. 1 – 8, March 1995.

CHAPTER 3

ON THE IMPACT OF PILOT DENSITY IN THE CHANNEL ESTIMATION OF OFDM SYSTEMS

In this chapter we investigate the impact of the pilot density (and associated pilot distances for both frequency and time domains) in the performance of the channel estimation for OFDM systems, when using dedicated sub-carriers to transmit pilots with 2-D rectangular patterns.

The analytical formulation of the channel estimation MSE for the single-user downlink scenario with a generic channel estimation scheme for a given power efficiency is presented.

The attained results go beyond the commonly accepted rule of thumb that suggests that an oversampling factor of two will result in a good trade-off between performance and pilot overhead.

The analytical formulation was validated by system simulations. A scenario using the 2-D LS-DFT channel estimation scheme confirmed the analytical result. The lowest channel estimation MSE for a given value of power efficiency is achieved when the pilot density is the one that closely fulfils the 2-D sampling theorem.

3.1. Introduction to the OFDM Channel Estimation

Channel estimation has always been present in wireless communications systems to help the receiver mitigate the effects of the wireless multipath channel. In single carrier wireless communication systems, the channel estimator estimates the coefficients of the time-varying FIR filter that models the TD multipath channel [Ars01]. Though most of single carrier's channel estimation techniques can be adapted to multicarrier systems, its unique characteristics gave rise to the development of new channel estimation algorithms.

In multicarrier systems, the acquisition of accurate channel state information (CSI) is crucial to achieve high spectral efficiency, with emphasis on demodulation/decoding and resource allocation operations. For coherent detection, the frequency response of the channel at the individual sub-carriers' frequencies needs to be estimated to be used in the decoding process. The multipath wireless channel is commonly modelled in TD by a time-varying FIR filter with unknown coefficients. Because the CFR is required for decoding in FD, unlike the single carrier systems, the majority of the channel estimation algorithms try to get a CFR estimate and not a CIR estimate (or the respective estimate of the FIR filter coefficients) that would have to be transformed to FD.

The techniques to perform the channel estimation fall mainly in two major groups: blind and pilot-aided techniques.

The blind channel estimation algorithms use the statistical properties of the received signals to generate a channel estimate, with no knowledge of the transmitted data. To be accurate, this group of techniques needs to gather a large amount of information [Son00], [Wu03] that leads to poor performance in mobile systems where the channel varies rapidly under the influence of Doppler's effect and multipath propagation [Han03].

To overcome the limitations of blind estimation techniques in mobile environments, pilot-aided channel estimation techniques are commonly preferred. When using these techniques, the transmitter inserts determinist data in the transmitted symbols that will be used by the receiver to estimate the channel. Because this known information carries no user data, it represents an overhead that lowers the system's power efficiency.

If the determinist data makes up a complete OFDM symbol it is referred to as training symbol. Current systems employing training symbols usually place it at the beginning of a burst so that the receiver can get an initial estimate of the CFR that will be used in decoding process of the remaining symbols [Tan02], [Sun02]. This arrangement is adequate for small burst-type transmission and low mobility scenarios, where the CFR is considered constant throughout the burst. If continuous transmission or high mobility scenarios is to be

considered, the training symbol must be repeated regularly to deal with the mobility-induced channel variability.

A more elegant way of reducing the loss of power efficiency and dealing with high mobility scenarios is to multiplex the known information along with user data in the same OFDM symbol and repeat the transmission of these multiplexed symbols regularly. Though several multiplexing techniques were investigated, the use of a set of dedicated sub-carriers to convey the determinist data stood out as the most promising technique. In this arrangement, the known information is referred to as pilots or pilot symbols. The pilots are arranged in one-dimensional (1-D) or two-dimensional (2-D) patterns that are used by a number of algorithms [Hoe97], [Kai97], [Li00] to get the channel estimates. These techniques make up the group of pilot-aided channel estimators.

Many issues arise from the use of pilots to perform the channel estimation and have received a considerable attention in the past decade.

The allocation of power between the pilots and data symbols was addressed in several works. Though usually the power is evenly distributed among pilots and data symbols, in [Dow02] it was shown that the performance of the channel estimator can be improved by boosting the pilots' power (compared to that of the data symbols). The studies presented in [Bar02] and [Bar03] show that, for a given total pilot power, the lowest MSE of the least square (LS) estimator is achieved when the pilots' power at the different sub-carriers is evenly distributed.

The problem of finding the optimum pilot locations in the time-frequency pilot grid for a given number of pilots was investigated in different papers. In [Sun02a] and [Bar03] this problem is addressed by minimising the MSE of the LS estimates. The optimality is a balance of the system's power efficiency, the performance of the channel estimator and the characteristics of the estimated channel (delay spread and Doppler spread) [Cav91]. An optimum solution for a given channel may give a power performance for another channel with longer delay spread that will be undersampled.

If the system has information of the current multipath channel affecting the transmission, it can take advantage of this knowledge to dynamically adapt the used pilot structure. Investigation on this topic can be found in [Wan01], [Dow02], [Hou02] and [Dow03]. In such systems, the pilot allocation in the frequency domain depends on the estimate of the channel delay spread, while the distance between pilot-carrying symbols is a function of the maximum Doppler shift. Using the right amount of pilots improves the system's power efficiency while maintaining the performance of the channel estimator. For non-adaptive systems, the design of the pilot structure is usually based on the worst-case

scenario, where the time-frequency pilot grid is defined based on the expected maximum channel delay and Doppler shift.

The issue of the selection of the set of sub-carriers to use in different pilot-carrying symbols to most efficiently track the channel's variations in both time and frequency domains was also widely addressed [Tuf97], [Bad99], [Gar99], [Gar00], [Jeo01], [Bar03], [Dow03] and [Cho05]. This selection defines the pilot pattern and it will have impact in the performance of the channel estimator. One of the most widely adopted pilot arrangements is the rectangular pilot pattern, where the pilots are always transmitted in the same sub-carriers. The simulation results in [Tuf97] indicate that denser pilot patterns, using different sub-carriers at the band edges and in different symbols is expected to yield better performance of the channel estimator for time-varying multipath channels. The results in [Bar03] and [Dow03] indicate that a lower MSE is attained by the LS estimator over several OFDM symbols when the pilots are cyclically shifted from one pilot-carrying OFDM symbols to the next. Both simulation and analysis have proven that the hexagonal pilot pattern yields the best performance among all possible 2-D patterns [Bad99], [Gar99], [Gar00], [Jeo01] and [Cho05].

The adoption of a 2-D pilot pattern imposes the need to estimate the channel for the data-carrying sub-carriers. Different interpolation techniques were proposed that either started by performing the frequency domain interpolation, estimating all the pilot-carrying symbols, prior to performing the symbol domain interpolation to estimate the remaining ones, did the interpolation operations in the reverse order, or even simultaneously. Further details of the different investigated interpolation techniques will be given in the next chapter.

Another issue that affects the performance of the channel estimator is the lack of pilot sub-carriers at both edges of the transmission band. The estimation of the edge sub-carriers must be obtained via extrapolation [Bou01], [Shi04]. Studies reveal that the estimation MSE is higher for edge sub-carriers than for those in the middle of the band, whose estimate is obtained via interpolation [Tuf97], [Mor01], [Jia03]. In [Mor01] a solution for this problem was proposed. Increasing the number of pilot sub-carriers in the band edges reduces the extrapolation error. This solution leads to a decrease in the system's power efficiency. A similar improvement was reported in [Jia03] that exploited the periodicity of the Fourier transform without decreasing the system's power efficiency. Using the fact that the sub-carriers in the lower and upper edges are highly correlated, the channel estimator can use this knowledge to improve the estimate of the sub-carriers at both edges.

The insertion of pilots should also contribute to the simplicity of the estimation algorithms and the overall complexity reduction of the used equipments. In [Li00a] and [Li02], the use of constant modulus pilots was shown to lead to a significant complexity reducing of the estimation algorithms, by simplifying the required matrix operations.

In the remaining of the chapter, the analytical study of the influence of the pilot distances (frequency and time) and associated density on the performance of a generic channel estimator is addressed. The study goes beyond the rule of thumb in [Kai97] that suggested that an oversampling factor of two would result in a good trade-off between performance and pilot overhead, introducing an analytical expression that relates the MSE of a generic channel estimator and the system's power efficiency.

The analytical expression is derived using the previously introduced assumptions of equipowered and equidistant pilots [Neg98], [Bar03], and using the common rectangular pilot pattern adopted in several standards.

The accuracy of the analytical expression was compared against simulation results using a 2-D LS – discrete Fourier transform (LS-DFT) channel estimation scheme and BRAN-A broadband wireless channel model [BRAN].

The remaining of the chapter is organized as follows. Next section introduces the pilot-aided channel estimation scheme that will be used in the section 3.3, where the analytic expression of channel estimation MSE is introduced. In section 3.4, the MSE analytical expression is compared against system simulation results. Some concluding remarks are presented in the following section.

3.2. Pilot-Aided Channel Estimation

To explore the time and frequency diversity, the OFDM symbols are organized in frames. An example of an OFDM frame is depicted in Figure 3.1.

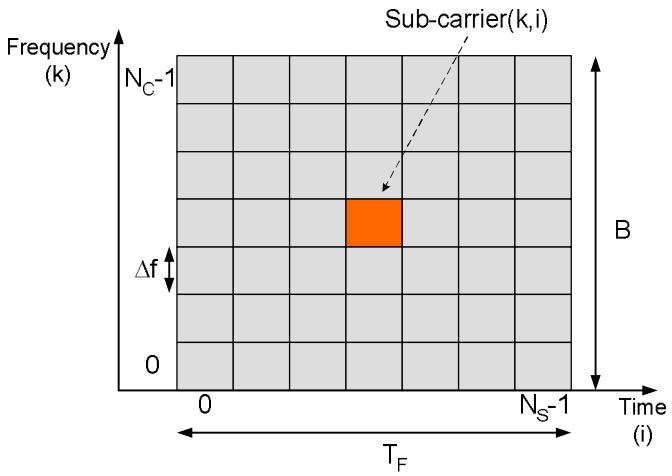

Figure 3.1. OFDM frame structure.

The frame is made-up of N_S consecutives symbols with duration

$$T_F = T_S N_S . \tag{3.1}$$

The diversity is explored by the channel coder that interleaves the coded data in uncorrelated symbols (time diversity) and sub-carriers (frequency diversity) within the frame. The maximum diversity gain is defined as the product of the time diversity and frequency diversity [Kai98],

$$G_{Div} = \frac{T_F}{T_c}\frac{B}{B_c}. \tag{3.2}$$

To help the receiver estimate the CFR, in pilot-aided channel estimation schemes some of the sub-carriers in the OFDM frame are dedicated to convey pilots.

Considering the results in [Neg98] and [Bar03], when LS estimation is to be used, the minimum MSE is obtained when the pilots in the frequency domain are equispaced and equipowered. This is justified by the fact that when the pilots are inserted in adjacent sub-carriers, the DFT matrix used in the LS estimation approaches to an ill conditioned matrix and the performance of the channel estimation is vulnerable to noise [Neg98].

The use of 2-D pilot patterns has been shown to outperform 1-D pilot patterns [Hoe97]. Figure 3.2 depicts an example of a rectangular pilot structure. The pilot separation in the frequency domain in noted as N_f and in the time domain as N_i. Other structures that can be found in the literature are diagonal, random and diamond patterns [Kai97], [Bad99], [Gar99], [Gar00], [Bad05].

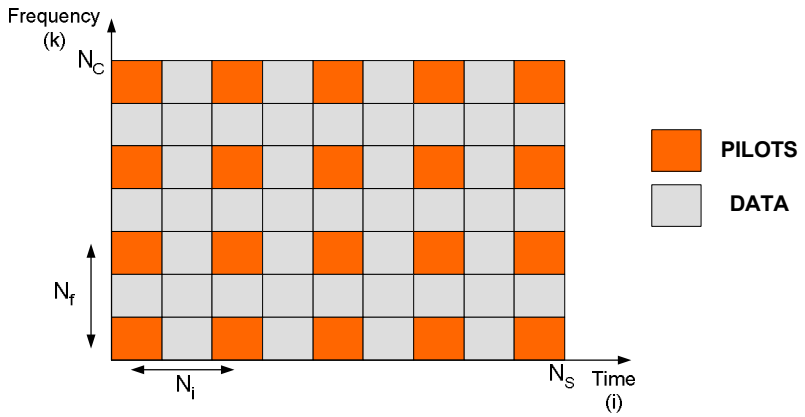

Figure 3.2. Example of rectangular pilot structure.

The 2-D rectangular pilot pattern, like any regular 2-D pattern [Dud84], [Mer83], can be represented by a non-singular matrix **V** formed by 2 basis vectors $\mathbf{v}_k = \begin{bmatrix} N_f & 0 \end{bmatrix}^T$ and $\mathbf{v}_i = \begin{bmatrix} 0 & N_i \end{bmatrix}^T$,

$$\mathbf{V} = \begin{bmatrix} \mathbf{v}_k & \mathbf{v}_i \end{bmatrix} = \begin{bmatrix} N_f & 0 \\ 0 & N_i \end{bmatrix}, \tag{3.3}$$

such that the set of the pattern points is defined by,

$$\left\{ \mathbf{a} = \begin{bmatrix} k, i \end{bmatrix}^T : \mathbf{a} = \mathbf{V}\mathbf{m}, \forall \mathbf{m} \in \mathbb{Z}^2 \right\}, \tag{3.4}$$

and the pilot pattern density D_p is $D_p = \left|\det(\mathbf{V})\right|^{-1} = \left(N_i N_f\right)^{-1}$. The basis vectors for the rectangular pilot pattern are depicted in Figure 3.3.

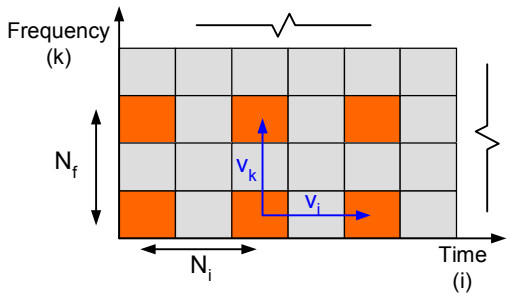

Figure 3.3. Basis vectors for rectangular pilot pattern.

The inclusion of the channel estimation scheme forces some changes in the OFDM baseband transmitter and receiver models introduced in the previous chapter. The new models are presented in Figure 3.4 and Figure 3.5. The changes from the previous model are highlighted. In the transmitter, a framing block is introduced that multiplexes pilots and data according to the used estimation scheme. In the receiver, a de-framing block separates the values received in the pilot and data sub-carriers. The values in received in the data sub-carriers are fed to the equalizer, while the remaining ones are passed to the channel estimation block. This block generates the CFR estimate for the entire frame that will be used by the equalizer to perform the coherent demodulation.

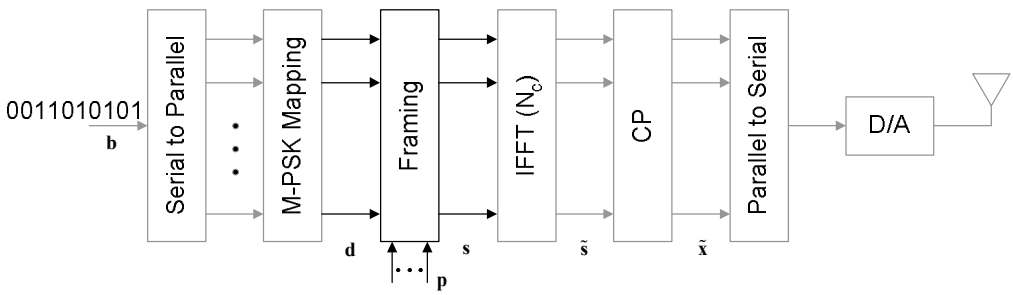

Figure 3.4. Pilot-aided OFDM baseband transmitter model.

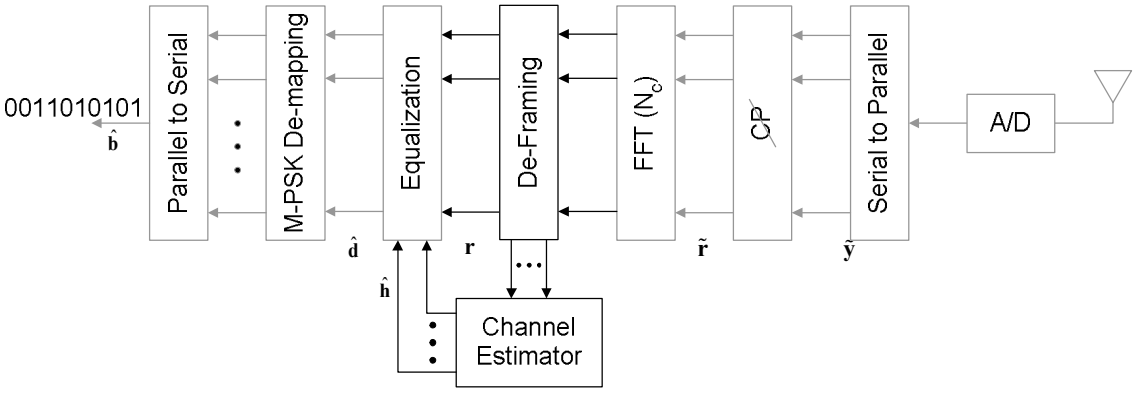

Figure 3.5. Pilot-aided OFDM baseband receiver model.

As stated in the previous chapter, we assume that the CIR remains constant for the duration of the symbol and that the insertion of a long enough CP in the transmitter assures that the orthogonality of the sub-carriers in maintained after transmission.

Suppose that the receiver is perfectly synchronized and is disturbed by independent and identically distributed (*iid*) zero mean AWGN samples with a variance σ_n^2.

3.3. Channel Estimation MSE Analytical Formulation

The receiver's channel estimator treats the channel's response for each sub-carrier as independent and starts by obtaining the LS estimates $\hat{\mathbf{H}}_{LS}$ of the channel for the set of pilot positions with-in the frame, $\wp$,

$$\hat{H}_{LS}[k,i] = H[k,i] + \frac{N[k,i]}{S[k,i]}, \forall (k,i) \in \wp, \tag{3.5}$$

where $\mathbf{H}$, $\mathbf{N}$ and $\mathbf{S}$ are $N_C \times N_S$ matrices that contain, respectively, the CFR, the noise samples and the transmitted symbols and after uses a 2-D DFT interpolator to obtain the estimates in the remaining frame positions.

Interpreting the LS estimates as noisy samples of the CFR, for the interpolator filter to be able to recover the CFR without aliasing, the pilot distances N_f and N_i need to be carefully selected. The pilot distance to be used in the frequency domain depends on the minimum coherence bandwidth of the channel, which, as introduced on the previous chapter, is related to the channel's delay spread and associated maximum propagation delay $\tau_{\max}$. To fulfil the Nyquist sampling theorem [Hoe97], [Moo00], the pilot distance N_f needs to be

small enough so that variations of the channel's response can be captured and the CFR perfectly reconstructed by the interpolator filter,

$$N_f \leq \left(\tau_{\max}\Delta f\right)^{-1}. \tag{3.6}$$

When the condition in (3.6) is not met, the channel information gathered in the pilot sub-carriers is insufficient and an irreducible error floor in the channel estimate, because the channel is undersampled and aliasing occurs [Ars03].

For mobility scenarios, where the channel varies from symbol to symbol, the pilot distance in time-domain N_i must be selected so that it allows the channel estimator to track the channel's variations. This distance depends on the channel's minimum coherence time, which is related to the maximum Doppler frequency f_D introduced in the previous chapter. The pilot distance N_i must fulfil the condition,

$$N_i \leq \left(2 f_D T_S\right)^{-1}, \tag{3.7}$$

so that the time variability is sufficiently sampled and aliasing thus not occur in the time domain.

In the absence of noise, the discrete CFR can be reconstructed using an ideal 2-D *sinc* filter, $W_P[k,i]$,

$$W_p[k,i] = sinc\left(\frac{1}{N_f}k\right) sinc\left(\frac{1}{N_i}i\right), \tag{3.8}$$

that oversamples the LS estimates by a factor N_f in the frequency domain and N_i in the time domain,

$$H[k,i] = \sum_{m=-\infty}^{+\infty}\sum_{l=-\infty}^{+\infty} H_S[k+m, i+l] W_P[m,l], \tag{3.9}$$

where,

$$H_S[k,i] = \begin{cases} H[k,i], \{k,i\} \in \wp \\ 0, \textit{remaining} \end{cases}. \tag{3.10}$$

The frequency response of the ideal 2-D *sinc* filter is depicted in Figure 3.6, where the filter's cut-off frequencies for both axis and gain are shown.

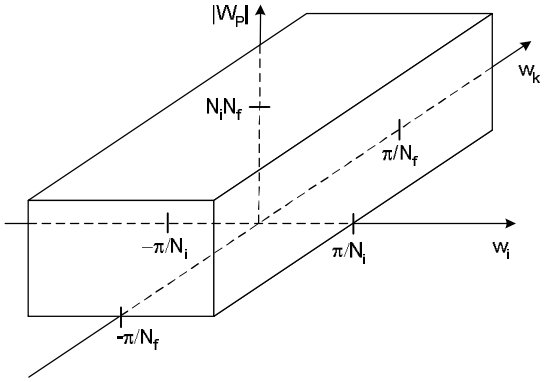

Figure 3.6. Ideal 2-D *sinc* filter.

The real LS estimates are noisy samples of the channel, that are used as the input to the 2-D estimation filter $W[k,i]$, to obtain the channel estimate $\hat{H}[k,i]$,

$$\hat{H}[k,i] = \sum_{m=-\infty}^{+\infty} \sum_{l=-\infty}^{+\infty} \hat{H}'_{LS}[k+m, i+l] W[m,l], \tag{3.11}$$

where,

$$\hat{H}'_{LS}[k,i] = \begin{cases} \hat{H}_{LS}[k,i], \{k,i\} \in \wp \\ 0, \textit{remaining} \end{cases}. \tag{3.12}$$

Splitting $\hat{\mathbf{H}}'_{LS}$ in $\hat{\mathbf{H}}'_{LS} = \mathbf{H}_S + \mathbf{N}_S$, where the elements of the matrix containing the noise samples $\mathbf{N}_S$ are defined by,

$$N_S[k,i] = \begin{cases} \dfrac{N[k,i]}{S[k,i]}, \{k,i\} \in \wp \\ 0, \textit{remaining} \end{cases}, \tag{3.13}$$

the channel estimation can be rewritten as,

$$\begin{aligned} \hat{H}[k,i] &= H[k,i] + \sum_{m=-\infty}^{+\infty} \sum_{l=-\infty}^{+\infty} \left(H_S[k+m, i+l] + N_S[k+m, i+l] \right) W[m,l] \\ &\quad - \sum_{m=-\infty}^{+\infty} \sum_{l=-\infty}^{+\infty} H_S[k+m, i+l] W_P[m,l] \\ &= H[k,i] + \sum_{m=-\infty}^{+\infty} \sum_{l=-\infty}^{+\infty} H_S[k+m, i+l] \left(W[m,l] - W_P[m,l] \right) \\ &\quad + \sum_{m=-\infty}^{+\infty} \sum_{l=-\infty}^{+\infty} N_S[k+m, i+l] W[m,l] \end{aligned}, \tag{3.14}$$

which can be interpreted as if the channel estimation is the summation of the real channel $H[k,i]$ with two terms that negatively affect the estimate. The first term is due to the imperfect estimation filter,

$$\sum_{m=-\infty}^{+\infty}\sum_{l=-\infty}^{+\infty} H_S[k+m,i+l]\left(W[m,l]-W_P[m,l]\right), \tag{3.15}$$

and the second is due to the presence of noise,

$$\sum_{m=-\infty}^{+\infty}\sum_{l=-\infty}^{+\infty} N_S[k+m,i+l]W[m,l]. \tag{3.16}$$

Defining the error filter $W_e[k,i]=W[k,i]-W_P[k,i]$, the estimation error of the k-th sub-carrier of the i-th symbol can be written as,

$$\begin{aligned} E[k,i] &= \hat{H}[k,i]-H[k,i] \\ &= \sum_{m=-\infty}^{+\infty}\sum_{l=-\infty}^{+\infty} H_S[k+m,i+l]W_e[m,l]+\sum_{m=-\infty}^{+\infty}\sum_{l=-\infty}^{+\infty} N_S[k+m,i+l]W[m,l]. \\ &= H_S[k,i]*W_e[k,i]+N_S[k,i]*W[k,i] \end{aligned} \tag{3.17}$$

Applying 2-D discrete-time Fourier transform (DTFT) to (3.17), it can be equivalently written as,

$$E(w_k,w_i)=H_S(w_k,w_i)W_e(w_k,w_i)+N_S(w_k,w_i)W(w_k,w_i). \tag{3.18}$$

Using the 2-D discrete Parseval's theorem [Mer83], the channel estimation MSE can be written as,

$$\sigma_e^{\,2}=\frac{1}{4\pi^2}\int_{-\pi}^{\pi}\int_{-\pi}^{\pi} E\left\{\left|E(w_k,w_i)\right|^2\right\}dw_k dw_i. \tag{3.19}$$

Considering that the noise $N_S(w_k,w_i)$ and the channel's response $H_S(w_k,w_i)$ are independent and recalling that $\mathbf{N}_S$ is made-up of AWGN samples,

$$\begin{aligned} E\left\{\left|E(w_k,w_i)\right|^2\right\} &= S_{H_S}(w_k,w_i)\left|W_e(w_k,w_i)\right|^2+E\left\{\left|N_S(w_k,w_i)\right|^2\right\}\left|W(w_k,w_i)\right|^2 \\ &= S_{H_S}(w_k,w_i)\left|W_e(w_k,w_i)\right|^2+\sigma_{N_S}^2\left|W(w_k,w_i)\right|^2 \end{aligned}, \tag{3.20}$$

where $S_{H_S}(w_k, w_i) = E\left\{\left|H_S(w_k, w_i)\right|^2\right\}$. Recalling that $N_S[k,i]$ is a sampled version of $N[k,i]$ with a density D_P and considering that the pilots are transmitted with unit energy, $\sigma^2_{N_S} = \sigma^2_n D_P$. The channel estimation MSE can be rewritten as,

$$\sigma_e^2 = \frac{1}{4\pi^2}\int_{-\pi}^{\pi}\int_{-\pi}^{\pi} S_{H_S}(w_k, w_i)\left|W_e(w_k, w_i)\right|^2 dw_k dw_i + \frac{\sigma_n^2 D_P}{4\pi^2}\int_{-\pi}^{\pi}\int_{-\pi}^{\pi}\left|W(w_k, w_i)\right|^2 dw_k dw_i. \quad (3.21)$$

The sampled channel's PSD $S_{H_S}(w_k, w_i)$ is a replicated and scaled version of the original channel's PSD $S_H(w_k, w_i)$ [Dud84],

$$S_{H_S}(w_k, w_i) = \frac{1}{(N_i N_f)^2}\sum_{i=0}^{N_i-1}\sum_{k=0}^{N_f-1} S_H\left(w_k - \frac{2\pi}{N_f}k, w_i - \frac{2\pi}{N_i}i\right). \quad (3.22)$$

Figure 3.7 presents the relationship between $S_{H_S}(w_k, w_i)$ and $S_H(w_k, w_i)$, assuming that the channel's PSD is limited in both frequency axes and that the pilot distances N_f and N_i are small enough to fulfil the 2-D sampling theorem, according to (3.6) and (3.7). The left figure represents the original channel's PSD and the right one the sampled version. The position of the replicas is defined by [Dud84],

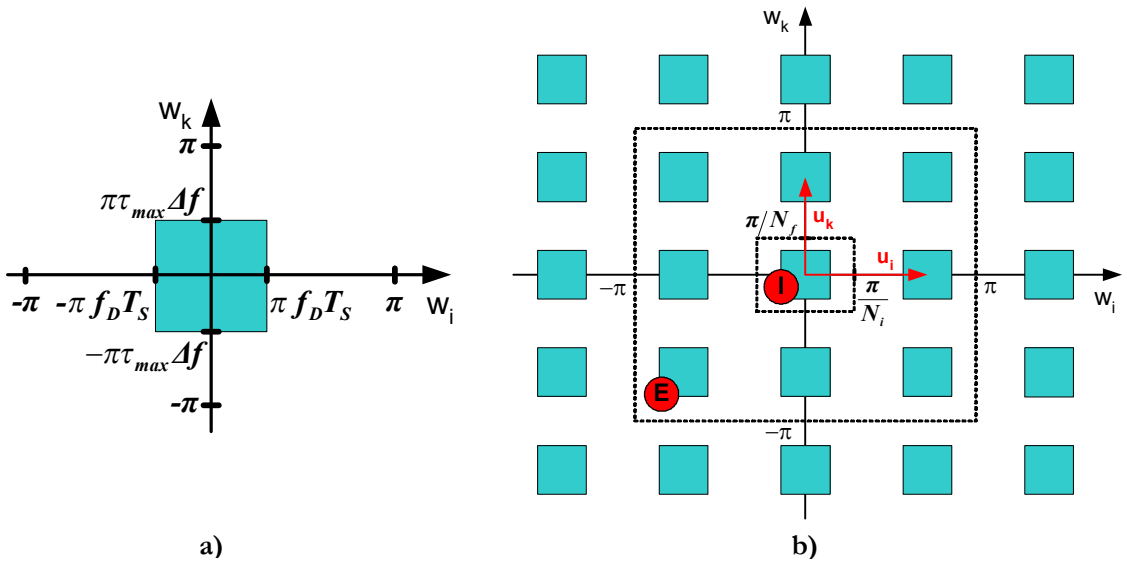

Figure 3.7. Relationship between the channel's PSDs; a) original; b) sampled.

$$\mathbf{U} = \begin{bmatrix} \mathbf{u}_k & \mathbf{u}_i \end{bmatrix} = \begin{bmatrix} 2\pi/N_f & 0 \\ 0 & 2\pi/N_i \end{bmatrix}. \tag{3.23}$$

Keeping in mind that the 2-D *sinc* filter is only non-zero in the area I (marked in Figure 3.7), the 2-D DTFT of the error filter is given by,

$$W_e(w_k, w_i) = \begin{cases} W(w_k, w_i) - N_i N_f, & |w_i| \le \pi/N_i \wedge |w_k| \le \pi/N_f \\ W(w_k, w_i), & \textit{remaining} \end{cases}. \tag{3.24}$$

Considering that the interpolator filters most of the energy of the channel replicas inside the area E (marked in Figure 3.7),

$$\begin{cases} \pi/N_i < |w_i| < \pi \\ \pi/N_f < |w_n| < \pi \end{cases}, \tag{3.25}$$

the error introduced by the first term of (3.21) in this area is negligible and the channel estimation MSE can be rewritten,

$$\sigma_e^2 \approx \frac{1}{4\pi^2} \iint_I S_{H_S}(w_k, w_i) \left| W(w_k, w_i) - N_i N_f \right|^2 dw_k dw_i + \frac{\sigma_n^2 D_P}{4\pi^2} \int_{-\pi}^{\pi} \int_{-\pi}^{\pi} \left| W(w_k, w_i) \right|^2 dw_k dw_i . \tag{3.26}$$

In the area I,

$$\begin{cases} |w_i| \le \pi/N_i \\ |w_n| \le \pi/N_f \end{cases}, \tag{3.27}$$

the sampled channel's PSD is just a scaled version of the original channel's PSD,

$$S_{H_S}(w_k, w_i) = \frac{1}{(N_i N_f)^2} S_H(w_k, w_i) = D_P^2 S_H(w_k, w_i). \tag{3.28}$$

Using (3.28) in (3.26),

$$\begin{aligned}\sigma_e^2 &\approx \frac{D_P^2}{4\pi^2}\iint_I S_H(w_k,w_i)\left|W(w_k,w_i)-(N_iN_f)\right|^2 dw_k dw_i + \frac{\sigma_n^2 D_P}{4\pi^2}\int_{-\pi}^{\pi}\int_{-\pi}^{\pi}\left|W(w_k,w_i)\right|^2 dw_k dw_i \\ &\approx \frac{D_P^2}{4\pi^2}\iint_I S_H(w_k,w_i)\left|W(w_k,w_i)\right|^2 dw_k dw_i - \frac{2D_P}{4\pi^2}\iint_I S_H(w_k,w_i)\,\mathrm{Re}\left\{W(w_k,w_i)\right\} dw_k dw_i \\ &+ \frac{D_P}{4\pi^2}\iint_I S_H(w_k,w_i)\,dw_k dw_i + \frac{\sigma_n^2 D_P}{4\pi^2}\int_{-\pi}^{\pi}\int_{-\pi}^{\pi}\left|W(w_k,w_i)\right|^2 dw_k dw_i \\ &\approx AD^2 + \left(\sigma_n^2 E_F - B\right)D + E_C\end{aligned} \quad ,(3.29)$$

where,

$$\begin{aligned}A &= \frac{1}{4\pi^2}\iint_I S_H(w_k,w_i)\left|W(w_k,w_i)\right|^2 dw_k dw_i \\ B &= \frac{2}{4\pi^2}\iint_I S_H(w_k,w_i)\,\mathrm{Re}\left\{W(w_k,w_i)\right\} dw_k dw_i \\ E_C &= \frac{1}{4\pi^2}\iint_I S_H(w_k,w_i)\,dw_k dw_i \\ E_F &= \frac{1}{4\pi^2}\int_{-\pi}^{\pi}\int_{-\pi}^{\pi}\left|W(w_k,w_i)\right|^2 dw_k dw_i\end{aligned} \quad . \tag{3.30}$$

The OFDM system's energy per bit E_b is given by,

$$E_b = \frac{\overline{S}_{symbol} T_S}{b_{data}}, \tag{3.31}$$

where $\overline{S}_{symbol}$ is the average OFDM symbol power and b_{data} is the number of data bits sent per symbol. Due to the presence of pilot sub-carriers in the frame, the average number of data bits per symbol depends on the pilot density D_P,

$$b_{data} = N_C \log_2(m)(1-D_P), \tag{3.32}$$

where m is the size of the constellation. Replacing in (3.31),

$$E_b = \frac{\overline{S}_{symbol} T_S}{\log_2(m)(1-D_P)N_C}. \tag{3.33}$$

The one-sided noise PSD N_O is given by,

$$N_O = \frac{\sigma_n^2}{N_C \Delta f} = \frac{\sigma_n^2 t_S}{N_C}, \tag{3.34}$$

where t_S is the OFDM symbol duration (without CP). The system's power efficiency E_b/N_O is defined by,

$$E_b/N_O = \frac{\overline{S}_{symbol}}{\sigma_n^2}\frac{T_S}{t_S}\frac{1}{\log_2(m)(1-D)}. \tag{3.35}$$

Expressing the noise power as a function of the power efficiency,

$$\sigma_n^2 = \left(E_b/N_o\right)^{-1}\overline{S}_{symbol}\frac{T_S}{t_S}\frac{1}{\log_2(m)(1-D_P)}, \tag{3.36}$$

the channel estimation MSE can be directly expressed as a function of E_b/N_O, by replacing in (3.29),

$$\sigma_e^2 \approx AD^2 + \left(\frac{\left(E_b/N_O\right)^{-1}\overline{S}_{symbol}}{\log_2(m)(1-D_P)}\frac{T_S}{t_S}E_F - B\right)D + E_C. \tag{3.37}$$

Equation (3.37) shows that the channel estimation MSE is dependent of the CFR, the noise present in the process and the frequency response of the estimation scheme used.

3.3.1 2-D LS-DFT channel estimator

The 2-D LS-DFT channel estimation scheme uses the 2-D *sinc* filter expressed in (3.8) to perform the interpolation that will return the estimates of the channel for the frame positions where data sub-carriers were transmitted. In this scenario, $\mathbf{W} = \mathbf{W}_P$, the error filter $\mathbf{W}_e = 0$ and (3.18) is reduced to

$$E(w_k, w_i) = N_S(w_k, w_i)W(w_k, w_i), \tag{3.38}$$

as the interpolator does not cause any distortion. Examining (3.26) it is straightforward that the channel estimation MSE with this scheme is $\sigma_e^2 = \sigma_n^2$, or expressed in terms of power efficiency by rewriting (3.37),

$$\sigma_e^2 = \left(E_b/N_O\right)^{-1}\overline{S}_{symbol}\frac{T_S}{t_S}\frac{1}{\log_2(m)(1-D_P)}. \tag{3.39}$$

A closer examination of (3.39) puts in evidence that, for a given value of power efficiency, the lowest MSE achieved with this channel estimation scheme is for the lowest

value of pilot density D_P (with associated pilot distances N_f and N_i) that closely fulfil the 2-D sampling theorem.

3.4. Simulation Results

A simulation scenario was implemented where $N_C = 1024$ sub-carriers were QPSK modulated. The system has a carrier frequency $f_c = 5GHz$ and a sampling interval $\Delta t = 10ns$. The transmission of symbols was carried out over BRAN-A model channels [BRAN]. The surfaces presented in Figure 3.8 to Figure 3.13 summarize the attained results. The red surfaces represent the simulation results while the analytical values are represented by the blue ones. The green dot points out the best density D_P (and respective pair (N_i, N_f)). The simulations were performed for MT speeds of 10km/h and 200km/h. The power efficiency, E_b/N_O, was set to the values 0dB, 10dB, 20dB and 30dB.

Observing the surfaces, we can conclude that in the area of interest, where the 2-D sampling theorem is fulfilled (there is no aliasing and the channel estimator performs the best), the analytical formulation of the channel estimation MSE closely follows the simulations results. This validates the approximation performed in the formulation process. Outside this area the surfaces diverge, as it would be expected, since the analytical formulation does not take into account the distortion caused by the aliasing. The optimum pilot density attained by simulation confirms the analytical result.

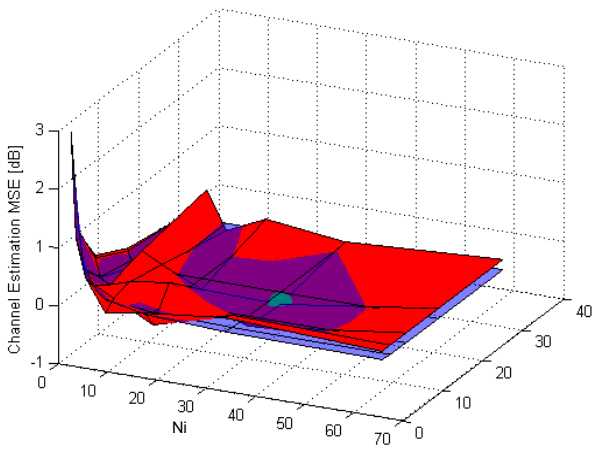

Figure 3.8. Channel estimation MSE surface (BRAN-A, MT speed=10km/h, Eb/N0=0dB).

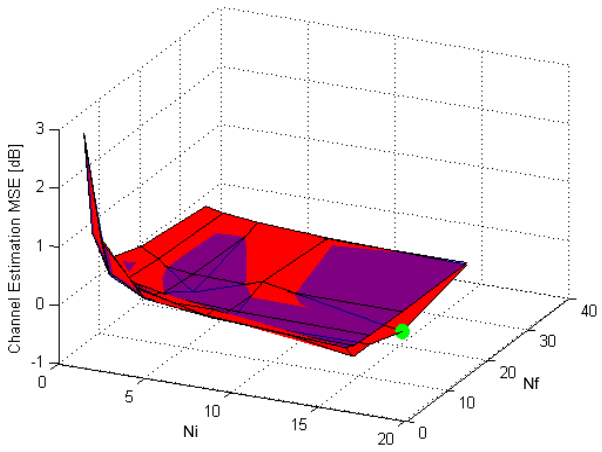

Figure 3.9. Channel estimation MSE surface (BRAN-A, MT speed=200km/h, Eb/N0=0dB).

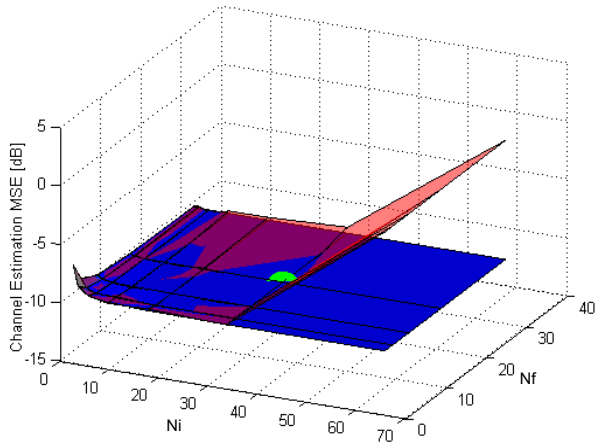

Figure 3.10. Channel estimation MSE surface (BRAN-A, MT speed=10km/h, Eb/N0=10dB).

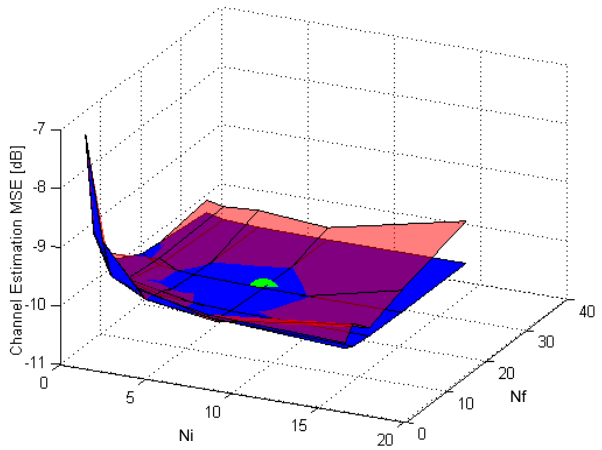

Figure 3.11. Channel estimation MSE surface (BRAN-A, MT speed=200km/h, Eb/N0=10dB).

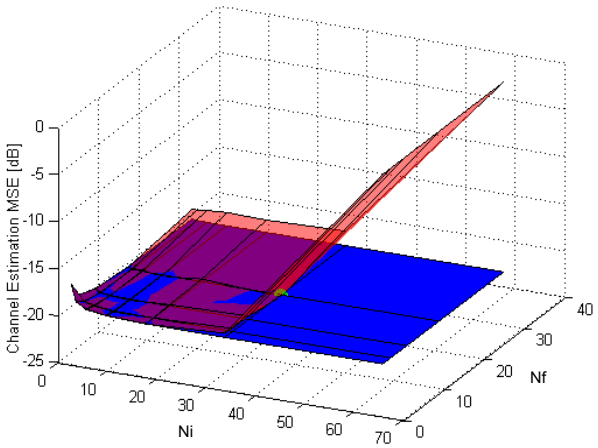

Figure 3.12. Channel estimation MSE surface (BRAN-A, MT speed=10km/h, Eb/N0=20dB).

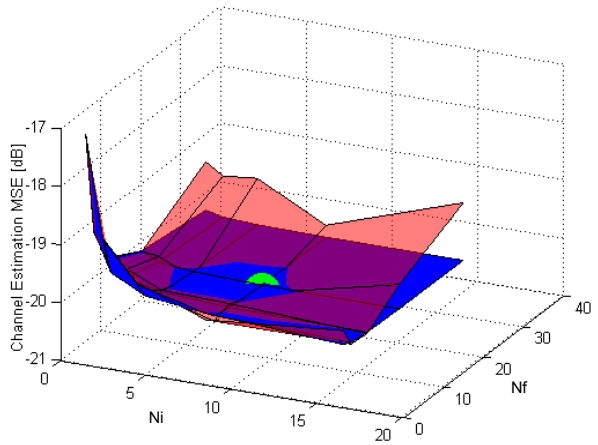

Figure 3.13. Channel estimation MSE surface (BRAN-A, MT speed=200km/h, Eb/N0=20dB).

3.5. Conclusions

The analytical formulation of the channel estimation MSE as a function of the pilot density (and distances) for a given power efficiency was presented.

Simulation results validate the analytical formulation in the area of interest, confirming that in the simulated scenario the optimum density is the one that closely fulfils the 2-D sampling theorem.

The channel estimation MSE is very sensitive to the fulfilment of the sampling frequency in the time axis, due to Doppler spectrum energy being concentrated near the Doppler frequency. Even a small overlap of the channel PSD replicas causes a considerable increase of the channel estimation MSE.

The multipath wireless channels that systems have to deal with in real scenarios commonly present an approximately exponentially decaying PDP, with most of the energy concentrated in a small set of initial samples and the remaining energy scattered in the longer CIR tail. The BRAN-A channel model used for simulation follows this tendency. When the pilot spacing N_f is increased until the sampling frequency in the frequency axis is not fulfilled, the tails of the CIR replicas start to overlap with the main set of samples of the other CIR replicas. For small overlaps, the distortion (aliasing) on the CIR estimate is not as severe as in the time axis, because the tail of the CIR has little energy.

As we increase the E_b/N_O at the receiver, the distortion caused by the aliasing becomes more and more severe. This can be observed by the increased slope of the MSE surfaces from top to bottom.

3.6. References

[Ars01] H. Arslan, G. Bottomley, "Channel Estimation in Narrowband Wireless Communication Systems," *Wireless Communications and Mobile Computing*, vol. 1, no. 2, pp. 201–219, April 2001.

[Ars03] H. Arslan, T. Yucek, "Estimation of Frequency Selectivity for OFDM Based New Generation Wireless Communication Systems," in *Proc. World Wireless Congress*, vol. 1, San Francisco, USA, May 2003.

[Bad05] F. Bader, R. Gonzalez, "Pilot time-frequency location adjustment in OFDM systems based on the channel variability parameters", *IEEE International Workshop on Multi-Carrier Spread Spectrum*, Munich, Germany, September 2005.

[Bad99] F. Bader, S. Zazo, J. Páez-Borrallo, "Optimum pilot pattern for the Uplink Multicarrier-CDMA systems," in *Proc. Symposium on Wireless Personal Multimedia Communications.*, Amsterdam, Netherlands, 1999.

[Bar02] I. Barhumi, G. Leus, M. Moonen, "Optimal Training Sequences for Channel Estimation in MIMO OFDM Systems in Mobile Wireless Channels," in *Proc. International Zurich Seminar on Broadband Communications*, vol. 44, pp. 1–6, Zurich, Switzerland, Feb. 2002.

[Bar03] I. Barhumi, G. Leus, M. Moonen, "Optimal Training Design For Mimo–Ofdm Systems in Mobile Wireless Channels," *IEEE Transactions on Signal Processing*, vol. 51, no. 6, pp. 1615–1624, June 2003.

[Bou01] S. Boumard, A. Mammela, "Channel Estimation Versus Equalization in an OFDM WLAN System," in *Proc. IEEE Vehicular Technology Conference*, vol. 1, pp. 653–657, Rhodes, Greece, May 2001.

[BRAN] ETSI Project Broadband Radio Access Networks (BRAN), HIPERLAN Type 2, Technical specification; Physical layer, October 1999.

[Cav91] J. K. Cavers, "An Analysis of Pilot Symbol Assisted Modulation for Rayleigh Fading Channels," *IEEE Transactions on Vehicular Technology*, vol. 40, pp. 686–693, Nov. 1991.

[Cho05] J.-W. Choi, Y.-H. Lee, "Optimum pilot pattern for channel estimation in OFDM systems," *IEEE Transactions on Wireless Communications*, Vol. 4, Issue 5, pp. 2083-2088, Sept. 2005.

[Dow02] A. Dowler, A. Doufexi, A. Nix, "Performance Evaluation of Channel Estimation Techniques for a Mobile Fourth Generation Wide Area OFDM System," in *Proc. IEEE Vehicular Technology Conference*, vol. 4, pp. 2036–40, Vancouver, Canada, Sept. 2002.

[Dow03] A. Dowler, A. Nix, "Performance Evaluation of Channel Estimation Techniques in a Multiple Antenna OFDM System," in *Proc. IEEE Vehicular Technology Conference*, vol. 2, pp. 1214–1218, Orlando, USA, Oct. 2003.

[Dud84] D. E. Dudgeon, R. M. Mersereau, *Multidimensional Digital Signal Processing*, Prentice-Hall, New Jersey, 1984.

[Gar00] M. J. Garcia, S. Zazo, J. Borrallo, "Pilot Patterns for Channel Estimation in OFDM," *IEE Electronic Letters*, vol.36, no. 12, pp. 1049–1050, June 2000.

[Gar99] M. J. Garcia, J. Borrallo, S. Zazo, "Efficient Pilot Patterns for Channel Estimation in OFDM Systems over HF Channels," in *Proc. IEEE Vehicular Technology Conference*, vol. 4, pp. 2193–2197, Amsterdam, Netherlands, Sept. 1999.

[Han03] B. Han *et al.*, "An Iterative Joint Channel Estimation and Symbol Detection Algorithm Applied in OFDM System with High Data To Pilot Power Ratio," in *Proc. IEEE International Conference on Communications*, vol. 3, pp. 2076–2080, Anchorage, USA, May 2003.

[Hoe97] P. Hoeher, S. Kaiser, P. Robertson, "Two-dimensional pilot-symbol-aided channel estimation by Wiener filtering," in *Proc. IEEE International Conference on Acoustics, Speech, and Signal Processing*, pp. 1845-1848, Munich, Germany, April 1997.

[Hou02] C. Hou, S. Song, D. Cao, "Channel Estimation for Adaptive OFDM System and Effects of Estimation Error on System Performance," in *Proc. IEEE International Workshop on Mobile and Wireless Communications Networks*, vol. 1, pp. 200–204, Stockholm, Sweden, Sept. 2002.

[Jeo01] W. G. Jeon, K. H. Paik, Y. S. Cho, "Two-Dimensional MMSE Channel Estimation for OFDM Systems with Transmitter Diversity," in *Proc. IEEE Vehicular Technology Conference*, vol. 3, pp. 1682–1685, Atlantic City, USA, Oct. 2001.

[Jia03] Z. Jianhua, Z. Ping, "An Improved 2–Dimensional Pilot–Symbols Assisted Channel Estimation in OFDM Systems," in *Proc. IEEE Vehicular Technology Conference*, vol. 3, pp. 1595–1599, Jeju, Korea, Apr. 2003.

[Kai97] S. Kaiser, P. Hoeher, "Performance of multi-carrier CDMA systems with channel estimation in two dimensions," in *Proc. IEEE Personal, Indoor and Mobile Radio Communications Symposium*, pp. 115-119, Helsinki, Finland, September 1997.

[Kai98] S. Kaiser, "Multi-Carrier CDMA Mobile Radio System- Analysis and Optimization of Detection, Decoding and Channel Estimation," *Ph.D. Thesis*, ISBN 3-18-353110-0, Munich, Germany, Jan. 1998.

[Li00] Y. Li, "Pilot-symbol-aided channel estimation for OFDM in wireless systems," *IEEE Transactions on Vehicular Technology*, Vol. 49, Issue 4, pp.1207-1215, July 2000.

[Li00a] Y. Li, "Optimum Training Sequences for OFDM Systems with Multiple Transmit Antennas," in *Proc. IEEE Global Telecommunications Conference*, vol. 3, pp. 1478–1482, San Francisco, USA, Nov. 2000.

[Li02] Y. Li, "Simplified Channel Estimation for OFDM Systems with Multiple Transmit Antennas," *IEEE Transactions on Wireless Communications*, vol. 1, no. 1, pp. 67–75, Jan. 2002.

[Mer83] R. M. Mersereau, T. C. Speake, "The processing of periodically sampled multidimensional signals," *IEEE Transactions on Signal Processing*, vol. ASSP-31, pp. 188-194, Feb. 1983.

[Moo00] J. Moon, S. Choi, "Performance of channel estimation methods for OFDM systems in a multipath fading channels", *IEEE Transactions on Consumer Electronics*, vol. 46, no. 1, pp. 161-170, Feb. 2000.

[Mor01] M. Morelli, U. Mengali, "A Comparison of Pilot–Aided Channel Estimation Methods for OFDM Systems," *IEEE Transactions on Signal Processing*, vol. 49, no. 12, pp. 3065–3073, Dec. 2001.

[Neg98] R. Negi, J. Cioffi, "Pilot Tone Selection for Channel Estimation in a Mobile OFDM System," *IEEE Transactions on Consumer Electronics*, vol. 44, no. 3, pp. 1122–1128, Aug. 1998.

[Shi04] M. Shin, H. Lee, C. Lee, "Enhanced Channel Estimation Technique for MIMO–OFDM Systems," *IEEE Transactions on Vehicular Technology*, vol. 53, no. 1, pp. 261–265, Jan. 2004.

[Son00] Y. Song, S. Roy, L. A. Akers, "Joint blind estimation of channel and data symbols in OFDM," in *Proc. IEEE Vehicular Technology Conference*, Vol. 1, pp.46-50, Tokyo, Japan, May 2000.

[Sun02] Y. Sun, X. Wang, K. Liu, "A Joint Channel Estimation and Unequal Error Protection Scheme for Video Transmission in OFDM Systems," in *Proc. IEEE International Conference on Image Processing*, vol. 1, pp. 549–552, Rochester, USA, Sept. 2002.

[Sun02a] Q. Sun *et al.*, "Estimation of Continuous Flat Fading MIMO Channels," *IEEE Transactions on Wireless Communications*, vol. 1, no. 4, pp. 549–553, Oct. 2002.

[Tan02] H. Tang, K. Y. Lau, R. W. Brodersen, "Interpolation-Based Maximum Likelihood Channel Estimation Using OFDM Pilot Symbols," in *Proc. IEEE Global Telecommunications Conference*, vol. 2, pp. 1860–1864, Taipei, Taiwan, Nov. 2002.

[Tuf97] F. Tufvesson, T. Maseng, "Pilot Assisted Channel Estimation for OFDM in Mobile Cellular Systems," in *Proc. IEEE Vehicular Technology Conference*, vol. 3, pp. 1639–1643, Phoenix, USA, May 1997.

[Wan01] X. Wang, K. J. R. Liu, "OFDM Channel Estimation Based on Time-Frequency Polynomial Model of Fading Multipath Channel," in *Proc. IEEE Vehicular Technology Conference*, vol. 1, pp. 460–464, Atlantic City, USA, Oct. 2001.

[Wu03] S. Wu, Y. Bar-Ness, "OFDM Channel Estimation in the Presence of Frequency Offset and Phase Noise," in *Proc. IEEE International Conference on Communications*, vol. 5, pp. 3366–3370, Anchorage, USA, May 2003.

CHAPTER 4

AN OFDM SYMBOL DESIGN FOR REDUCED COMPLEXITY MMSE CHANNEL ESTIMATION

In this chapter we revisit the MMSE pilot-aided channel estimation for broadband OFDM systems. The careful design of OFDM symbol leads to the proposal of a simplified TD MMSE estimator. By exploring the Fourier properties of the symbol, the investigated method eliminates the need to use direct or inverse discrete Fourier transforms (IDFT) before the channel estimation, by using the TD received symbol samples as the input to the MMSE filter. Moreover, performing the estimation in TD (where the CIR energy is mainly limited to a small set of samples), makes way to a simple, nonetheless efficient estimation of the filter parameters. The performance of the channel estimation scheme, using the estimated parameters, presents a tolerable degradation when compared with the ideal situation (a-priori knowledge of the channel correlation and noise variance), while exhibiting a reduced computational load. The feasibility of the investigated method is substantiated by system simulation using indoor and outdoor wireless channel models.

4.1. Introduction to Channel Estimation Techniques

Future mobile broadband applications will require reliable high data-rate wireless communication systems. In recent years, OFDM-based transmission systems [Nee00], [Stu04], [Pau04] emerged as the scheme with the potential to fulfil these conditions, with bandwidth efficiency and robustness to frequency selective channels, common in mobile personal communication systems. For systems using differential modulation schemes [Wei04], [Has05], [Can05], [Him06], channel estimation is not mandatory, but a performance loss of 3-4 dB is observed when comparing with systems employing coherent modulation techniques. This performance loss dictates the use of coherent detection OFDM systems in recent standards [802.11g], [802.16], [LTE]. In such systems, the channel estimation accuracy is crucial for the system's performance. Channel estimation performance evaluations and overviews can be found in [San96], [Har02], [Kan03] and [Ozd07].

As mentioned in the previous chapter, the use of pilots to help estimate the channel may be divided into two groups: training symbol based schemes and pilot-aided schemes.

The training symbols are used in commercial products using the WLAN [802.11g] and fixed WIMAX [802.16d] standards. The training symbols are typically inserted in the beginning of the burst and may be immediately repeated, so that the receiver's channel estimation scheme can exploit the correlation of the received training symbols to improve the estimate [Jeo00], or sent regularly so that the channel variation may be tracked [Sun02].

A number of techniques have been investigated to estimate the CFR of the remaining data-carrying symbols of the OFDM frame. The simplest solution is to extend the CFR estimate of the training symbols until the arrival of a new training symbol [Sun02], [Yeh99]. This technique has the drawback of poor performance for time-varying multipath channels, where the estimate error grows as the CFR estimate is used for received symbols farthest from the training symbol. For fast varying channels, the CFR estimate for data-carrying symbols can be obtained by interpolation methods. Linear interpolation can be found in [Jeo00] and [Yu03] and higher order interpolation polynomials were investigated in [Wan01], [Cha02] and [Col02].

For systems that can handle higher latency and more complex algorithms, data-aided techniques can be used to track the channel changes. This set of techniques uses the decoded data as pseudo-pilots to generate CFR estimates [Mig95], [Sun02]. The new CFR estimate will be used for the next received symbol. These algorithms enhance the system's performance for limited mobility scenarios. For high mobility scenarios, the error from using an outdated channel estimate from the previous symbol limits its performance.

In pilot-aided channel estimation schemes, pilots are multiplexed along with data sub-carriers as introduced in the previous chapter. Such a scheme is used, for example, in the recent LTE standard [LTE]. The channel estimates may be obtained in the time domain – CIR estimate – that is after transformed to frequency domain with the use of an FFT operation, or frequency domain, where the channel is first estimated for the pilot positions and then interpolated or extrapolated for the remaining sub-carriers and symbols.

The initial estimate in the pilot sub-carriers for a large number of channel estimation schemes is the LS estimation [Chi94]. This classical estimator treats the channel to be estimated as an unknown constant vector [Kay98], not taking advantage of the correlation of the channel across the sub-carriers in frequency and time domains. The minimization of the LS error criterion may not translate into minimizing the estimation error, but under the Gaussian assumption is equivalent to the maximum likelihood (ML) estimator. The LS estimator can also be applied in the TD by transforming the received values in the pilot sub-carriers to TD, with the use of an IDFT operation, [Bee95], [Edf96], yielding the same estimate. The use of the ML estimator to estimate the channel was investigated in [Mor01], [Lar01], where the knowledge of the limited length of the CIR was explored to improve the final estimate. If a minimum variance unbiased (MVU) estimator exists, the ML estimator will asymptotically tend to it for an infinite observation vector.

The classical estimators do not use *a-priori* information on the channel statistics to obtain the estimate. The Bayesian estimators [Kay98] constitute another group of estimation techniques that exploit the knowledge of prior information about the channel statistics to lead them to an improved estimate. The MMSE estimator requires the *a-priori* knowledge of the process' PDF. Under the Gaussian noise assumption, the linear MMSE estimator yields the minimum Bayesian MSE, like the unrestricted MMSE, and requires only the prior knowledge of the first two moments of the PDF, mean and covariance. For this reason this last technique stands-out as the most widely adopted either in FD [Hoe97] or in TD [Bee95]. Since the prior information is not available at the receiver, finding the most robust estimator to channel correlation mismatches and tracking the channel changes grew to be an important research topic [Li98]. The *maximum-a-posteriori* estimation (MAP) is also a Bayesian estimator with the same requirements as the MMSE. This estimator also yields the minimum Bayesian MSE and its utilization in pilot-aided channel estimation for OFDM systems was investigated in [Gao08], [Kim08]. Due to the higher implementation requirements, this technique did not receive as much attention as the MMSE scheme.

A wealth of iterative methods, that asymptotically achieve the performance of the previous techniques, has been investigated to perform the channel estimation. The utilization of the Expectation-Maximization (EM) algorithm [Moo96] was proven effective in estimating the fast-varying multipath channels that OFDM systems face [Ald03], [Xie03], but the

computation required to calculate and maximize the conditional expectation makes its use in real-time systems limited. The use of the Least Mean Square (LMS) and Recursive Least Square (RLS) iterative algorithms was addressed in [Col02], [Sch05] and [Bar03], [Ngu09]. The inability of these last two algorithms to use prior information limits its performance.

Some of the estimation schemes output the full channel estimate (for both data and pilot sub-carriers) [Hoe97], but a large number of the pilot-aided channel estimation schemes require an interpolator that outputs the channel estimates for the data sub-carriers.

Similarly to training symbol based schemes, the simplest interpolation is to extend the channel estimates in the pilot positions until the closest pilots in both frequency and time domains [Rin96]. Acceptable performance is only achieved if the CFR for neighbouring pilots is significantly correlated. Thus, the pilots need to be very close together in both dimensions (the channel is significantly oversampled) or the channel must vary slowly and have a limited delay spread. The linear interpolation method [Col02], [Ath03] enhances the performance of the previous scheme [Col02a] by using a first order polynomial to define the line that connects two neighbouring pilots. The channel estimates for the data carrying sub-carriers are taken from the defined lines.

When transmission occurs over highly frequency and/or time selective channels, linear interpolation feels short and higher order polynomial interpolation algorithms were investigated [Wan01], [Dow02], [Lee03] and proved to be more accurate in estimating highly selective channels. The investigation in [Lee03] showed that a better performance of the channel estimation scheme is achieved if the order of the interpolator is dynamically adapted according to the channel statistics. The most usual higher order polynomial interpolators are the spline interpolator [Dow02], [Col02a], the Gaussian interpolator [Kan03] and the polynomial fitting interpolator [Cha00], [Wan01], [Cha02].

The above interpolators can be seen as low-pass filters that use the knowledge that the CIR is limited to L_p significant taps/samples, a value smaller than the number of pilot sub-carriers, $L_p \ll N_P$, to filter out noise from the remaining time domain samples. Because they are not ideal, the estimator's performance will always be limited either from the wanted noise that is not filtered out or/and by some CIR taps that are unwillingly removed or attenuated/distorted.

The transform domain techniques use the same knowledge that the CFR depends on a small number of independent variables (the number of CIR taps). By applying different orthogonal transforms to the CFR estimates at the pilot positions, they try to isolate the CIR taps from the noise. The samples that hold only noise may be removed before performing the interpolation for the remaining sub-carriers. The interpolation process uses a larger number of the original estimates at the pilot positions to get the final estimates, when compared with the

previous set of techniques. Therefore, the error of the channel estimate is significantly lowered for this set of techniques. The best performance will be achieved by the transform that shrinks the number of samples with CIR energy to a minimum. The last step in the estimation scheme consists in applying the inverse transform to return to the original domain and, thus, obtain the final CFR estimate. The most common transforms used in the channel estimation techniques that can be found in the literature are discrete Fourier [Bee95], [Li99], [Li99a], [Li00], [Gar01], [Col02], [Li02], discrete cosine [Yeh00], [Yeh04], Karhunen-Loeve [Edf98], [Ste02] and Hadamard [Li01].

The Fourier transform based channel estimation techniques received a significant interest due to its ability to isolate the independent variables (CIR taps) under the channel assumptions stated in the previous chapter and its efficient implementation, thanks to the use of FFT operations. This group of techniques is in the aim of the algorithms proposed in this chapter.

The investigation on this topic can be divided in two groups. In the first group, the initial LS CFR estimates in the pilot sub-carriers are transformed to time-domain via an IFFT operation [Chi94], [Bee95], [Chi96], [Edf96], [Li00], [Li02]. This operation concentrates the energy of the channel to a small number of samples. Different time-domain schemes were investigated to improve the initial estimate, remove the samples that only have noise or separate the CIRs from different channels. The improved estimate is then transformed back to frequency domain with an FFT operation to get the final CFR estimate.

The second group of Fourier transform based techniques starts by performing an FFT operation on the initial LS CFR estimates at the pilot sub-carriers [Zha97], [Won01], [Sun02] and then apply techniques similar to the ones in the first group to improve the initial estimate. An IFFT operation returns the estimate to the original domain to get the final CFR estimate. The use of an initial FFT operation has the effect of concentrating the channel energy in a different segment of the FFT output vector, but under the same channel knowledge, both schemes achieve the same estimation performance [Won04].

The time domain pilot-aided channel estimation schemes haven't received much attention due to the unsurpassable fact that the equalization is performed in the frequency domain. Nevertheless, some investigation on the topic can be found in the literature. The design of the pilot sequences is explored in [Yeh99] and [Min00]. The pilot-carrying received symbols are processed to explore the correlation among the several CIR replicas to reduce the noise in the estimate. The use of superimposed pseudo-random pilot sequences was investigated in [Yeh99] and [Wan03]. In these schemes, the CIR estimate is obtained through the correlation of the received symbols with copies of transmitted pseudo-random sequences that are stored in the receiver (known *a-priori*).

Although published work on TD channel estimation put in evidence that the estimation process can be performed directly in TD, due to the common FD pilot arrangement, most of the publications on the topic of pilot-aided channel estimation use the FD LS estimates as the starting point for the estimation process. The results in [Rib07] show that this operation can be performed in TD by a simple linear operation on the received signal. Furthermore, the utilization of an MMSE estimator filter, whose input is directly linked to the received symbol samples (with no DFT/IDFT operations performed before the estimation filter [Bee95]), is largely simplified. In TD the CIR energy is limited to a small set of samples, resulting that the effective size of the matrices involved in the filtering can be significantly reduced and very accurate estimates are attained with significantly lower complexity.

This chapter contains a proposal for a pilot-aided TD MMSE channel estimator for OFDM systems where pilots are multiplexed along with data symbols in different sub-carriers within the OFDM symbol. The estimator structure is undemanding and the complexity reduced. Exploiting an initial TD channel estimate, the method uses a simple scheme to estimate the MMSE filter parameters: the slowly-varying delays of the multipath channel and the noise variance.

The chapter is organized as follows. Next Section gives a brief introduction to the wireless multipath channel and the OFDM baseband model. In Section 4.3 the investigated channel estimation algorithm is developed. The feasibility of the new method is substantiated by simulation results presented in Section 4.4. Finally, conclusions are drawn in Section 4.5.

4.2. OFDM in Mobile Wireless Channels

Let's consider that the system transmits over a multipath Rayleigh fading wireless channel, whose model was defined in Chapter 2,

$$\tilde{h}[n] = \sum_{l=0}^{L_p-1} \alpha_l \delta[n-\tau_l]. \tag{4.1}$$

The paths are assumed to be statistically independent, with normalized average power, $\sum_{l=0}^{L_p-1} \sigma_h^2[l] = 1$, where $\sigma_h^2[l]$ is the average power of path l. The channel is time-variant due to the motion of the MT, but we will assume that the CIR is constant during one OFDM symbol. The time dependence of the CIR is not present in the notation for simplicity. Assuming that the insertion of a long enough CP in the transmitter assures that the orthogonality of the sub-carriers is maintained after transmission, the CFR can be expressed as

$$h[k] = \sum_{l=0}^{L_p-1} \alpha_l \exp\left[-j\frac{2\pi}{N_C} k\tau_l\right]. \tag{4.2}$$

Let's consider the pilot-aided OFDM baseband transmitter model introduced in the previous chapter, here depicted in Figure 4.1 and the alternative pilot-aided OFDM baseband receiver model depicted in Figure 4.2. The changes from the previous receiver model are highlighted. The channel estimation block uses the time-domain vector $\tilde{\mathbf{r}}$ as the input to the estimation process. The de-framing block separates the values in data and pilot sub-carriers, but the latter are discarded.

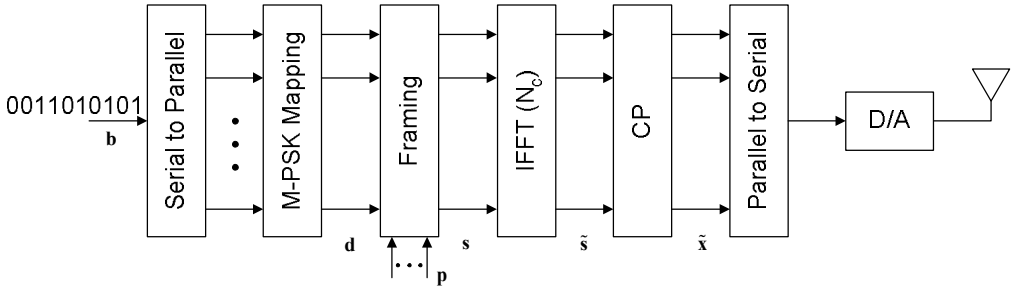

Figure 4.1. Pilot-aided OFDM baseband transmitter model.

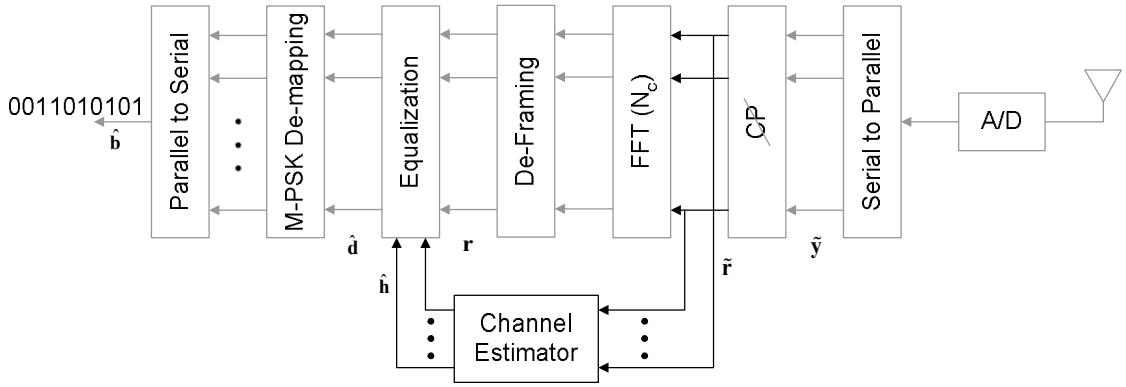

Figure 4.2. Pilot-aided OFDM baseband receiver model.

To assist in the channel estimation process, pilot symbols are multiplexed together with data symbols in different sub-carriers. The pilot symbols are collected in vector $\mathbf{p}$. Vectors $\mathbf{p}$ and $\mathbf{d}$ contain non-zero values at disjoint positions (sub-carriers). The resulting FD vector is $\mathbf{s} = \mathbf{d} + \mathbf{p}$.

The IDFT block transforms the input vector into the TD vector $\tilde{\mathbf{s}}$. After prefixing the L samples long CP, the resulting TD transmitted vector is

$$\tilde{\mathbf{x}} = \mathbf{A}_{CP}\mathbf{F}^H\mathbf{s} = \mathbf{A}_{CP}\left(\tilde{\mathbf{d}} + \tilde{\mathbf{p}}\right). \tag{4.3}$$

The TD vectors $\tilde{\mathbf{d}}$ and $\tilde{\mathbf{p}}$ collect, respectively, the components of the data symbols and pilot symbols present in $\tilde{\mathbf{s}}$.

The transmission over the wireless channel results in the received signal

$$\tilde{\mathbf{y}} = \tilde{\mathbf{H}}_{lin}\tilde{\mathbf{x}} + \bar{\tilde{\mathbf{n}}}, \tag{4.4}$$

where the vector $\bar{\tilde{\mathbf{n}}}$ is made-up of *iid* zero mean AWGN samples with variance σ_n^2.

With the assumption that a long enough CP was used for transmission, removing the CP from the received symbol with pilot and data results in the vector $\tilde{\mathbf{r}}$,

$$\begin{aligned}\tilde{\mathbf{r}} &= \mathbf{R}_{CP}\tilde{\mathbf{y}} = \mathbf{R}_{CP}\tilde{\mathbf{H}}_{lin}\mathbf{A}_{CP}\left(\tilde{\mathbf{d}} + \tilde{\mathbf{p}}\right) + \mathbf{R}_{CP}\bar{\tilde{\mathbf{n}}} \\ &= \tilde{\mathbf{H}}_{circ}\left(\tilde{\mathbf{d}} + \tilde{\mathbf{p}}\right) + \tilde{\mathbf{n}}\end{aligned}, \tag{4.5}$$

where $\tilde{\mathbf{n}} = \mathbf{R}_{CP}\bar{\tilde{\mathbf{n}}}$ is the resulting TD column N_C-noise vector. The vector $\tilde{\mathbf{r}}$ is the input to both DFT and channel estimation blocks.

The channel estimation block uses the pilot component present in $\tilde{\mathbf{r}}$ for the estimation process. The output vector $\hat{\mathbf{h}}$ consists of the FD channel estimates for all sub-carriers.

The DFT block transforms vector $\tilde{\mathbf{r}}$ to F. The resulting FD column N_C-vector can be expressed as

$$\mathbf{r} = \mathbf{F}\tilde{\mathbf{r}} = \mathbf{Q}\left(\mathbf{d} + \mathbf{p}\right) + \mathbf{n}, \tag{4.6}$$

where $\mathbf{Q}$ is a $N_C \times N_C$ diagonal matrix whose diagonal elements are defined by (4.2) and $\mathbf{n}$ is the FD noise vector.

The de-framing block separates the signals in the sub-carriers conveying pilots and data symbols. The values in the data sub-carriers are collected in vector $\hat{\mathbf{d}}$ and fed to the decision block. Together with the channel estimate, the decision block is now able to decide what where the transmitted symbols, according to some decision rule, and generate the estimate of the transmitted data $\hat{\mathbf{b}}$.

4.3. OFDM Symbol Design for Reduced Complexity MMSE Channel Estimation

The proposed method estimates the channel from the TD received symbols carrying pilots and data, taking advantage of the properties of the designed OFDM symbol (Figure

4.3). Extending the results in [Rib07] to the use of a TD MMSE criterion, all the processing required to estimate the CIR is performed immediately in TD. It eliminates the need to move from TD to FD and back to TD to finally obtain the CIR estimate, common to the methods in [Bee95], [Chi94], [Chi96], [Edf96]] (Figure 4.4). The simple TD operation is successful in simultaneously removing the data-dependent component in $\tilde{\mathbf{r}}$, generating the TD LS channel estimate and improving this initial estimate using the TD MMSE criterion, that optimally weighs the average power of the CIR taps to the noise variance.

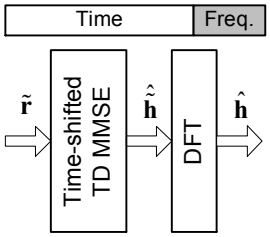

Figure 4.3. TD pilot-aided MMSE channel estimation.

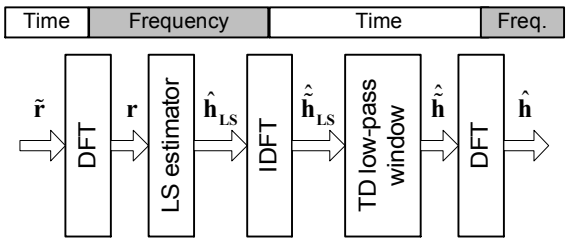

Figure 4.4. Pilot-aided DFT-based channel estimation.

4.3.1 Design of the OFDM symbol

Consider the set of sub-carriers $\wp$ dedicated to convey pilot symbols,

$$\wp = \left\{0, N_f, 2N_f, \cdots, N_C - N_f\right\}, \tag{4.7}$$

where the pilot distance N_f can range from 1 (particular case where all sub-carriers in the OFDM symbol are dedicated to transmit pilots – training symbol) to N_C, fulfilling the condition

$$\frac{N_C}{N_f} = N_t \in \mathbb{N}. \tag{4.8}$$

The transmitted pilots all have equal value (without loss of generality, in following, the pilots will have the value "1"), resulting in the *k*-th element of the pilot vector $\mathbf{p}$,

$$p[k] = \sum_{m=0}^{N_f-1} \delta\left[k - mN_f\right]. \tag{4.9}$$

Conversely, the *n*-th element of the corresponding TD vector $\tilde{\mathbf{p}}$ is

$$\tilde{p}[n] = \begin{cases} \dfrac{1}{N_f}, & \text{if } n = mN_t, \quad m = 0,1,..,N_f - 1 \\ 0, & \textit{remaining} \end{cases} = \frac{1}{N_f} \sum_{m=0}^{N_f-1} \delta\left[n - mN_t\right]. \tag{4.10}$$

The *n*-th element of $\tilde{\mathbf{d}}$ can be expressed by

$$\tilde{d}[n] = N_C^{-1/2} \sum_{\substack{k=0 \\ k \notin \wp}}^{N_C-1} d[k] e^{j2\pi \frac{kn}{N_C}}, \tag{4.11}$$

where $d[k]$ is the *k*-th element of $\mathbf{d}$ (complex data symbol conveyed by the *k*-th sub-carrier).

Using equations (4.10) and (4.11), the *n*-th element of $\tilde{\mathbf{r}}$ is

$$\tilde{r}[n] = \sum_{l=0}^{L-1} \tilde{h}[l]\tilde{d}[n-l] + \frac{1}{N_f} \sum_{m=0}^{N_f-1} \tilde{h}\left[n - mN_t\right] + \tilde{n}[n]. \tag{4.12}$$

Equation (4.12) puts in evidence that the received signal is the sum of three distinct components: the data vector $\tilde{\mathbf{d}}$ and pilot vector $\tilde{\mathbf{p}}$ transmitted over the wireless channel, and the AWGN. Looking carefully at the component dependent on the pilot vector, it becomes clear that it is made-up of N_f scaled replicas of the CIR. Moreover, the CIR replicas are separated by N_t samples.

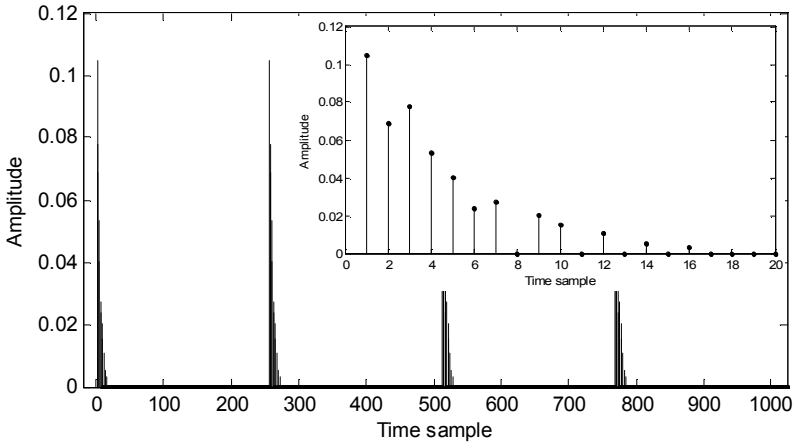

Figure 4.5. Received signal for the single antenna transmitter (pilot sub-carriers only; data sub-carriers not loaded).

For the purpose of illustration, Figure 4.5 shows an example of a received pilot vector transmitted through an 18 path BRAN-A [BRAN] wireless channel with a maximum delay spread of 390ns, $N_C = 1024$ sub-carriers and a pilot distance $N_f = 4$. The zoomed figure in the top right corner of Figure 4.5 details the first received replica of the CIR.

Given the normalized channel bandwidth $\frac{\tau_{\max}}{N_C \Delta t}$, where $\tau_{\max}$ is the maximum channel delay spread and Δt is the sampling interval, the minimum pilot distance N_f that can be used with no overlap in adjacent channel replicas, thus enabling the best performance of the channel estimator, is

$$N_f \leq \frac{N_C \Delta t}{\tau_{\max}}. \tag{4.13}$$

Otherwise, the overlapping of consecutive replicas will cause distortion in the estimation process and impose an irreducible MSE floor on the estimate.

4.3.2 Time analysis of DFT-based channel estimation

Let's briefly perform a TD analysis of the operations of the DFT-based channel estimator [Chi96] depicted in Figure 4.4, when using the OFDM symbol design of the previous section. The estimator initiates by transforming the TD vector $\tilde{\mathbf{r}}$ into the FD vector $\mathbf{r}$ using a DFT operation. It proceeds with the FD LS estimation of sub-carriers conveying pilots. The k-th element of the LS estimate vector $\hat{\mathbf{h}}_{\mathbf{LS}}$ is

$$\hat{h}_{LS}[k] = r[k] \sum_{m=0}^{N_f - 1} \delta\left[k - mN_f\right]. \tag{4.14}$$

The LS estimate vector is transformed to TD with the use of an IDFT operation, $\hat{\tilde{\mathbf{h}}}_{\mathbf{LS}} = \mathbf{F}^{H} \hat{\mathbf{h}}_{\mathbf{LS}}$. The n-th element of the resulting vector is

$$\begin{aligned} \hat{\tilde{h}}_{LS}[n] &= N_C^{-1/2} \sum_{k=0}^{N_C - 1} r[k] \sum_{m=0}^{N_f - 1} \delta\left[k - mN_f\right] \exp\left[j \frac{2\pi}{N_C} kn \right], \\ &= \frac{1}{N_f} \sum_{m=0}^{N_f - 1} \tilde{h}\left[n - mN_t\right] + \tilde{v}[n] \end{aligned} \tag{4.15}$$

where the noise component $\tilde{v}[n]$ is defined by

$$\tilde{v}[n] = N_C^{-1/2} \sum_{k \in \wp} n[k] \exp\left[j \frac{2\pi}{N_C} kn \right]. \tag{4.16}$$

The TD rectangular low-pass window $\tilde{\mathbf{t}}$, defined by

$$\tilde{t}[n] = N_f\left(u[n] - u[n - N_t + 1]\right), \tag{4.17}$$

is used to select the first CIR replica present in $\hat{\tilde{\mathbf{h}}}_{\mathbf{LS}}$ and thus attain the CIR estimate vector $\hat{\tilde{\mathbf{h}}}$,

$$\begin{aligned}\hat{\tilde{h}}[n] &= \tilde{t}[n]\hat{\tilde{h}}_{LS}[n] \\ &= \begin{cases}\tilde{h}[n] + N_f\tilde{v}[n], & n = 0,\cdots,N_t - 1\cdot \\ 0, & \textit{remaining}\end{cases}\end{aligned} \tag{4.18}$$

The CFR estimate vector $\hat{\mathbf{h}}$ is the result of transforming the CIR estimate back to FD, $\hat{\mathbf{h}} = \mathbf{F}\hat{\tilde{\mathbf{h}}}$.

4.3.3 Attaining the CIR estimate from the TD samples

Considering that the condition in (4.13) is fulfilled, an adequate processing that succeeds in removing the data dependent component from (4.12) would open way to easily obtain estimates of the CIR immediately from the received vector $\tilde{\mathbf{r}}$. The operation that achieves this goal is [Rib07]

$$\hat{\tilde{\mathbf{h}}} = \mathbf{T}\tilde{\mathbf{r}}, \tag{4.19}$$

where the $(N_t \times N_C)$ matrix $\mathbf{T} = \left[\mathbf{I}_{N_t} \cdots \mathbf{I}_{N_t}\right]$. The n-th element of $\hat{\tilde{\mathbf{h}}}$ is

$$\begin{aligned}\hat{\tilde{h}}[n] &= \begin{cases}\sum_{m=0}^{N_f-1}\tilde{r}[n + mN_t], & n = 0,\cdots,N_t - 1 \\ 0, & \textit{remaining}\end{cases} \\ &= \left(u[n] - u[n - N_t + 1]\right)\sum_{m=0}^{N_f-1}\tilde{r}[n + mN_t] \\ &= \left(u[n] - u[n - N_t + 1]\right)\times \\ &\times\left(\frac{1}{N_f}\sum_{m=0}^{N_f-1}\sum_{l=0}^{N_f-1}\tilde{h}[n + (m-l)N_t] + \sum_{m=0}^{N_f-1}\tilde{n}[n + mN_t] + \sum_{m=0}^{N_f-1}\sum_{l=0}^{L-1}\tilde{h}[l]\tilde{d}[n + mN_t - l]\right) \\ &= \begin{cases}\tilde{h}[n] + N_f\tilde{v}[n], & n = 0,\cdots,N_t - 1 \\ 0, & \textit{remaining}\end{cases}\end{aligned} \tag{4.20}$$

The last step in (4.20) was possible considering that the data component was eliminated due to the fact that

$$\begin{aligned}&\sum_{m=0}^{N_f-1}\sum_{l=0}^{L-1}\tilde{h}[l]\tilde{d}[n+mN_t-l]=\\&=N_C^{-1/2}\sum_{l=0}^{L-1}\tilde{h}[l]\sum_{\substack{k=0\\k\notin\wp}}^{N_C-1}d[k]\exp\left[j\frac{2\pi}{N_C}k(n-l)\right]\sum_{m=0}^{N_f-1}\exp\left[j\frac{2\pi}{N_C}kmN_t\right]=0\end{aligned}. \tag{4.21}$$

The result in (4.21) is best understood considering that only the sub-carriers $k\in\wp$ add constructively in the operation performed in (4.20). Correspondingly, the resulting noise component in (4.20) is justified considering that

$$\begin{aligned}\sum_{m=0}^{N_f-1}\tilde{n}[n+mN_t]&=N_C^{-1/2}\sum_{k=0}^{N_C-1}n[k]\exp\left[j\frac{2\pi}{N_C}kn\right]\sum_{m=0}^{N_f-1}\exp\left[j\frac{2\pi}{N_C}kmN_t\right]\\&=N_fN_C^{-1/2}\sum_{k\in\wp}n[k]\exp\left[j\frac{2\pi}{N_C}kn\right]=N_f\tilde{v}[n]\end{aligned}. \tag{4.22}$$

The result in (4.20) demonstrates that the simple operation in (4.19) yields the same CIR estimate attained by (4.18).

4.3.4 MMSE smoothing filter

The initial CIR estimate of (4.19) can be improved with the use of a smoothing filter. With the knowledge that the CIR energy is limited to the set of taps $\{L_p\}$, with L_p elements, an MMSE filter will optimally weigh the CIR energy to the noise variance inside this set and remove the outside noise, so to achieve the lowest possible estimate MSE.

The MMSE filter is implemented by the $(N_t\times N_t)$ matrix [Kay98]

$$\tilde{\mathbf{W}}_{MMSE}=\mathbf{R}_{\tilde{h}\hat{h}}\mathbf{R}_{\hat{h}\hat{h}}^{-1}, \tag{4.23}$$

where the $(N_t\times N_t)$ filter input correlation matrix is

$$\mathbf{R}_{\hat{h}\hat{h}}=E\{\hat{\mathbf{h}}\hat{\tilde{\mathbf{h}}}^H\}=\mathbf{R}_{\tilde{h}\tilde{h}}+\sigma_n^2/N_t\,\mathbf{I}_{N_t}, \tag{4.24}$$

and the $(N_t\times N_t)$ filter input–output cross-correlation matrix is

$$\mathbf{R}_{\tilde{h}\hat{h}}=E\{\tilde{\mathbf{h}}\hat{\tilde{\mathbf{h}}}^H\}=\mathbf{R}_{\tilde{h}\tilde{h}}, \tag{4.25}$$

with the $(N_t\times N_t)$ channel correlation diagonal matrix

$$\mathbf{R}_{\tilde{h}\tilde{h}} = E\{\tilde{\mathbf{h}}\tilde{\mathbf{h}}^H\} = diag\left(\left[\sigma_{\tilde{h}}^2[0],\cdots,\sigma_{\tilde{h}}^2\left[L_p-1\right],0,\cdots,0\right]\right). \tag{4.26}$$

Replacing equations (4.24) to (4.26) in (4.23), the MMSE filter becomes,

$$\tilde{\mathbf{W}}_{MMSE} = diag\left(\left[\frac{\sigma_{\tilde{h}}^2[0]}{\sigma_{\tilde{h}}^2[0]+\frac{\sigma_n^2}{N_t}},\cdots,\frac{\sigma_{\tilde{h}}^2\left[L_p-1\right]}{\sigma_{\tilde{h}}^2\left[L_p-1\right]+\frac{\sigma_n^2}{N_t}},0,\cdots,0\right]\right). \tag{4.27}$$

The final CIR estimate can be expressed by

$$\hat{\tilde{\mathbf{h}}}_{MMSE} = \tilde{\mathbf{W}}_{MMSE}\hat{\tilde{\mathbf{h}}}. \tag{4.28}$$

Taking into consideration that the filter is implemented with a diagonal matrix with L_p non-zero elements, the MMSE filtering in (4.28) can be performed simultaneously with the operation in (4.19). In fact, the merge of both operations reduces the computational load of (4.19), by limiting the summation interval in (4.20) to the set $\{L_p\}$. The elements of the final CIR estimate can be found by

$$\begin{aligned}\hat{\tilde{h}}_{MMSE}[n] &= \begin{cases}\dfrac{\sigma_{\tilde{h}}^2[n]}{\sigma_{\tilde{h}}^2[n]+\dfrac{\sigma_n^2}{N_t}}\displaystyle\sum_{m=0}^{N_f-1}\tilde{r}[n+mN_t], & n\in\{L_p\}\\ 0, \quad remaining\end{cases}\\ &= \begin{cases}\dfrac{\sigma_{\tilde{h}}^2[n]\left(\tilde{h}[n]+N_f\tilde{v}[n]\right)}{\sigma_{\tilde{h}}^2[n]+\dfrac{\sigma_n^2}{N_t}}, & n\in\{L_p\}\\ 0, \quad remaining\end{cases}\end{aligned}. \tag{4.29}$$

4.3.5 MMSE filter design

Examining (4.27) it is clear that the computation of the filter coefficients requires only L_p complex divisions, unlike its FD counterpart [Hoe97] that needs a computationally demanding full matrix inversion.

The MMSE filter is a function of two design parameters: the channel correlation matrix $\mathbf{R}_{\tilde{h}\tilde{h}}$ and the noise variance σ_n^2, none of which available to the receiver in a real scenario. Moreover, if the transmission is performed over a time-varying channel, these parameters must be tracked to maintain the filter's performance.

Making use of $\hat{\tilde{\mathbf{h}}}$, where the CIR energy is limited to the set of taps $\{L_p\}$, the estimate of the filter parameter is significantly simplified when compared to other FD estimation methods [Yuc06].

The channel correlation matrix is dependent on the complex values and delays of the channel paths. The variation of the complex path values is linked to the Doppler shift, leading to considerable variations between consecutive symbols for high values of MT velocity.

On the other hand, the delays may be considered constant for the duration of t symbols provided that its variation $\Delta\tau$ is much smaller than the system's temporal resolution, $\Delta\tau \ll \Delta t$. For a radial movement between transmitter and receiver with velocity v, the variation of delay in t symbols is $\Delta\tau = \frac{vtT_S}{c}$, leading to

$$t \ll \frac{c\Delta t}{vT_S}, \tag{4.30}$$

where the speed of light $c = 3\times10^8\, m/s$ and T_S is the OFDM symbol duration.

For $v = 100 km/h$ and with the system parameters defined in the simulation results section, the delays can be considered constant for $t \approx 1000$ symbols.

Considering that the delays remain constant for q pilot-carrying symbols, we propose a simple method to estimate the slowly-varying delays $\hat{\tau}_l$ (and associated average power values $\hat{\sigma}_h^2[l]$) and noise variance $\hat{\sigma}_n^2$.

The estimation of the noise variance $\hat{\sigma}_n^2$ uses the samples $\left\{\hat{\tilde{h}}[n],\ n \notin \{L_p\}\right\}$,

$$\hat{\sigma}_n^2 = \frac{N_t}{(N_t - L_p)q}\sum_{t=1}^{q}\sum_{n\notin\{L_p\}}\left|\hat{\tilde{h}}_t[n]\right|^2. \tag{4.31}$$

The elements of the main diagonal of the channel correlation matrix $\mathbf{R}_{\tilde{h}\tilde{h}}$ are estimated by

$$\hat{\sigma}_h^2[n] = \frac{1}{q}\sum_{t=1}^{q}\sum_{n\in\{L_p\}}\left|\hat{\tilde{h}}_t[n]\right|^2 - \frac{\hat{\sigma}_n^2}{N_t}. \tag{4.32}$$

On the simulation results presented in the next section, we have updated the filter parameters on every OFDM frame. This option proved to be a good trade-off between computational load and estimation performance.

4.3.6 Complexity analysis of TD-based channel estimators

The investigated method requires $\frac{L_p}{N_C}$ multiplications and $\frac{L_p N_f}{N_C}$ additions per tap to implement the time-shifted TD MMSE block, resulting in a total complexity per CFR sub-carrier of $\frac{L_p}{N_C}+\frac{\log_2(N_C)}{2}$ multiplications and $\frac{L_p N_f}{N_C}+\log_2(N_C)$ additions, if the complexity of the tracking procedure is discarded.

TABLE 4.1. DFT CHANNEL ESTIMATION COMPLEXITY (OPS. PER SUB-CARRIER).

	LS Estimate	DFT / IDFT	TD weighting window	Required ops. per tap
Multiplications	1	$\frac{\log_2(N_C)}{2}$	1	$2+\log_2(N_C)$
Additions	–	$\log_2(N_C)$	–	$2\log_2(N_C)$

TABLE 4.2. COMPLEXITY COMPARISON (OPS. PER SUB-CARRIER).

	TD MMSE	LS-DFT [Chi96]	DFT + MMSE [Bee95]
Multiplications	≈5	12	75
Additions	≈10	20	85

The complexity of the method in [Chi96] is summarized in Table 4.1. To calculate each CFR sub-carrier estimate it requires a total of $2+\log_2(N_C)$ multiplications and $2\log_2(N_C)$ additions. To further implement the TD MMSE method in [Bee95] with a $(N_t \times N_t)$ MMSE matrix, it requires $\frac{N_t^2}{N_C}$ additional multiplications and equal number of additions, resulting in a total complexity of $1+\log_2(N_C)+\frac{N_t^2}{N_C}$ multiplications and $2\log_2(N_C)+\frac{N_t^2}{N_C}$ additions.

Table 4.2 compares the complexity between the investigated method and the methods in [Bee95] and [Chi96] for the indoor simulation scenario ($L_p = 9$ taps channel) described in Section 4.4. It puts in evidence the considerable computational load reduction achieved by the proposed method, with no performance trade-off.

4.3.7 Analysis of TD-based channel estimators' MSE

Assuming that the noise in the TD samples is *iid*, the noise variance in (4.19) is σ_n^2, resulting in the initial channel estimation MSE

$$\sigma_{e,INI}^2 = \sigma_n^2 . \tag{4.33}$$

By eliminating the noise in the samples where there is no CIR energy, the noise variance in the channel estimation method in [Rib07] is reduced and the resulting channel estimation MSE is

$$\sigma_{e,STC}^2 = \sigma_n^2 \frac{L_p}{N_t} = \sigma_{e,INI}^2 \frac{L_p}{N_t} . \tag{4.34}$$

This MSE tends to the initial MSE when L_p goes to N_t (limiting condition in (4.13)).

An error floor will limit the performance for high values of SNR if the set $\{L_p\}$ is not properly estimated and some CIR energy is removed.

In the investigated channel estimation method, the resulting MSE is [Edf96]

$$\sigma_{e,MMSE}^2 = \sigma_n^2 \frac{L_p}{N_t} \sum_{l \in \{L_p\}} \frac{\sigma_h^2[l]}{\sigma_h^2[l] + \frac{\sigma_n^2}{N_t}} . \tag{4.35}$$

Observing (4.35), we can conclude that when $SNR \to \infty$, $\sigma_{e,MMSE}^2 \to \sigma_{e,STC}^2$. Results presented in the next section confirm this analysis.

4.4. Simulation Results

A simulation scenario was implemented where $N_C = 1024$ sub-carriers were QPSK modulated. The system used a carrier frequency $f_C = 5GHz$ and the sampling interval was set to $\Delta t = 50ns$. The transmitted OFDM symbols carried pilots and data using the proposed pilot structure, with a pilot separation $N_f = 4$. The OFDM frame consists of 24 symbols.

Two channel models with exponential decaying PDP were used to simulate indoor ($50ns$ *rms* delay spread) and outdoor environments ($250ns$ *rms* delay spread).

To validate the proposed method, BER and channel estimation simulations were performed, using Eb/No values in the range of *0dB* to *20dB*. Its performance is plotted

against the one of the methods in [Rib07] and [Chi96]. The proposed method is simulated using the ideal MMSE filter and using the estimated parameters. The method in [Rib07] is simulated using the perfect set of delays $\{L_p\}$, that represents the upper bound on the method's performance.

The normalized channel estimation MSE results are depicted in Figure 4.6 and Figure 4.7, respectively for indoor and outdoor channels. The proposed method and the methods in [Rib07] and [Chi96] are noted as "TD MMSE", "TD STC" and "TD LS-DFT", respectively. The proposed method using the filter with estimated parameters is noted "TD MMSE (Param.Est.)".

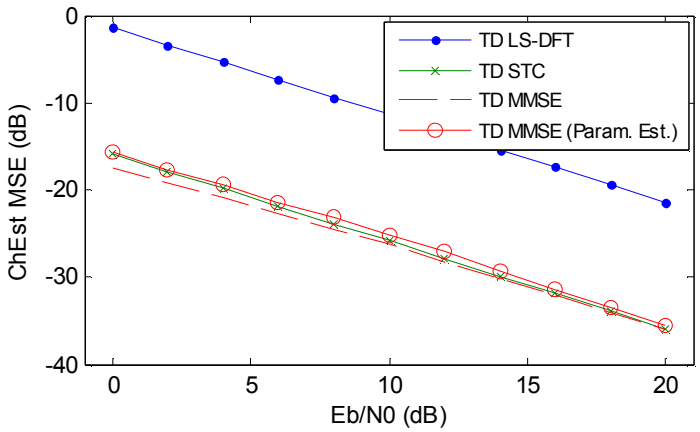

Figure 4.6. Channel estimation MSE (indoor scenario).

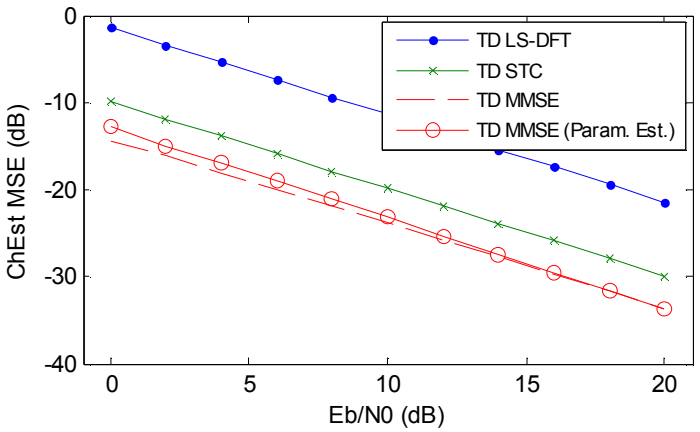

Figure 4.7. Channel estimation MSE (outdoor scenario).

The BER results are depicted in Figure 4.8 and Figure 4.9, respectively for indoor and outdoor channels. The plot noted as "Perfect CSI" represents the situation where the perfect CSI is used in the decision block.

On both scenarios, the method in [Chi96] and the proposed method present a consistent performance. The method in [Chi96] always achieves the worst performance due to the fact that it does not take advantage of the channel characteristics; in the indoor scenario, $\approx 16dB$ and $\approx 14,5dB$ degradation in the channel estimation MSE when compared with the proposed method for the lower and higher values of Eb/No, respectively ($\approx 3dB$ and $\approx 2,5dB$ in the BER results); in the outdoor scenario, $\approx 13dB$ and $\approx 12dB$ degradation in the channel estimation MSE when compared with the proposed method for the lower and higher values of Eb/No, respectively ($\approx 3dB$ and $\approx 2,5dB$ in the BER results).

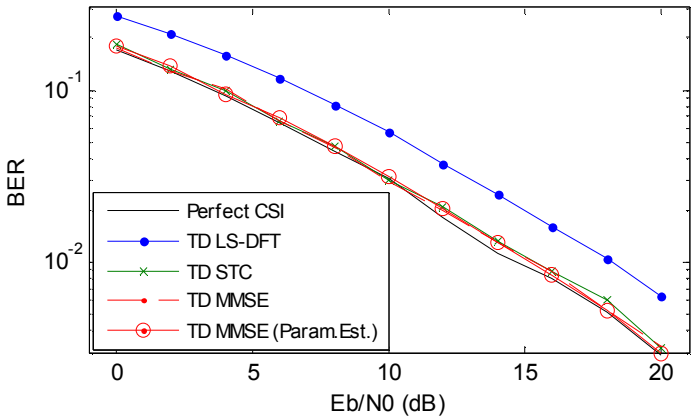

Figure 4.8. System BER performance (indoor scenario).

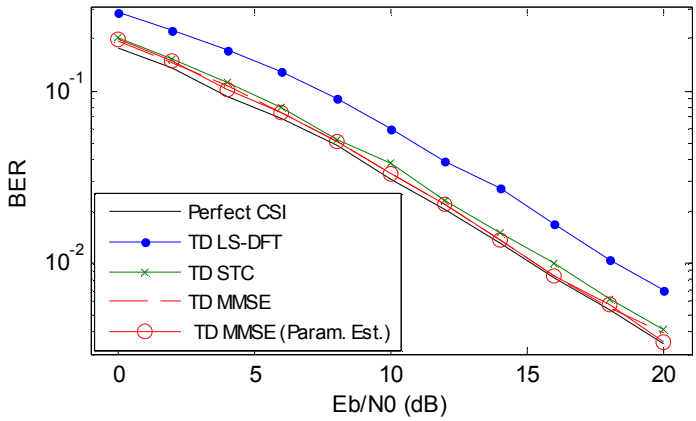

Figure 4.9. System BER performance (outdoor scenario).

In contrast, the proposed method always achieves the best performance with a BER performance near the ideal perfect CSI. It presents the ability of dealing with the increasing channel delay spread by always weighing the energy of channel taps vs. noise variance.

The performance of the method in [Rib07] is closely dependent on the channel delay spread. Its performance is bounded by the two previous methods. A channel with a short

delay spread will result in the best performance (by having the CIR energy concentrated in just a few taps, most of the noise is eliminated in the estimation process). As the channel delay spread increases, the performance tends to that of the method in [Chi96].

Results show that the MMSE filter using the estimated parameters presents a performance near the ideal situation were the filter used the true channel correlation and noise variance.

4.5. Conclusions

We have presented a pilot sequence design and associated TD MMSE channel estimation algorithm for OFDM systems. The investigated method eliminates the use of DFT/IDFT operation before the estimation process, resulting in an undemanding structure with very low computational load.

It was demonstrated that the operations up to the CIR estimate can be equivalently performed in TD with a simple linear operation. By working in TD, the channel correlation matrix is diagonal, with a small number of non-zero elements, noticeably reducing the computational load of implementing the MMSE estimation, with no performance penalty. Also, the estimation of MMSE filter parameters is simplified when compared with the FD counterpart. A simple method to estimate the required filter parameters is introduced and its performance evaluated by simulations. Results show that the performance degradation is negligible when compared with the ideal MMSE filter.

4.6. References

[802.11g] IEEE Std. 802.11g-2003, "Local and metropolitan area networks – Specific requirements – Part 11: Wireless LAN medium access control (MAC) and physical layer (PHY) specifications – Amendment 4: Further higher data rate extension in the 2.4 GHz band," June 2003.

[802.16] IEEE Std. 802.16-2009, "Local and metropolitan area networks – Part 16: Air interface for broadband wireless access systems," May 2009.

[802.16d] IEEE Std. 802.16-2004, "Local and metropolitan area networks – Part 16: Air interface for fixed broadband wireless access systems," Oct. 2004.

[Ald03] C. Aldana, E. Carvalho, J. Cioffi, "Channel estimation for multicarrier multiple input multiple output systems using the EM algorithm," *IEEE Transactions on Signal Processing*, vol. 51, no. 12, pp. 3280 – 3291, December 2003.

[Ath03] C. Athaudage, A. Jayalath, "Low–Complexity Channel Estimation for Wireless OFDM Systems," in *Proc. IEEE International Symposium on Personal, Indoor and Mobile Radio Communications*, vol. 1, pp. 521 – 525, Beijing, China, Sept. 2003.

[Bar03] I. Barhumi, G. Leus, M. Moonen, "Optimal Training Design for MIMO OFDM Systems in Mobile Wireless Channels," *IEEE Transactions on Signal Processing*, vol. 51, no. 6, pp. 1615 – 1624, June 2003.

[Bee95] J.-J. van de Beek, O. Edfors, M. Sandell, S. K. Wilson, P. O. Borjesson, "On channel estimation in OFDM systems," in *Proc. IEEE Vehicular Technology Conference*, vol. 2, pp. 815 – 819, Chicago, USA, July 1995.

[BRAN] ETSI Project Broadband Radio Access Networks (BRAN), "HIPERLAN Type 2, Technical specification; Physical layer," October 1999.

[Can05] A. Cano, X. Ma, G. Giannakis, "Block-Differential Modulation over Doubly Selective Wireless Fading Channels," *IEEE Transactions on Communications*, vol. 53, no. 12, pp. 2157 – 2166, Dec. 2005.

[Cha00] M. Chang and Y. T. Su, "2D Regression Channel Estimation for Equalizing OFDM Signals," in *Proc. IEEE Vehicular Technology Conference*, vol. 1, pp. 240 – 244, Tokyo, Japan, May 2000.

[Cha02] M. Chang, Y. Su, "Model–Based Channel Estimation for OFDM Signals in Rayleigh Fading," *IEEE Transactions on Communications*, vol. 50, no. 4, pp. 540 – 544, April 2002.

[Chi94] A. Chini, "Multicarrier modulation in frequency selective fading channels," Ph.D. dissertation, Carleton University, Canada, 1994.

[Chi96] A. Chini, M. S. El-Tanany, S. A. Mahmoud, "Transmission of high rate ATM packets over indoor radio channels," *IEEE Journal on Selected Areas in Communications*, vol. 14, no. 4, pp. 469 – 476, April 1996.

[Col02] S. Coleri, M. Ergen, A. Puri, A. Bahai, "Channel Estimation Techniques Based on Pilot Arrangement in OFDM Systems," *IEEE Transactions on Broadcasting*, vol. 48, no. 3, pp. 223–229, Sept. 2002.

[Col02a] S. Coleri, M. Ergen, A. Puri, A. Bahai, "A Study of Channel Estimation in OFDM Systems," in *Proc. IEEE Vehicular Technology Conference*, vol. 2, pp. 894 – 898, Vancouver, Canada, Sept. 2002.

[Dow02] A. Dowler, A. Doufexi, A. Nix, "Performance Evaluation of Channel Estimation Techniques for a Mobile Fourth Generation Wide Area OFDM System," in *Proc. IEEE Vehicular Technology Conference*, vol. 4, pp. 2036 – 2040, Vancouver, Canada, Sept. 2002.

[Edf96] O. Edfors, "Low-complexity algorithms in digital receivers," Ph.D. dissertation, Lulea University of Technology, Sweden, 1996.

[Edf98] O. Edfors, M. Sandell, J.-J. van de Beek, S. Wilson, P. Borjesson, "OFDM Channel Estimation By Singular Value Decomposition," *IEEE Transactions on Communications*, vol. 46, no. 7, pp. 931 – 939, July 1998.

[Gao08] J. Gao, H. Liu, "Low-Complexity MAP Channel Estimation for Mobile MIMO-OFDM Systems," *IEEE Transactions on Wireless Communications*, vol. 7, no. 3, pp. 774 – 780, March 2008.

[Gar01] M. J. Garcia, J. Paez-Borrallo, S. Zazo, "DFT–Based Channel Estimation in 2D-Pilot-Symbol-Aided OFDM Wireless Systems," in *Proc. IEEE Vehicular Technology Conference*, vol. 2, pp. 810 – 814, Rhodes, Greece, May 2001.

[Har02] I. Harjula, A. Mammela, Z. Li, "Comparison of Channel Frequency and Impulse Response Estimation for Space Time Coded OFDM Systems," in *Proc. IEEE Vehicular Technology Conference*, vol. 4, pp. 2081 – 2085, Vancouver, Canada, Sept. 2002.

[Has05] W. Hashim, F. Said, B. Allen, A. Aghvami, A. Ismail, "Performance Comparison of Differential Space-Time Signalling Schemes for OFDM Systems," in *Proc. IEEE International Conference on Networks*, vol. 2, pp. 1 – 6, Kuala Lumpur, Malaysia, Nov. 2005.

[Him06] T. Himsoon, S. Weifeng, K. Liu, "Single-block Differential Transmit Scheme for Broadband Wireless MIMO–OFDM Systems," *IEEE Transactions on Signal Processing*, vol. 54, no. 9, pp. 3305 – 3314, Sept. 2006.

[Hoe97] P. Hoeher, S. Kaiser, P. Robertson, "Two-dimensional pilot-symbol-aided channel estimation by Wiener filtering," in *Proc. IEEE International Conference on Acoustics, Speech, and Signal Processing*, Munich, pp. 1845 – 1848, Germany, April 1997.

[Jeo00] W. Jeon, K. Paik, Y. Cho, "An Efficient Channel Estimation Technique for OFDM Systems with Transmitter Diversity," in *Proc. IEEE International Symposium on Personal, Indoor and Mobile Radio Communications*, vol. 2, pp. 1246 – 1250, London, UK, Sept. 2000.

[Kan03] S. Kang, Y. Ha, E. Joo, "A Comparative Investigation on Channel Estimation Algorithms for OFDM in Mobile Communications," *IEEE Transactions on Broadcasting*, vol. 49, no. 2, pp. 142 – 149, June 2003.

[Kay98] S. Kay, *Fundamentals of Statistical Signal Processing*, Englewood Cliffs, NJ, USA, Prentice-Hall, 1998.

[Kim08] J. Kim, J. Lim, "MAP-Based Channel Estimation for MIMO–OFDM Over Fast Rayleigh Fading Channels," *IEEE Transactions on Vehicular Technology*, vol. 57, no. 3, pp. 1963 – 1968, May 2008.

[Lar01] E. Larsson, L. Guoqing, L. Jian, G. Giannakis, "Joint symbol timing and channel estimation for OFDM based WLANs," *IEEE Communications Letters*, vol. 5, no. 8, pp. 325 – 327, August 2001.

[Lee03] S. Lee, D. Lee, H. Choi, "Performance Comparison of Space-Time Codes and Channel Estimation in OFDM Systems with Transmit Diversity for Wireless LANs," in *Proc. Asia-Pacific Conference on Communications*, vol. 1, pp. 406 – 410, Penang, Malaysia, Sept. 2003.

[Li00] Y. Li, "Pilot-symbol-aided channel estimation for OFDM in wireless systems," *IEEE Transactions on Vehicular Technology*, vol. 49, no. 4, pp. 1207 – 1215, July 2000.

[Li01] Y. Li, N. Sollenberger, "Clustered OFDM with Channel Estimation for High Rate Wireless Data," *IEEE Transactions on Communications*, vol. 49, no. 12, pp. 2071 – 2076, Dec. 2001.

[Li02] Y. Li, "Simplified channel estimation for OFDM systems with multiple transmit antennas," *IEEE Transactions on Wireless Communications*, vol. 1, pp. 67 – 75, Jan. 2002.

[Li03] Y. Li, Z. Li, Y. Cai, Y. Xu, "An improved channel estimation scheme for OFDM systems by tracking the subspace," in *Proc. IEEE International Symposium on Personal, Indoor and Mobile Radio Communications*, vol. 2, pp. 1109 – 1113, Beijing, China, Sept. 2003.

[Li98] Y. Li, L. J. Cimini, N. R. Sollenberger, "Robust channel estimation for OFDM systems with rapid dispersive fading," *IEEE Transactions on Communications*, vol. 46, pp. 902 – 915, July 1998.

[Li99] Y. Li, N. Seshadri, S. Ariyavisitakul, "Channel estimation for OFDM systems with transmitter diversity in mobile wireless channels," *IEEE Journal on Selected Areas in Communications*, vol. 17, no. 3, pp. 461 – 471, March 1999.

[Li99a] Y. Li, "Pilot-Symbol-Aided Channel Estimation for OFDM in Wireless Systems," in *Proc. IEEE Vehicular Technology Conference*, vol. 2, pp. 1131 – 1135, Houston, USA, May 1999.

[LTE] ETSI Technical Specification TS 136 201 v8.3.0, "LTE; Evolved universal terrestrial radio access (E-UTRA); Long Term Evolution (LTE) physical layer; General description," April 2009.

[Mig95] V. Mignone, A. Morello, M. Visintin, "CD3–OFDM: A New Channel Estimation Method to Improve the Spectrum Efficiency in Digital Terrestrial Television

Systems," in *Proc. International Broadcasting Convention*, vol. 1, pp. 122–128, Amsterdam, Netherlands, Sept. 1995.

[Min00] H. Minn, V. Bhargava, "An investigation into time-domain approach for OFDM channel estimation," *IEEE Transactions on Broadcasting*, vol. 46, no. 4, pp. 240 – 248, Dec. 2000.

[Moo96] T. Moon, "The expectation-maximization algorithm," *IEEE Signal Processing Magazine*, vol. 13, no. 6, pp. 47 – 60, June 1996.

[Mor01] M. Morelli, U. Mengali, "A comparison of pilot-aided channel estimation methods for OFDM systems," *IEEE Transactions on Signal Processing*, vol. 49, no. 12, pp. 3065 – 3073, December 2001.

[Nee00] R. V. Nee, R. Prasad, *OFDM for Wireless Multimedia Communications*, 1st edition, Artech House, 2000.

[Ngu09] H. Nguyen-Le, T. Le-Ngoc, C. Ko, "RLS-Based Joint Estimation and Tracking of Channel Response, Sampling, and Carrier Frequency Offsets for OFDM," *IEEE Transactions on Broadcasting*, vol. 55, no. 1, pp. 84 – 94, March 2009.

[Ozd07] M. Ozdemir, H. Arslan, "Channel Estimation for Wireless OFDM Systems," *IEEE Communications Surveys*, vol. 9, no. 2, pp. 18 – 48, 2nd Quarter 2007.

[Pau04] A. J. Paulraj, D. A. Gore, R. U. Nabar, H. Bolcskei, "An overview of MIMO communications - a key to gigabit wireless," *Proceedings of the IEEE*, vol. 92, no. 2, pp. 198 – 218, Feb. 2004.

[Rib07] C. Ribeiro, A. Gameiro, "Direct time-domain channel impulse response estimation for OFDM-based systems," in *Proc. IEEE Vehicular Technology Conference*, pp. 1082 – 1086, Baltimore, USA, Oct. 2007.

[Rin96] J. Rinne, M. Renfors, "Pilot Spacing in Orthogonal Frequency Division Multiplexing Systems on Practical Channels," *IEEE Transactions on Consumer Electronics*, vol. 42, no. 3, pp. 959 – 962, Nov. 1996.

[San96] M. Sandell, O. Edfors, "*A Comparative Study of Pilot-Based Channel Estimators for Wireless OFDM*," Lulea University of Technology, Lulea, Sweden, Sept. 1996.

[Sch05] D. Schafhuber, G. Matz, "MMSE and adaptive prediction of time-varying channels for OFDM systems," *IEEE Transactions on Wireless Communications*, vol. 4, no. 2, pp. 593 – 602, March 2005.

[Sim04] O. Simeone, Y. Bar-Ness, U. Spagnolini, "Pilot-based channel estimation for OFDM systems by tracking the delay-subspace," *IEEE Transactions on Wireless Communications*, vol. 3, pp. 315 – 325, Jan. 2004.

[Ste02] M. Stege, P. Zillmann, G. Fettweis, "MIMO Channel Estimation with Dimension Reduction," in *Proc. IEEE International Symposium on Wireless Personal Multimedia Communications*, vol. 2, pp. 417 – 421, Honolulu, USA, Oct. 2002.

[Stu04] G. L. Stuber, J. R. Barry, S. W. McLaughlin, Y. Li, M. A. Ingram and T. G. Pratt, "Broadband MIMO-OFDM wireless communications," *Proceedings of the IEEE*, vol. 92, no. 2, pp. 271 – 294, Feb. 2004.

[Sun02] Y. Sun, X. Wang, K. Liu, "A Joint Channel Estimation and Unequal Error Protection Scheme for Video Transmission in OFDM Systems," in *Proc. IEEE International Conference on Image Processing*, vol. 1, pp. 549 – 552, Rochester, USA, Sept. 2002.

[Sun03] S. Sun, I. Wiemer, C. Ho, T. Tjhung, "Training sequence assisted channel estimation for MIMO OFDM," in *Proc. IEEE Wireless Communications and Networking Conference*, vol. 1, pp. 38 – 43, New Orleans, March 2003.

[Wan01] X. Wang, K. Liu, "OFDM Channel Estimation Based on Time-Frequency Polynomial Model of Fading Multipath Channel," in *Proc. IEEE Vehicular Technology Conference*, vol. 1, pp. 460 – 464, Atlantic City, USA, Oct. 2001.

[Wan03] D. Wang, G. Zhu, Z. Hu, "A Combined Channel Estimation in Time-Frequency Domain for OFDM System in Mobile Channel," in *Proc. IEEE International Symposium on Personal, Indoor and Mobile Radio Communications,* vol. 1, pp. 940 –944, Beijing, China, Sept. 2003.

[Wei04] S. Weifeng, K. Liu, "Differential Space–Frequency Modulation for MIMO-OFDM Systems via a smooth Logical Channel," in *Proc. IEEE Global Telecommunications Conference*, vol. 2, pp. 913 – 917, San Francisco, USA, Dec. 2004.

[Won01] C. Wong, C. Law, Y. Guan, "Channel Estimator for OFDM Systems with 2-Dimensional Filtering in the Transform Domain," in *Proc. IEEE Vehicular Technology Conference*, vol. 1, pp. 717 – 721, Rhodes, Greece, May 2001.

[Won04] T. Wong, B. Park, "Training Sequence Optimization in MIMO Systems with Colored Interference," *IEEE Transactions on Communications*, vol. 52, no. 11, pp. 1939 – 1947, Nov. 2004.

[Xie03] Y. Xie, C. Georghiades, "Two EM-type channel estimation algorithms for OFDM with transmitter diversity," *IEEE Transactions on Communications*, vol. 51, no. 1, pp. 106 – 115, January 2003.

[Yan01] B. Yang, K. Letaief, R. Cheng, Z. Cao, "Channel estimation for OFDM transmission in multipath fading channels based on parametric channel modelling," *IEEE Transactions on Communications*, vol. 49, pp. 467 – 478, March 2001.

[Yeh00] Y. Yeh, S. Chen, "Efficient Channel Estimation Based on Discrete Cosine Transform," in *Proc. IEEE International Conference on Acoustics, Speech, and Signal Processing*, vol. 4, pp. 676 – 679, Hong Kong, China, April 2000.

[Yeh04] Y. Yeh, S. Chen, "DCT–Based Channel Estimation for OFDM Systems," in *Proc. IEEE International Conference on Communications*, vol. 4, pp. 2442 – 2446, Paris, France, June 2004.

[Yeh99] C. Yeh, Y. Lin, "Channel estimation using pilots tones in OFDM systems," *IEEE Transactions on Broadcasting*, vol. 45, pp. 400 – 409, Dec. 1999.

[Yu03] H. Yu, M. Kim, S. Lee, "Channel Estimation and Equalization for High Speed Mobile OFDM Systems," in *Proc. Asilomar Conference on Signals, Systems and Computers*, vol. 1, pp. 693 – 697, Monterey, Canada, Nov. 2003.

[Yuc06] T. Yucek, H. Arslan, "Delay spread and time dispersion estimation for adaptive OFDM systems," in *Proc. Wireless Communications and Networking Conference*, vol.3, pp.1433 – 1438, Las Vegas, USA, 2006.

[Zha97] Y. Zhao, A. Huang, "A Novel Channel Estimation Method for OFDM Mobile Communication Systems Based on Pilot Signals and Transform-Domain Processing," in *Proc. IEEE Vehicular Technology Conference*, vol. 3, pp. 2089 – 2093, Phoenix, USA, May 1997.

CHAPTER 5

CHANNEL ESTIMATION FOR MIMO-OFDM SYSTEMS

In this chapter we propose a channel estimation scheme for the broadband MIMO OFDM systems. The design of the pilot sequences to explore the properties of the DFT opens way to the extraction of the CIR in the time-domain from the symbols carrying data and pilots from all transmit antennas. The pilot sequences we advocate allow the separation of the CIRs for the different channels from the data components when the symbols are transmitted over Rayleigh fading multipath channels and are robust against co-channel interference. The feasibility of our approach is substantiated by system simulation results obtained using BRAN broadband mobile wireless channel models.

5.1. Introduction to MIMO-OFDM Channel Estimation

Future mobile broadband applications will require reliable high data-rate wireless communication systems. In recent years, MIMO-OFDM transmission systems [Nee00], [Sam02], [Pau04] [Stu04], emerged as the scheme with the potential to fulfil these conditions, with bandwidth efficiency and robustness to frequency selective channels common in mobile personal communication systems.

The accurate extraction of the channel state information is crucial to realize the full potential of the MIMO-OFDM system. The performance of the channel estimator is vital for diversity combining, coherent detection and decoding, and resource allocation operations. The co-channel interference inherent to the system, where the received signal is the superposition of the signals transmitted simultaneous from the different antennas, puts an additional challenge on the design of the channel estimation algorithm.

Due to the time-variant nature of the channels involved in the transmission process, the channel estimation methods commonly found on commercial systems are pilot-based [802.11g], [802.16], [LTE], *i.e.* the channel information is extracted from known transmitted symbols that, although decreasing system efficiency since no data information is conveyed, provide better performance than blind methods.

In systems with a large number of transmit antennas, the pilots must be sent efficiently to minimize the decrease of the system's efficiency, but still enable the receiver to estimate all the channels accurately, with minimum co-channel interference.

The initial proposals for pilot-aided channel estimation schemes for MIMO-OFDM transformed the problem of estimating overlapping channels in the estimation of multiple Single-Input Single-Output (SISO) OFDM channels. This was achieved by allocating dedicated pilot sub-carriers to each transmit antenna. The receiver estimates each channel from the pilot sub-carriers belonging to each transmit antenna and then applies an interpolator to get the full channel estimate [Jeo00], [[Dow02]. This type of pilot allocation can be found in the fixed WIMAX standard [802.16d].

Although this type of pilot allocation simplifies the channel estimation, it presents some drawbacks. As the number of transmit antennas increase, the spectral efficiency lowers considerably since a large number of sub-carriers will be assigned exclusively to transmit pilots. Moreover, the fact that the pilot sub-carriers are not loaded in all but the transmit antenna for which the sub-carrier is allocated, increases the critical PAPR parameter [Dow03], that strongly impacts in the performance of the power amplifier.

A pilot-aided channel estimation scheme that attempted to minimize the co-channel interference was published in [Li99]. The proposed algorithm exhibits a high computational load. A simplified and enhanced algorithm, introducing a data-aided scheme for the data transmission mode, is presented in [Li02]. In [Ste05] overlapped pilots are proposed for channel estimation where different transmitters use the same pilot sub-carriers, avoiding the decrease in efficiency with increasing number of transmitters. However, the performance results are not very favourable. The topic attracted a significant attention and has been the focus of investigation in multiple publications [Shi04], [Zha05], [Zam07] and references therein.

The design of training symbols and pilot sequences with the ability to decouple the co-channel interference and minimize the channel estimation MSE for MIMO-OFDM was addressed in several publications [Li02], [Bar03], [Min06]. The use of different orthogonal sequences was addressed in several works. The use of Hadamard sequences was proposed in [Lei02], [Dow03]. The Golay sequences were considered in [Suh03] and complex exponential sequences were investigated in [Min02], [Aue03].

Most publications on the topic of training-signal or pilot-aided channel estimation use the FD LS estimates as the starting point for the analysis of the estimation algorithm or the design of the training sequence. It was established in the previous chapter that, fir SISO OFDM, a TD LS estimate could be obtained using a simple linear operation on the received signal, if the used pilot sequence fulfils certain conditions (training sequences were treated as particular pilot sequences with no data symbols in-between consecutive pilot sub-carriers).

In this chapter we develop MIMO-OFDM pilot sequence designs and associated channel estimation methods that succeed in extracting each CIR estimate with minimal computational load. Using different sub-carriers to convey the pilots for each transmit antenna or the same sub-carriers for all antennas, coded with different phase-shifting sequences, together with the result from the previous chapter, the algorithms separate the different CIRs and eliminate the co-channel interference under given conditions. The STC algorithm [Li99] and the TD LMMSE criterion [Edf96] are incorporated in the estimation scheme to improve the estimate with little or no added computational cost.

The remaining of the chapter is organized as follows. Section 5.2 briefly presents the baseband system model for MIMO-OFDM systems. The next section proposes low complexity algorithms for the three common pilot schemes that can be found in the literature. Section 5.4 presents several simulation results that validate the investigated algorithms and discusses the attained results. Finally, conclusions are drawn in Section 5.5.

5.2. MIMO-OFDM Baseband System Model

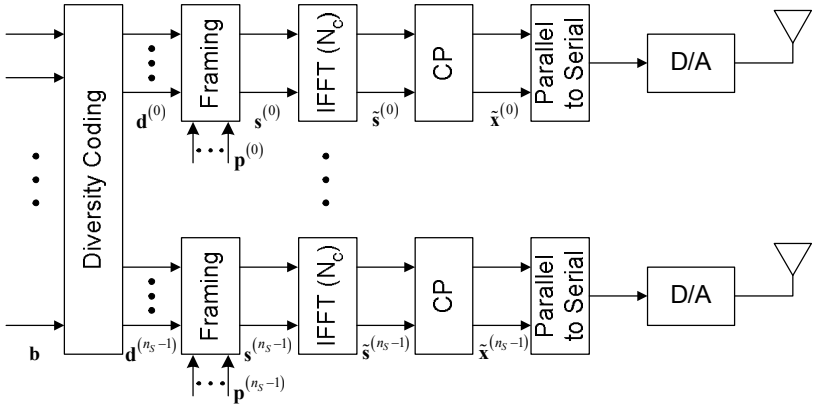

Figure 5.1 Pilot-aided MIMO-OFDM baseband transmitter model.

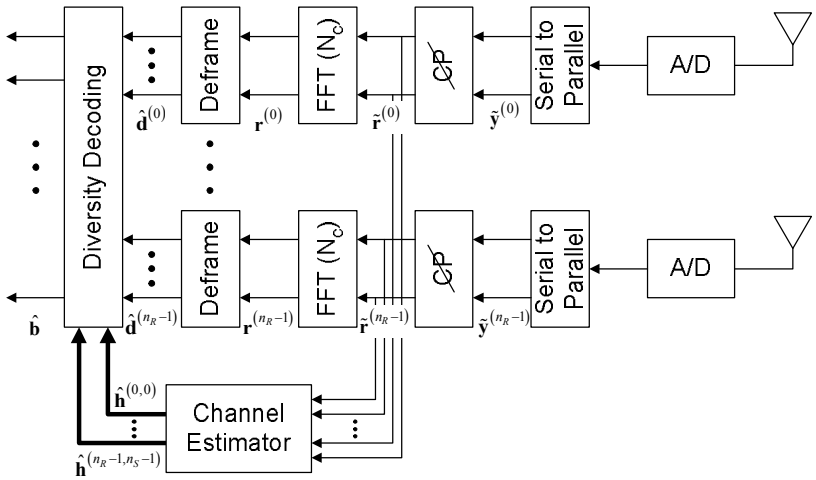

Figure 5.2. Pilot-aided MIMO-OFDM baseband receiver model.

Let's consider the MIMO-OFDM baseband transmitter with n_S transmit antennas depicted in Figure 5.1 and the associated baseband receiver with n_R receive antennas depicted in Figure 5.2. The binary data vector $\mathbf{b}$ is coded into n_S modulating vectors $\left\{\mathbf{d}^{(s)} : s = 0, \cdots, n_S - 1\right\}$. Using some sort of diversity coding [Fos96], [Ala98], [Wol98], [Tar99], the transmit antennas simultaneously send the n_S OFDM signals modulated by $\mathbf{d}^{(s)}$.

To assist in the channel estimation process, pilot symbols are multiplexed together with data symbols in each transmit path. Each path uses a different FD pilot vector $\mathbf{p}^{(s)}$. Vectors $\mathbf{d}^{(s)}$ and $\mathbf{p}^{(s)}$ contain non-zero values at disjoint positions (sub-carriers). The resulting FD signal transmitted by antenna s is $\mathbf{s}^{(s)} = \mathbf{d}^{(s)} + \mathbf{p}^{(s)}$.

The OFDM modulator present on each transmit path performs an N_C-points IDFT operation to transform the vector $\mathbf{s}^{(s)}$ to the TD vector $\tilde{\mathbf{s}}^{(s)}$. An L_p samples long CP is prefixed to each of the n_S vectors $\tilde{\mathbf{s}}^{(s)}$. Antenna s TD transmitted vector $\tilde{\mathbf{x}}^{(s)}$ is,

$$\tilde{\mathbf{x}}^{(s)} = \mathbf{A}_{CP}\mathbf{F}^H\mathbf{s}^{(s)} = \mathbf{A}_{CP}\left(\tilde{\mathbf{d}}^{(s)} + \tilde{\mathbf{p}}^{(s)}\right), \tag{5.1}$$

where the TD vectors $\tilde{\mathbf{d}}^{(s)}$ and $\tilde{\mathbf{p}}^{(s)}$ collect, respectively, the components of data symbols and pilot symbols present in $\tilde{\mathbf{s}}^{(s)}$.

The transmission over uncorrelated wireless multipath channels results in a received signal vector $\tilde{\mathbf{y}}$ at receive antenna r consisting of n_S superimposed transmitted signal samples,

$$\tilde{\mathbf{y}}^{(r)} = \sum_{s=0}^{n_S-1}\tilde{\mathbf{y}}^{(r,s)} + \bar{\tilde{\mathbf{n}}} = \sum_{s=0}^{n_S-1}\tilde{\mathbf{H}}_{lin}^{(r,s)}\tilde{\mathbf{x}}^{(s)} + \bar{\tilde{\mathbf{n}}}. \tag{5.2}$$

The vector $\tilde{\mathbf{y}}^{(r,s)} = \tilde{\mathbf{H}}_{lin}^{(r,s)}\tilde{\mathbf{x}}^{(s)}$ represents the contribution from transmit antenna s to the received signal; $\tilde{\mathbf{H}}_{lin}^{(r,s)}$ is the $(N_C+L)\times(N_C+L)$ lower triangular Toeplitz channel convolution matrix with first column $\left[\left(\tilde{\mathbf{h}}^{(r,s)}\right)^T \ \mathbf{0}_{1\times N_C}\right]^T$, where $\tilde{\mathbf{h}}^{(r,s)}$ is the column L_p-vector with the discrete-time CIR from transmit antenna s to receive antenna r and $\mathbf{0}_{1\times N_C}$ is a null N_C-vector.

With the assumption that the signals in the receive antennas are mutually uncorrelated, that transmission occurs over multipath Rayleigh fading wireless channels, whose model was defined in Chapter 2, and that the CIR remains constant for the duration of one OFDM symbol, the channel estimation at the receiver will be independent for all channels and, in the following, the receive antenna index will be dropped for notation simplicity.

The OFDM demodulator in each receiving path starts by removing the CP from each symbol. The resulting vector for symbols with pilots and data is,

$$\begin{aligned}\tilde{\mathbf{r}} = \mathbf{R}_{CP}\tilde{\mathbf{y}} &= \sum_{s=0}^{n_S-1}\mathbf{R}_{CP}\tilde{\mathbf{H}}_{lin}^{(s)}\mathbf{A}_{CP}\left(\tilde{\mathbf{d}}^{(s)} + \tilde{\mathbf{p}}^{(s)}\right) + \mathbf{R}_{CP}\bar{\tilde{\mathbf{n}}} \\ &= \sum_{s=0}^{n_S-1}\tilde{\mathbf{H}}_{circ}^{(s)}\left(\tilde{\mathbf{d}}^{(s)} + \tilde{\mathbf{p}}^{(s)}\right) + \tilde{\mathbf{n}} = \sum_{s=0}^{n_S-1}\tilde{\mathbf{r}}^{(s)} + \tilde{\mathbf{n}}\end{aligned}, \tag{5.3}$$

where $\tilde{\mathbf{r}}^{(s)} = \tilde{\mathbf{H}}_{circ}^{(s)}\left(\tilde{\mathbf{d}}^{(s)} + \tilde{\mathbf{p}}^{(s)}\right)$ represents the contribution from transmit antenna s to the received vector and $\tilde{\mathbf{H}}_{circ}^{(s)} = \mathbf{R}_{CP}\tilde{\mathbf{H}}_{lin}^{(s)}\mathbf{A}_{CP}$ is the $N_C \times N_C$ circulant matrix for channel s, with circulant vector $\left[\left(\tilde{\mathbf{h}}^{(s)}\right)^T \quad \mathbf{0}_{1\times(N_C-L)}\right]^T$. The n_R vectors $\tilde{\mathbf{r}}^{(s)}$ are fed to the channel estimation block. Each of these vectors is independently transformed to FD with a DFT operation. The resulting FD column N_C-vector can be expressed as,

$$\mathbf{r} = \mathbf{F}\tilde{\mathbf{r}} = \sum_{s=0}^{n_S-1}\mathbf{Q}^{(s)}\left(\mathbf{d}^{(s)} + \mathbf{p}^{(s)}\right) + \mathbf{n}, \tag{5.4}$$

where $\mathbf{Q}^{(s)}$ is the $N_C \times N_C$ diagonal matrix whose diagonal elements are the CFR vector $\mathbf{h}^{(s)}$ and $\mathbf{n}$ is the FD noise vector.

The de-framing block in each receive path separates the signals in the sub-carriers conveying pilots and data symbols. The signals in the data sub-carriers are fed to the diversity decoding block along with the $n_R n_S$ channel estimate vectors $\hat{\mathbf{h}}^{(r,s)}$ to generate the estimated data vector $\hat{\mathbf{b}}$.

5.3. TD Pilot-Aided Channel Estimation for MIMO-OFDM

The channel estimation algorithm must estimate the $n_S n_R$ channels from the receive antennas' signals. The proposed methods estimate the channels from the symbols carrying pilots and data (the training sequence is a particular case and the results can be easily extended to it). All the processing required to estimate the CIR is performed immediately on the TD received vector $\tilde{\mathbf{r}}$, eliminating the need to go from TD to FD and back to TD to finally obtain the CIR estimate [Li99], [Li02]. The proposed algorithms have very low computational load and no performance trade-offs. Under given conditions, the co-channel interference is entirely eliminated. Data-aided channel estimation algorithms [Li02] can be incorporated to further improve the algorithms' performance.

In pilot-aided channel estimation schemes for OFDM with multiple transmit antennas, 3 pilot schemes are commonly found in commercial systems.

In the overlapping pilot scheme, the transmitter uses the same symbols and the same sub-carriers to transmit pilots from all transmit antennas. To reduce the co-channel interference caused by the superposition of the signals from the different transmit antennas at the receiving antennas, the pilot sequences for each antenna are coded; in the frequency-multiplexed scheme, the transmitter uses the same symbols to convey pilots from all transmit

antennas, using different sets of sub-carriers for different antennas; in the symbol-multiplexed scheme, the transmitter uses different symbols to convey pilots from different transmit antennas;

5.3.1 Channel estimation for overlapping scheme

Consider the set of regularly spread sub-carriers $\wp$, dedicated to convey pilots,

$$\wp = \left\{k_{ini}, k_{ini} + N_f, k_{ini} + 2N_f, \cdots, k_{ini} + N_C - N_f\right\} \tag{5.5}$$

where k_{ini} is index of the first pilot-carrying sub-carrier with $k_{ini} \in \left\{0, \cdots, N_f - 1\right\}$ and the pilot distance N_f can range from 1 (particular case where all sub-carriers in the OFDM symbol are dedicated to transmit pilots – training symbol) to N_C, fulfilling the condition

$$\frac{N_C}{N_f n_S} \in \mathbb{N}. \tag{5.6}$$

The set $\wp$ is common to all transmit antennas (pilot sub-carriers overlap in the receive antennas). This pilot scheme is depicted in Figure 5.3.

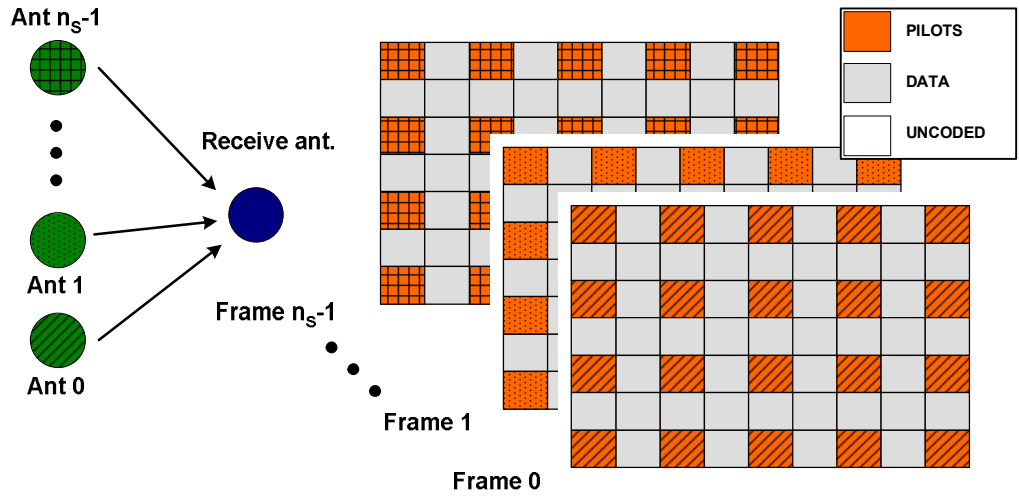

Figure 5.3. Overlapping pilot scheme for OFDM systems with multiple transmit antennas.

The system uses equal power pilots and distinct phase-shifted pilot sequences in each transmit antenna to allow the separation of the sequences in the receiving antennas. The k-th element of the column N_C-vector $\mathbf{p}^{(s)}$ is defined by,

$$p^{(s)}[k] = \sum_{m=0}^{N_t - 1} \delta\left[k - k_{ini} - mN_f\right] \exp\left[-j2\pi \frac{s}{n_S} m\right], \tag{5.7}$$

where $N_t = \frac{N_C}{N_f}$. As an example, for the case of $n_S = 4$ transmit antennas, the frequency-domain pilot vectors will be,

$$\begin{cases} \mathbf{p}^{(0)} = [+1 \;\; 0 \;\cdots\; 0 \;\; +1 \;\; 0 \;\cdots\; 0 \;\; +1 \;\; 0 \;\cdots\; 0 \;\; +1 \;\; 0 \;\cdots\; 0 \;\; +1 \;\cdots] \\ \mathbf{p}^{(1)} = [+1 \;\; 0 \;\cdots\; 0 \;\; -i \;\; 0 \;\cdots\; 0 \;\; -1 \;\; 0 \;\cdots\; 0 \;\; +i \;\; 0 \;\cdots\; 0 \;\; +1 \;\cdots] \\ \mathbf{p}^{(2)} = [+1 \;\; 0 \;\cdots\; 0 \;\; -1 \;\; 0 \;\cdots\; 0 \;\; +1 \;\; 0 \;\cdots\; 0 \;\; -1 \;\; 0 \;\cdots\; 0 \;\; +1 \;\cdots] \\ \mathbf{p}^{(3)} = [+1 \;\; 0 \;\cdots\; 0 \;\; +i \;\; 0 \;\cdots\; 0 \;\; -1 \;\; 0 \;\cdots\; 0 \;\; -i \;\; 0 \;\cdots\; 0 \;\; +1 \;\cdots] \end{cases} \tag{5.8}$$

This definition of pilot sequence gives rise to the corresponding TD vector $\tilde{\mathbf{p}}^{(s)}$, whose n-th element is,

$$\begin{aligned} \tilde{p}^{(s)}[n] &= N_C^{-1/2} \sum_{k=0}^{N_C-1} \sum_{m=0}^{N_t-1} \delta\left[k - k_{ini} - mN_f\right] \exp\left[-j2\pi \frac{s}{n_S} m\right] \exp\left[j \frac{2\pi}{N_C} kn\right] \\ &= N_C^{1/2} N_f^{-1} \exp\left[j \frac{2\pi}{N_C} k_{ini} n\right] \sum_{m=0}^{N_f-1} \delta\left[n - \frac{s}{n_S} N_t - mN_t\right] \end{aligned}, \tag{5.9}$$

or equivalently,

$$\begin{cases} \tilde{p}^{(0)}[n] = N_C^{1/2} N_f^{-1} \exp\left(j \frac{2\pi}{N_C} k_{ini} n\right) \sum_{m=0}^{N_f-1} \delta\left[n - mN_t\right] \\ \tilde{p}^{(1)}[n] = N_C^{1/2} N_f^{-1} \exp\left(j \frac{2\pi}{N_C} k_{ini} n\right) \sum_{m=0}^{N_f-1} \delta\left[n - \frac{1}{n_S} N_t - mN_t\right] \\ \vdots \\ \tilde{p}^{(n_S-1)}[n] = N_C^{1/2} N_f^{-1} \exp\left(j \frac{2\pi}{N_C} k_{ini} n\right) \sum_{m=0}^{N_f-1} \delta\left[n - \frac{n_S-1}{n_S} N_t - mN_t\right] \end{cases} . \tag{5.10}$$

Equation (5.10) shows that the transmit antennas' pilot sequences do not overlap in TD, allowing the separation of each transmit antenna's CIR on TD, as it will be demonstrated.

The n-th element of $\tilde{\mathbf{d}}^{(s)}$ can be expressed by,

$$\tilde{d}^{(s)}[n] = N_C^{-1/2} \sum_{\substack{k=0 \\ k \notin \wp}}^{N_C-1} d^{(s)}[k] \exp\left[j \frac{2\pi}{N_C} kn\right], \tag{5.11}$$

where $d^{(s)}[k]$ is the k-th element of $\mathbf{d}^{(s)}$ (complex data symbol conveyed by the k-th sub-carrier).

Replacing equation (5.9) in equation (5.3), the n-th element of $\tilde{\mathbf{r}}$ is,

$$\begin{aligned}
\tilde{r}[n] &= \sum_{s=0}^{n_S-1} \tilde{r}^{(s)}[n] + \tilde{n}[n] = \sum_{s=0}^{n_S-1}\sum_{l=0}^{L_p-1} \tilde{h}^{(s)}[l]\tilde{d}^{(s)}[n-l] + \tilde{n}[n] \\
&+ N_C^{1/2} N_f^{-1} \sum_{s=0}^{n_S-1}\sum_{l=0}^{L_p-1}\sum_{m=0}^{N_f-1} \tilde{h}^{(s)}[l] \exp\left[j\frac{2\pi}{N_C} k_{ini}(n-l) \right] \delta\left[n-l-\frac{s}{n_S}N_t - mN_t \right] \\
&= \sum_{s=0}^{n_S-1}\sum_{l=0}^{L_p-1} \tilde{h}^{(s)}[l]\tilde{d}^{(s)}[n-l] + \tilde{n}[n] \\
&+ N_C^{1/2} N_f^{-1} \sum_{s=0}^{n_S-1}\sum_{m=0}^{N_f-1} \exp\left[j\frac{2\pi}{N_C} k_{ini}\left(mN_t + \frac{s}{n_S}N_t \right) \right] \tilde{h}^{(s)}\left[n-\frac{s}{n_S}N_t - mN_t \right] \\
&= \sum_{s=0}^{n_S-1}\sum_{l=0}^{L_p-1} \tilde{h}^{(s)}[l]\tilde{d}^{(s)}[n-l] + \tilde{n}[n] \\
&+ N_C^{1/2} N_f^{-1} \sum_{m=0}^{N_f-1} \exp\left[j\frac{2\pi}{N_C} k_{ini} mN_t \right] \tilde{h}^{(0)}[n-mN_t] \\
&+ N_C^{1/2} N_f^{-1} \sum_{m=0}^{N_f-1} \exp\left[j\frac{2\pi}{N_C} k_{ini}\left(mN_t + \frac{1}{n_S}N_t \right) \right] \tilde{h}^{(1)}\left[n-\frac{1}{n_S}N_t - mN_t \right] + \cdots \\
&+ N_C^{1/2} N_f^{-1} \sum_{m=0}^{N_f-1} \exp\left[j\frac{2\pi}{N_C} k_{ini}\left(mN_t + \frac{n_S-1}{n_S}N_t \right) \right] \tilde{h}^{(n_S-1)}\left[n-\frac{n_S-1}{n_S}N_t - mN_t \right]. \quad (5.12)
\end{aligned}$$

Equation (5.12) puts in evidence that antenna r received signal is the sum of three distinct components: the data vectors $\tilde{\mathbf{d}}^{(s)}$ and pilot vectors $\tilde{\mathbf{p}}^{(s)}$, transmitted over its channels, and the AWGN. Looking carefully at the component dependent on the pilot vectors, it becomes clear that it is made-up of N_f frequency-shifted and scaled replicas of each of the n_S CIR, corresponding to the n_S channels that link the transmit antennas with the considered receive antenna. Moreover, the replicas of each CIR are separated by N_t samples and transmit antenna s CIR replicas are time-shifted $N_t \frac{s}{n_S}$ samples from the reference position mN_t, $m \in \{0, \cdots, N_f - 1\}$.

Figure 5.4 shows an example of a TD received vector $\tilde{\mathbf{r}}$ when $n_S = 4$ antennas transmit one symbol carrying only pilots (data sub-carriers are not loaded) over independent BRAN-A model multipath channels [BRAN]. The top plot represents the overlapping of the signals from all transmit antennas in one receive antenna. The four lower plots show how the CIR replicas corresponding to each transmit antenna are phase-shifted and can be separated from the overall signal. It gives a clear image of the condition that each CIR must fulfil so that consecutive replicas do not overlap.

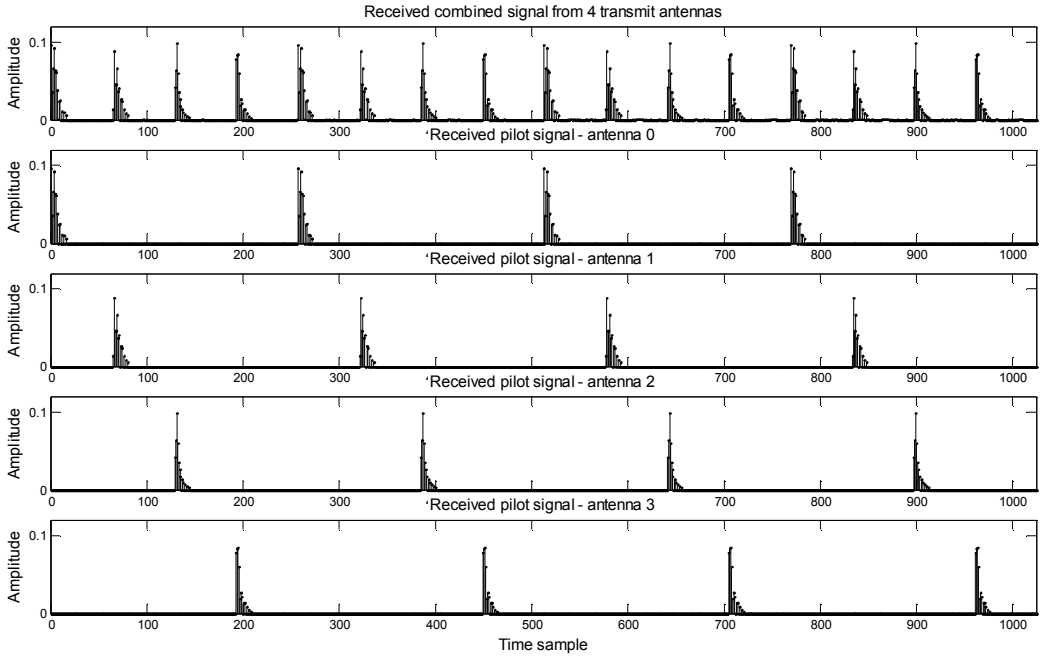

Figure 5.4. Decomposition of the combined received symbol (pilots only) for $n_S = 4$ transmit antennas.

Given the transmit antenna s maximum channel delay spread, $\tau_{\max}^{(s)}$, and the system's sampling interval, Δt, the minimum pilot distance that can be used without overlap of adjacent CIR replicas, thus enabling the best performance of the channel estimator, can be expressed as

$$N_f \leq \frac{N_C \Delta t}{n_S \tau_{\max}^{(s)}}. \tag{5.13}$$

As it will be demonstrated, if the condition in (5.13) is verified the co-channel interference will be completely eliminated. Otherwise, the overlapping of consecutive replicas will cause distortion in the estimation process and impose an MSE floor on the estimate.

Considering that the condition presented by (5.13) is fulfilled, the transmit antenna s CIR estimate vector $\hat{\tilde{\mathbf{h}}}^{(s)}$ can be obtained immediately from the TD received vector $\tilde{\mathbf{r}}$, similarly to the SISO case presented in the previous chapter,

$$
\begin{aligned}
\hat{\tilde{h}}^{(s)}[n] &= \begin{cases} \sum_{q=0}^{N_f-1} \exp\left[-j\frac{2\pi}{N_C}k_{ini}\left(qN_t+\frac{s}{n_S}N_t\right)\right]\tilde{r}\left[n+\frac{s}{n_S}N_t+qN_t\right], & n=0,1,\cdots,\frac{N_t}{n_S}-1 \\ 0, \quad remaining \end{cases} \\
&= \left(u[n]-u\left[n-\frac{N_t}{n_S}+1\right]\right)\sum_{q=0}^{N_f-1}\exp\left[-j\frac{2\pi}{N_C}k_{ini}\left(qN_t+\frac{s}{n_S}N_t\right)\right]\tilde{r}\left[n+\frac{s}{n_S}N_t+qN_t\right] \\
&= \left(u[n]-u\left[n-\frac{N_t}{n_S}+1\right]\right)\times \\
&\left(\begin{array}{l} N_C^{1/2}N_f^{-1}\sum_{q=0}^{N_f-1}\sum_{s=0}^{n_S-1}\sum_{m=0}^{N_f-1}\exp\left[-j\frac{2\pi}{N_C}k_{ini}\left(qN_t-mN_t\right)\right]\tilde{h}^{(s)}[n-qN_t+mN_t] \\ +\sum_{q=0}^{N_f-1}\exp\left[-j\frac{2\pi}{N_C}k_{ini}\left(qN_t+\frac{s}{n_S}N_t\right)\right]\tilde{n}\left[n+\frac{s}{n_S}N_t+qN_t\right] \\ +\sum_{q=0}^{N_f-1}\sum_{s=0}^{n_S-1}\sum_{l=0}^{L_p-1}\exp\left[-j\frac{2\pi}{N_C}k_{ini}\left(qN_t+\frac{s}{n_S}N_t\right)\right]\tilde{h}^{(s)}[l]\tilde{d}^{(s)}\left[n+\frac{s}{n_S}N_t+qN_t-l\right] \end{array}\right) \\
&= \begin{cases} \tilde{h}^{(s)}[n]+\sum_{q=0}^{N_f-1}\exp\left[-j\frac{2\pi}{N_C}k_{ini}\left(qN_t+\frac{s}{n_S}N_t\right)\right]\tilde{n}\left[n+\frac{s}{n_S}N_t+qN_t\right], & n=0,1,\cdots,\frac{N_t}{n_S}-1 \\ 0, \quad remaining \end{cases}
\end{aligned}
\qquad ,(5.14)
$$

where $u[n]$ is the unit step function. The operation in (5.14) estimates all n_S CIR and must be repeated for all n_R receive antennas. The result in (5.14) is possible because the data dependent component was eliminated, considering that,

$$
\begin{aligned}
&\sum_{q=0}^{N_f-1}\sum_{s=0}^{n_S-1}\sum_{l=0}^{L_p-1}\exp\left[-j\frac{2\pi}{N_C}k_{ini}\left(qN_t+\frac{s}{n_S}N_t\right)\right]\tilde{h}^{(s)}[l]\tilde{d}^{(s)}\left[n+\frac{s}{n_S}N_t+qN_t-l\right] \\
&= N_C^{-1/2}\sum_{s=0}^{n_S-1}\sum_{l=0}^{L_p-1}\left(\begin{array}{l} \tilde{h}^{(s)}[l]\exp\left[-j\frac{2\pi}{N_C}k_{ini}\frac{s}{n_S}N_t\right] \\ \times\sum_{\substack{k=0 \\ k\notin\wp}}^{N_C-1}d^{(s)}[k]\exp\left[j\frac{2\pi}{N_C}k\left(n+\frac{s}{n_S}N_t-l\right)\right]\sum_{q=0}^{N_f-1}\exp\left[j\frac{2\pi}{N_f}q\left(k-k_{ini}\right)\right] \end{array}\right)=0
\end{aligned}
\qquad .(5.15)
$$

The CIR estimate resulting of (5.14) is the equivalent of the TD LS CIR estimate for the SISO-OFDM system introduced in the previous chapter. Consider a constant envelope modulation (though it can be easily extended for any modulation) with transmit power equally distributed among the n_S antennas, $E\left\{\left|s^{(s)}[k]\right|^2\right\}=1/n_S$. Pilot and data sub-carriers are transmitted with equal power. Assuming that the noise in the TD samples is *iid*, the noise variance in (5.14) is σ_n^2/n_S, resulting in the channel estimation MSE,

$$\sigma^2_{e,INI} = N_f \sigma^2_n \,. \tag{5.16}$$

This initial estimate can be improved by incorporating other TD algorithms at little or no added computational load. With the knowledge that the CIR energy is concentrated in a small set of taps, the significant tap catching (STC) scheme [Li99] lowers the channel estimation MSE considerably. Further improvement is provided by the TD linear MMSE (LMMSE) filter [Edf96], if the channel correlation and noise variance are known a-priori (due to the CIR energy concentration, the estimation of these parameter is quite simpler in TD, when compared to FD).

5.3.2 Channel estimation for frequency-multiplexed scheme

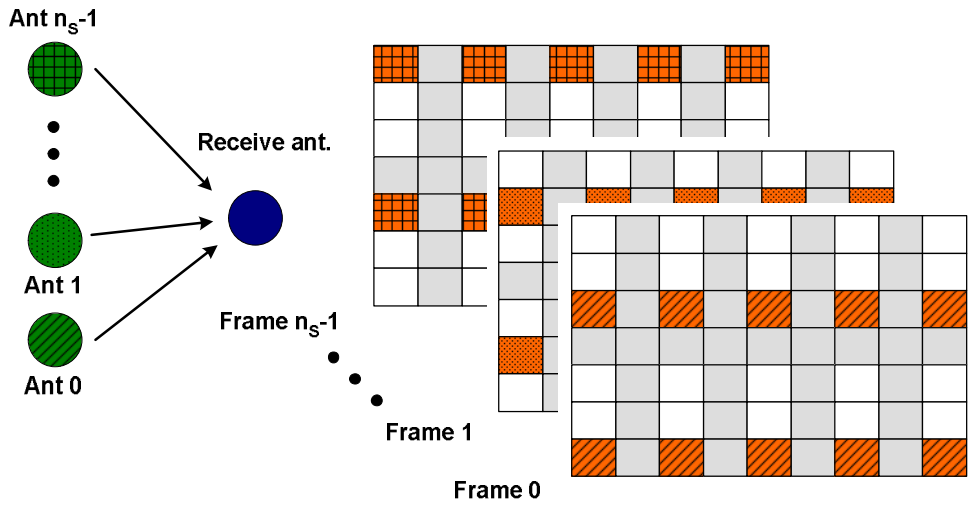

Figure 5.5. Frequency-multiplexed pilot scheme for OFDM systems with multiple transmit antennas.

Consider the set of regularly spread sub-carriers $\wp^{(s)}$, dedicated to convey pilots,

$$\wp^{(s)} = \left\{ k_{ini}^{(s)}, k_{ini}^{(s)} + N_f, k_{ini}^{(s)} + 2N_f, \cdots, k_{ini}^{(s)} + N_C - N_f \right\} \tag{5.17}$$

where $k_{ini}^{(s)}$ is index of the first pilot-carrying sub-carrier for the s transmit antenna, with $k_{ini}^{(s)} \in \{0, \cdots, N_f - 1\}$ and $k_{ini}^{(s)} = k_{ini}^{(w)} \Rightarrow s = w$. The n_S pilot vectors $\mathbf{p}^{(s)}$ contain non-zero values at disjoint positions (sub-carriers) and the pilot sub-carriers of any transmit antenna are not loaded (either with data symbols or pilots) on the remaining ones. This pilot scheme is depicted in Figure 5.5. The pilot distance N_f is common to all pilot vectors and can range from 1 to N_C, fulfilling the condition

$$\frac{N_C}{N_f} \in \mathbb{N}. \tag{5.18}$$

In this pilot scheme, the $n_S n_R$ channels can be estimated by the receiver in the FD as the pilot sub-carriers for each transmit antenna are distinct. After obtaining the channel estimates at the pilot positions, an interpolator is required to estimate the remaining sub-carriers data carry data symbols. As introduced in the previous chapter, the DFT-based interpolation is one of the most common interpolators, presenting a good trade-off between complexity and performance, mostly due to the use of the FFT algorithm.

Let's consider that the system uses equal power pilots on all transmit antennas with constant value (without loss of generality, will consider unit valued pilots in the analysis). The k-th element of the column N_C-vector $\mathbf{p}^{(s)}$ is defined by,

$$p^{(s)}[k] = \sum_{m=0}^{N_t-1} \delta\left[k - k_{ini}^{(s)} - mN_f\right], \tag{5.19}$$

where $N_t = \frac{N_C}{N_f}$.

This definition of pilot sequence gives rise to the corresponding TD vector $\tilde{\mathbf{p}}^{(s)}$, whose n-th element for transmit antenna s is,

$$\begin{aligned} \tilde{p}^{(s)}[n] &= N_C^{-1/2} \sum_{k=0}^{N_C-1} \sum_{m=0}^{N_t-1} \delta\left[k - k_{ini}^{(s)} - mN_f\right] \exp\left[j\frac{2\pi}{N_C}kn\right] \\ &= N_C^{1/2} N_f^{-1} \exp\left[j\frac{2\pi}{N_C}k_{ini}^{(s)}n\right] \sum_{m=0}^{N_f-1} \delta\left[n - mN_t\right] \end{aligned}. \tag{5.20}$$

Unlike the overlapping pilot scheme, equation (5.20) shows that the transmit antennas' pilot sequences overlap in TD. As it will demonstrated, the frequency shifting of each CIR replica will be explored to separate each transmit antenna's CIR from the TD superimposed received symbols carrying both pilots and data.

The n-th element of $\tilde{\mathbf{d}}^{(s)}$ can be expressed by,

$$\tilde{d}^{(s)}[n] = N_C^{-1/2} \sum_{\substack{k=0 \\ k \notin \wp}}^{N_C-1} d^{(s)}[k] \exp\left[j\frac{2\pi}{N_C}kn\right], \tag{5.21}$$

where $d^{(s)}[k]$ is the k-th element of $\mathbf{d}^{(s)}$ (complex data symbol conveyed by the k-th sub-carrier of transmit antenna s) and the set $\wp$ results from the union of the sets of pilot sub-carriers from all transmit antennas, $\wp = \wp^{(0)} \cup \wp^{(1)} \cup \cdots \cup \wp^{(n_S-1)}$.

Replacing equation (5.20) in equation (5.3), the n-th element of $\tilde{\mathbf{r}}$ is,

$$\begin{aligned}
\tilde{r}[n] &= \sum_{s=0}^{n_S-1} \tilde{r}^{(s)}[n] + \tilde{n}[n] = \sum_{s=0}^{n_S-1} \sum_{l=0}^{L_p-1} \tilde{h}^{(s)}[l]\tilde{d}^{(s)}[n-l] + \tilde{n}[n] \\
&+ N_C^{1/2} N_f^{-1} \sum_{s=0}^{n_S-1} \sum_{l=0}^{L_p-1} \sum_{m=0}^{N_f-1} \tilde{h}^{(s)}[l] \exp\left[j\frac{2\pi}{N_C} k_{ini}^{(s)} (n-l) \right] \delta[n-l-mN_t] \\
&= \sum_{s=0}^{n_S-1} \sum_{l=0}^{L_p-1} \tilde{h}^{(s)}[l]\tilde{d}^{(s)}[n-l] + \tilde{n}[n] \\
&+ N_C^{1/2} N_f^{-1} \sum_{s=0}^{n_S-1} \sum_{m=0}^{N_f-1} \exp\left[j\frac{2\pi}{N_C} k_{ini}^{(s)} mN_t \right] \tilde{h}^{(s)}[n-mN_t] \\
&= \sum_{s=0}^{n_S-1} \sum_{l=0}^{L_p-1} \tilde{h}^{(s)}[l]\tilde{d}^{(s)}[n-l] + \tilde{n}[n] \\
&+ N_C^{1/2} N_f^{-1} \sum_{m=0}^{N_f-1} \exp\left[j\frac{2\pi}{N_C} k_{ini}^{(0)} mN_t \right] \tilde{h}^{(0)}[n-mN_t] + \cdots \\
&+ N_C^{1/2} N_f^{-1} \sum_{m=0}^{N_f-1} \exp\left[j\frac{2\pi}{N_C} k_{ini}^{(n_S-1)} mN_t \right] \tilde{h}^{(n_S-1)}[n-mN_t]
\end{aligned} \quad . \tag{5.22}$$

Looking carefully at the component dependent on the pilot vectors in equation (5.22), it becomes clear that it is made-up of N_f phase-shifted and scaled replicas of each of the n_S CIR, corresponding to the n_S channels that link the transmit antennas with the considered receive antenna. The CIR replicas from different channels overlap and the replicas of each CIR are separated by N_t samples.

Given the transmit antenna s maximum channel delay spread, $\tau_{\max}^{(s)}$, and the system's sampling interval, Δt, the minimum pilot distance that can be used without overlap of adjacent CIR replicas from the same channel, thus enabling the best performance of the channel estimator, can be expressed as

$$N_f \leq \frac{N_C \Delta t}{\tau_{\max}^{(s)}}. \tag{5.23}$$

As it will be demonstrated, if the condition in (5.23) is verified the will be no aliasing of the sampled channel. Otherwise, the overlapping of consecutive CIR replicas will cause distortion in the estimation process and impose an MSE floor on the estimate.

Considering that the condition presented by (5.23) is fulfilled, the transmit antenna s CIR estimate vector $\hat{\tilde{\mathbf{h}}}^{(s)}$ can be obtained immediately from the TD received vector $\tilde{\mathbf{r}}$ with no co-channel interference,

$$\begin{aligned}
\hat{\tilde{h}}^{(s)}[n] &= \begin{cases} \sum_{q=0}^{N_f-1} \exp\left[-j\frac{2\pi}{N_C} k_{ini}^{(s)} q N_t\right] \tilde{r}[n+qN_t], & n=0,1,\cdots,N_t-1 \\ 0, & \textit{remaining} \end{cases} \\
&= \left(u[n]-u[n-N_t+1]\right) \sum_{q=0}^{N_f-1} \exp\left[-j\frac{2\pi}{N_C} k_{ini}^{(s)} q N_t\right] \tilde{r}[n+qN_t] \\
&= \left(u[n]-u[n-N_t+1]\right)\times \\
&\left(\begin{array}{l} N_C^{1/2} N_f^{-1} \sum_{q=0}^{N_f-1} \sum_{z=0}^{n_S-1} \sum_{m=0}^{N_f-1} \exp\left[-j\frac{2\pi}{N_C} N_t \left(q k_{ini}^{(s)} - m k_{ini}^{(z)}\right)\right] \tilde{h}^{(z)}[n-qN_t+mN_t] \\ + \sum_{q=0}^{N_f-1} \exp\left[-j\frac{2\pi}{N_C} k_{ini}^{(s)} q N_t\right] \tilde{n}[n+qN_t] \\ + \sum_{q=0}^{N_f-1} \sum_{s=0}^{n_S-1} \sum_{l=0}^{L_p-1} \exp\left[-j\frac{2\pi}{N_C} k_{ini}^{(s)} q N_t\right] \tilde{h}^{(s)}[l] \tilde{d}^{(s)}[n+qN_t-l] \end{array} \right. \\
&= \begin{cases} \tilde{h}^{(s)}[n] + \sum_{q=0}^{N_f-1} \exp\left[-j\frac{2\pi}{N_C} k_{ini}^{(s)} q N_t\right] \tilde{n}[n+qN_t], & n=0,1,\cdots,N_t-1 \\ 0, & \textit{remaining} \end{cases}
\end{aligned} \quad . \quad (5.24)$$

The operation in (5.24) estimates all n_S CIR and must be repeated for all n_R receive antennas. Similarly to the previous section, the result in (5.24) is possible because the data dependent component was eliminated, considering that,

$$\begin{aligned}
&\sum_{q=0}^{N_f-1} \sum_{s=0}^{n_S-1} \sum_{l=0}^{L_p-1} \exp\left[-j\frac{2\pi}{N_C} k_{ini}^{(s)} q N_t\right] \tilde{h}^{(s)}[l] \tilde{d}^{(s)}[n+qN_t-l] \\
&= N_C^{-1/2} \sum_{s=0}^{n_S-1} \sum_{l=0}^{L_p-1} \tilde{h}^{(s)}[l] \sum_{\substack{k=0 \\ k\notin\wp}}^{N_C-1} d^{(s)}[k] \exp\left[j\frac{2\pi}{N_C} k(n-l)\right] \sum_{q=0}^{N_f-1} \exp\left[j\frac{2\pi}{N_f} q\left(k-k_{ini}^{(s)}\right)\right] = 0
\end{aligned} \quad . \quad (5.25)$$

For the pilot dependent component, reminding the condition in (5.23), for $m \neq q \Rightarrow \tilde{h}^{(z)} = 0, \forall z \in \{0,\cdots,n_S-1\}$. When $m=q$, the pilot dependent component can be written as,

$$N_C^{1/2} N_f^{-1} \sum_{z=0}^{n_S-1} \tilde{h}^{(z)}[n] \sum_{q=0}^{N_f-1} \exp\left[-j\frac{2\pi}{N_C} N_t q \left(k_{ini}^{(s)} - k_{ini}^{(z)}\right)\right], \quad (5.26)$$

making it clear that for $z \neq s \Rightarrow \left(k_{ini}^{(s)} - k_{ini}^{(z)}\right) \neq 0 \wedge \left(k_{ini}^{(s)} - k_{ini}^{(z)}\right) \in \mathbb{N}$ and so equation (5.26) is null, leaving only the $\begin{cases} m = q \\ z = s \end{cases}$ case that justifies the result in (5.24).

The CIR estimate resulting of (5.24) is the equivalent of the TD LS CIR estimate for the SISO-OFDM system introduced in the previous chapter and the overlapping pilot scheme presented in the previous section.

Similarly to the previous section, let's consider a constant envelope modulation with transmit power equally distributed among the n_S antennas, $E\left\{\left|s^{(s)}[k]\right|^2\right\} = 1/n_S$. In this scheme, to achieve equal distribution of power among pilot and data sub-carriers, the pilots are transmitted with unit value, to compensate for the uncoded sub-carriers. This leads to the same overall pilot overhead and pilot power that the ones on the previous section. Assuming that the noise in the TD samples is *iid*, the noise variance in (5.24) is σ_n^2/n_S, resulting in same channel estimation MSE,

$$\sigma_{e,INI}^2 = N_f \sigma_n^2, \tag{5.27}$$

of the previous scheme. Much the same way, this initial estimate can be improved by using the knowledge that the CIR energy is concentrated in a small set of taps and implementing the STC scheme [Li99] or the TD LMMSE filter [Edf96], if the channel correlation and noise variance are known a-priori.

5.3.3 Channel estimation for symbol-multiplexed scheme

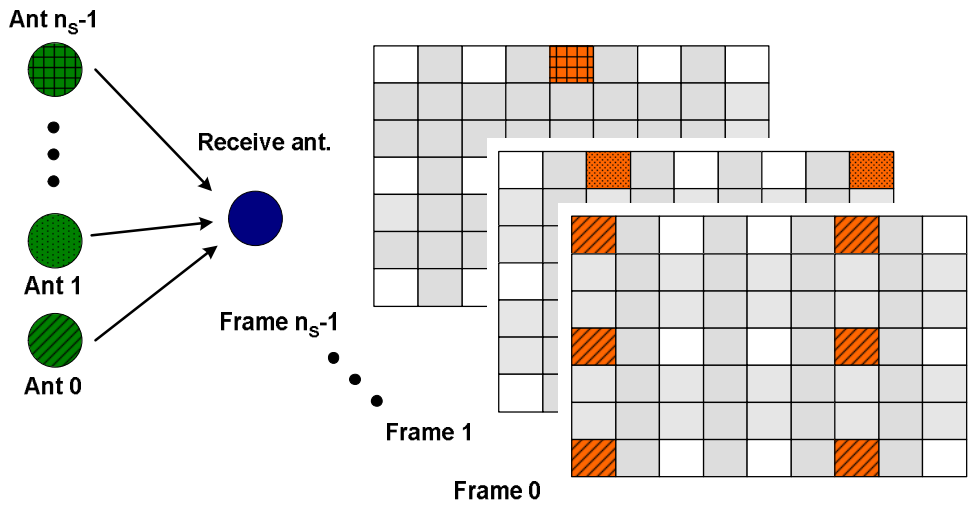

Figure 5.6. Symbol-multiplexed pilot scheme for OFDM systems with multiple transmit antennas.

Consider the set of regularly spread sub-carriers $\wp^{(s)}$, dedicated to convey pilots, identical to the previous section,

$$\wp^{(s)} = \left\{ k_{ini}^{(s)}, k_{ini}^{(s)} + N_f, k_{ini}^{(s)} + 2N_f, \cdots, k_{ini}^{(s)} + N_C - N_f \right\} \tag{5.28}$$

where $k_{ini}^{(s)}$ is index of the first pilot-carrying sub-carrier for the s transmit antenna, with $k_{ini}^{(s)} \in \left\{0, \cdots, N_f - 1\right\}$. Each pilot-carrying symbol conveys pilots from a single transmit antenna and the pilot-carrying sub-carriers on any transmit antenna are not loaded with data symbols on the remaining ones. This pilot scheme is depicted in Figure 5.6. If using the common FD channel estimation scheme, each channel is estimated using the corresponding pilot-carrying symbol.

Considering that the system uses equal power pilots on all transmit antennas with constant value, the FD and TD pilot vectors are defined by equations (5.19) and (5.20), respectively. The difference to the pilot scheme in the previous section is that there is no overlapping of pilot sequences in TD, as only one transmit antenna uses a particular symbol to multiplex its pilots (similarly to the SISO pilot-aided channel estimation scheme). Hence, this scheme is a particular case of the scheme in the previous section, where the CIR from the wanted channel needs only to be separated from the n_S superimposed data components (unlike the SISO scheme, where only one data component is superimposed).

The TD received vector for symbols carrying one pilot sequence and data is a simplification of (5.22),

$$\begin{aligned} \tilde{r}[n] = \sum_{s=0}^{n_S-1} \tilde{r}^{(s)}[n] + \tilde{n}[n] = \sum_{s=0}^{n_S-1} \sum_{l=0}^{L_p-1} \tilde{h}^{(s)}[l] \tilde{d}^{(s)}[n-l] + \tilde{n}[n] \\ + N_C^{1/2} N_f^{-1} \sum_{m=0}^{N_f-1} \exp\left[j \frac{2\pi}{N_C} k_{ini}^{(s)} m N_t \right] \tilde{h}^{(s)}[n - m N_t] \end{aligned}, \tag{5.29}$$

where it is clear that only N_f phase-shifted and scaled replicas of the CIR corresponding to the transmitted pilot sequence is present and the separation of the CIR replicas continues to be N_t samples.

The minimum pilot separation that enables the best performance of the channel estimator is expressed by (5.23). Fulfilling this condition, the TD LS estimate is a simplification of (5.24)

$$
\begin{aligned}
\hat{\tilde{h}}^{(s)}[n] &= \begin{cases} \sum_{q=0}^{N_f-1} \exp\left[-j\frac{2\pi}{N_C} k_{imi}^{(s)} q N_t\right] \tilde{r}[n+qN_t], & n=0,1,\cdots,N_t-1 \\ 0, & \textit{remaining} \end{cases} \\
&= \left(u[n]-u[n-N_t+1]\right)\times \\
&\left(\begin{array}{l} N_C^{1/2} N_f^{-1} \sum_{q=0}^{N_f-1}\sum_{m=0}^{N_f-1} \exp\left[-j\frac{2\pi}{N_C} N_t q k_{imi}^{(s)}\right] \tilde{h}^{(s)}[n-qN_t+mN_t] \\ + \sum_{q=0}^{N_f-1} \exp\left[-j\frac{2\pi}{N_C} k_{imi}^{(s)} q N_t\right] \tilde{n}[n+qN_t] \\ + \sum_{q=0}^{N_f-1}\sum_{s=0}^{n_S-1}\sum_{l=0}^{L_p-1} \exp\left[-j\frac{2\pi}{N_C} k_{imi}^{(s)} q N_t\right] \tilde{h}^{(s)}[l]\tilde{d}^{(s)}[n+qN_t-l] \end{array} \right) \\
&= \begin{cases} \tilde{h}^{(s)}[n] + \sum_{q=0}^{N_f-1} \exp\left[-j\frac{2\pi}{N_C} k_{imi}^{(s)} q N_t\right] \tilde{n}[n+qN_t], & n=0,1,\cdots,N_t-1 \\ 0, & \textit{remaining} \end{cases}
\end{aligned}
\quad . \qquad (5.30)
$$

The elimination of the data component in (5.30) is a particular case of equation (5.25) where

$$
\tilde{d}^{(s)}[n] = N_C^{-1/2} \sum_{\substack{k=0 \\ k\notin\wp^{(s)}}}^{N_C-1} d^{(s)}[k] \exp\left[j\frac{2\pi}{N_C} kn\right]. \qquad (5.31)
$$

Similarly to the previous section, considering a constant envelope modulation with transmit power equally distributed among the n_S antennas, $E\left\{\left|s^{(s)}[k]\right|^2\right\} = 1/n_S$, to achieve equal distribution of power among pilot and data sub-carriers, the pilots are transmitted with unit value.

In conclusion, the 3 pilot schemes yield the same channel estimation MSE defined by (5.27) for the same overall pilot overhead and pilot power. Due to the correspondence of results of the 3 pilot schemes, in the remaining of this chapter solely the overlapping pilot scheme is used.

5.3.4 Including the STC algorithm

The CIR energy of wireless multipath channels is commonly limited to a small set of taps. By identifying this set of significant taps and ignoring the remaining, we are removing noise from the channel estimate, thus improving it [Li02]. Considering the channel model introduced in Chapter 2, the CIR will only have L_p significant taps. Assuming that the set of significant taps is $\{L_p\}$, the initial channel estimate in (5.14) can be rewritten

$$\hat{\tilde{h}}^{(s)}[n]=\begin{cases}\sum_{q=0}^{N_f-1}\exp\left[-j\frac{2\pi}{N_C}k_{ini}\left(qN_t+\frac{s}{n_S}N_t\right)\right]\tilde{r}\left[n+\frac{s}{n_S}N_t+qN_t\right], & n\in\{L_p\}\\ 0, \quad remaining\end{cases}$$
$$=\begin{cases}\tilde{h}^{(s)}[n]+\sum_{q=0}^{N_f-1}\exp\left[-j\frac{2\pi}{N_C}k_{ini}\left(qN_t+\frac{s}{n_S}N_t\right)\right]\tilde{n}\left[n+\frac{s}{n_S}N_t+qN_t\right], & n\in\{L_p\}\\ 0, \quad remaining\end{cases} \quad (5.32)$$

By eliminating the noise in the non-significant taps, the noise variance in (5.32) is reduced to $\sigma_n^2\frac{L_pN_f}{N_C}$ and the resulting channel estimation MSE is,

$$\sigma_{e,STC}^2=\sigma_n^2\frac{n_SL_pN_f^2}{N_C}=\sigma_{e,INI}^2\frac{n_SL_pN_f}{N_C} \quad (5.33)$$

This MSE tends to the initial MSE when L_p goes to limiting condition $\frac{N_C}{n_SN_f}$. The channel estimation MSE achieved in [Li02] is the same as in (5.33) when $N_f=1$ (training symbol).

The use of the STC algorithm actually lowers the computational load by limiting the summation interval. An error floor will limit the performance for high values of SNR if the set $\{L_p\}$ is not properly estimated and some CIR energy is removed in the estimation process.

5.3.5 Including TD LMMSE filter

For low values of SNR, a significant improvement in the channel estimation can be achieved by using the TD LMMSE filter that minimizes the effect of the noise in the estimate.

Considering the channel model introduced in Chapter 2, where the resolvable paths and respective delays have values multiple of the OFDM system sampling interval, the TD MMSE filter $\tilde{\mathbf{W}}_{MMSE}$ is implemented by a diagonal matrix [Edf96] whose diagonal elements are defined by

$$\tilde{W}_{MMSE}[n,n]=\frac{R_{\tilde{h}\tilde{h}}[n,n]}{R_{\tilde{h}\tilde{h}}[n,n]+N_f^{-1}\sigma_n^2}, \quad (5.34)$$

where $\mathbf{R}_{\tilde{h}\tilde{h}}$ is the CIR diagonal correlation matrix. Because all paths of all channels are uncorrelated, the matrix will only have L_p non-zero values in the diagonal elements defined

by $\{L_p\}$. Therefore, the operation can be implemented simultaneously with the operation in (5.14),

$$\hat{\tilde{h}}^{(s)}[n] = \begin{cases} \dfrac{R_{\tilde{h}\tilde{h}}[n,n]}{R_{\tilde{h}\tilde{h}}[n,n] + N_f^{-1}\sigma_n^2} \displaystyle\sum_{q=0}^{N_f-1} \left[\begin{array}{l} \exp\left[-j\dfrac{2\pi}{N_C} k_{imi}\left(qN_t + \dfrac{s}{n_S} N_t \right) \right] \\ \times \tilde{r}\left[n + \dfrac{s}{n_S} N_t + qN_t \right] \end{array} \right], n \in \{L_p\} \\ 0, \quad remaining \end{cases} \quad (5.35)$$

$$= \begin{cases} \dfrac{R_{\tilde{h}\tilde{h}}[n,n]}{R_{\tilde{h}\tilde{h}}[n,n] + N_f^{-1}\sigma_n^2} \left[\tilde{h}^{(s)}[n] + \displaystyle\sum_{q=0}^{N_f-1} \left[\begin{array}{l} \exp\left[-j\dfrac{2\pi}{N_C} k_{imi}\left(qN_t + \dfrac{s}{n_S} N_t \right) \right] \\ \times \tilde{n}\left[n + \dfrac{s}{n_S} N_t + qN_t \right] \end{array} \right] \right], n \in \{L_p\} \\ 0, \quad remaining \end{cases}$$

The resulting channel estimation MSE [Edf96] is,

$$\sigma_{e,MMSE}^2 = \sigma_n^2 \frac{n_S N_f^2}{N_C} \sum_{l \in \{L_p\}} \frac{R_{\tilde{h}\tilde{h}}[l,l]}{R_{\tilde{h}\tilde{h}}[l,l] + N_C^{-1} n_S L_p N_f^2 \sigma_n^2}. \quad (5.36)$$

Observing (5.36), we can conclude that when SNR tends to infinity, $\sigma_{e,MMSE}^2 \to \sigma_{e,STC}^2$.

The use of LMMSE filter lowers the computational load by limiting the summation interval but requires additional calculations to estimate the channel correlation and noise variance.

5.4. Performance Evaluation

A simulation scenario was implemented using an Alamouti 2×1 OFDM system with $N_C = 1024$ QPSK modulated sub-carriers, sampling interval $\Delta t = 10ns$ and a CP with 200 samples. The transmitted OFDM symbols carried pilots and data using the proposed overlapping pilot structure, with a pilot separation $N_f = 4$. Since the investigated channel estimation schemes perform time-domain (sample-domain) estimation, the measurements presented in this section are only with respect to the symbols that carry both pilots and data. Channel estimation in the symbol domain that would involve estimating the channel's response of the symbols carrying only data is not considered.

The BRAN-A and BRAN-E channel models [BRAN] were used to simulate indoor ($50ns$ *rms* delay spread) and outdoor environments ($250ns$ *rms* delay spread), respectively.

Figure 5.7 shows the comparison between real and estimated channel's frequency response, when the transmitter sends pilot and data-carrying symbols through independent BRAN-A channels. The receiver's signal to noise ratio was set to $SNR = 10dB$ and the STC algorithm was used.

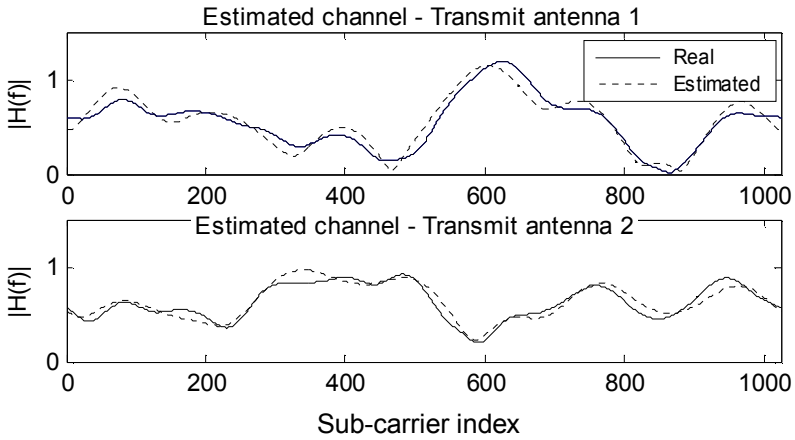

Figure 5.7. Comparison between real and estimated channel's frequency response. The solid line refers to the real channel while dashed line represents the estimated channel.

To validate the proposed method, BER and channel estimation simulations were performed using Eb/N0 values in the range of $0dB$ to $20dB$. The 3 channel estimation schemes presented in the previous section were simulated with both channel models.

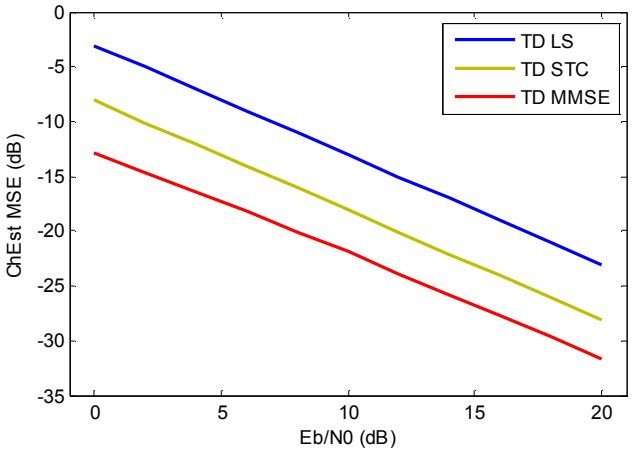

Figure 5.8. Channel estimation MSE (BRAN-A indoor channel).

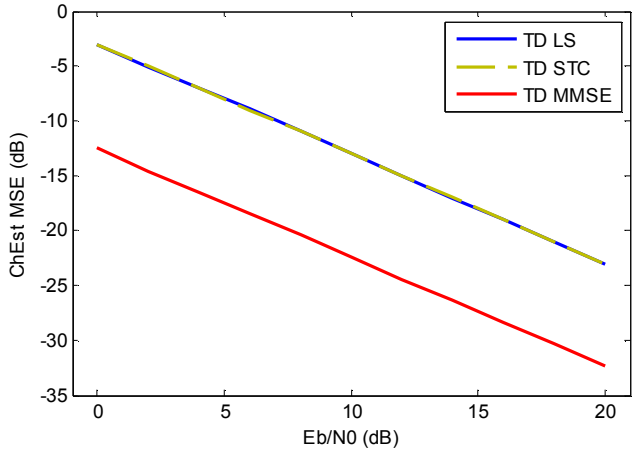

Figure 5.9. Channel estimation MSE (BRAN-E outdoor channel).

The normalized channel estimation MSE results are depicted in Figure 5.8 and Figure 5.9 , respectively for BRAN-A and BRAN-E channels. For both TD STC and TD MMSE methods, the perfect knowledge of the channels' PDP was used. As introduced in the previous section, the perfect knowledge of the channels' PDP allows the definition of the perfect TD windows, so that an error floor does not limit the performance of this method for high values of SNR. In addition, for TD MMSE algorithm, the real noise variance was also used so that the perfect filter is designed without mismatched between the filter parameters and the real ones (*c.f.* equation (5.34)).

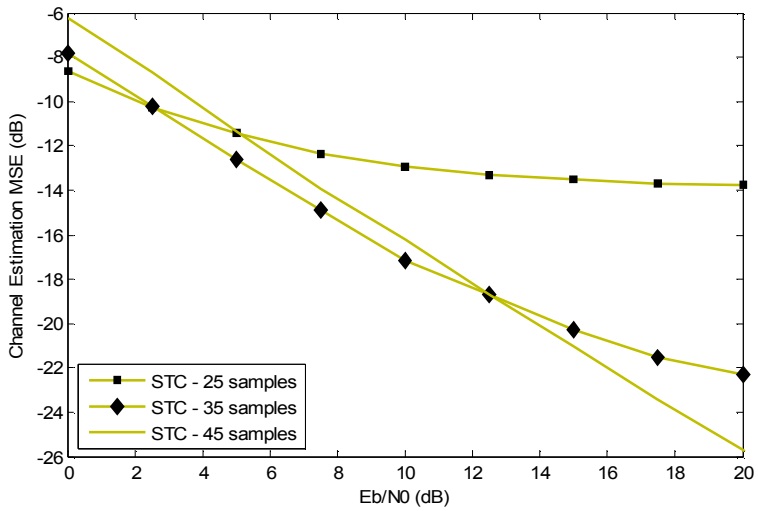

Figure 5.10. MSE for STC method as a function of the number of samples used in TD window.

To assess the performance of the STC method with fixed TD window, several simulations were performed using independent BRAN-A channels. Figure 5.10 presents the channel estimation MSE plots, when a TD window with a fixed number of consecutive samples is used (starting at sample 0), using Eb/N0 values in the range of 0*dB* to 20*dB*.

The utilization of the STC method with a fixed TD window implies a trade-off between the amount of distortion introduced by removing energy from significant channel taps and the amount of noise inputted to the estimation process. A MSE noise floor is present due to removing some of the channel's energy and it will be lower as the number of samples is increased (at the price of a worse performance for low values of SNR).

The BER results are depicted in Figure 5.11 and Figure 5.12, respectively for BRAN-A and BRAN-E channels.

On both scenarios, the TD LS and the TD MMSE methods present a consistent performance. The TD LS method always achieves the worst performance ($\approx 2dB$ degradation in the BER compared with the perfect CSI) due to the fact that it does not take advantage of the channel characteristics. In the opposite, the TD MMSE method always achieves the best performance, near the ideal situation. It has the ability of dealing with the increasing channel delay spread by always weighing the energy of channel taps vs. noise variance.

The performance of the TD STC method is closely dependent on the channel delay spread. Its performance is bond by the 2 previous methods. A channel with a short delay spread will result in the best performance (by having the CIR energy concentrated to just a few taps, most of the noise is eliminated in the estimation process). As the channel delay spread increases, the performance tends to that of the TD LS method.

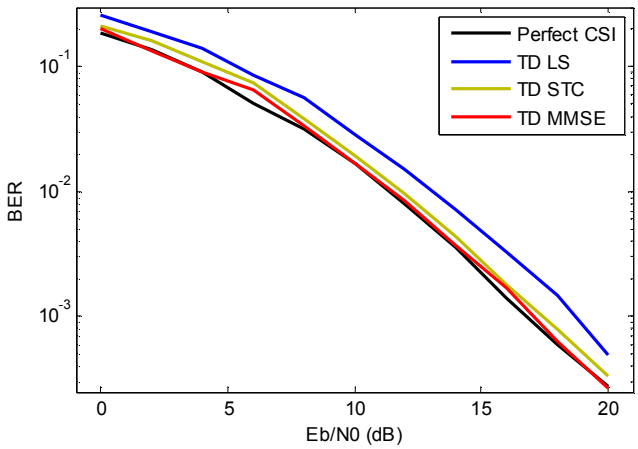

Figure 5.11. System BER performance (BRAN-A indoor channel).

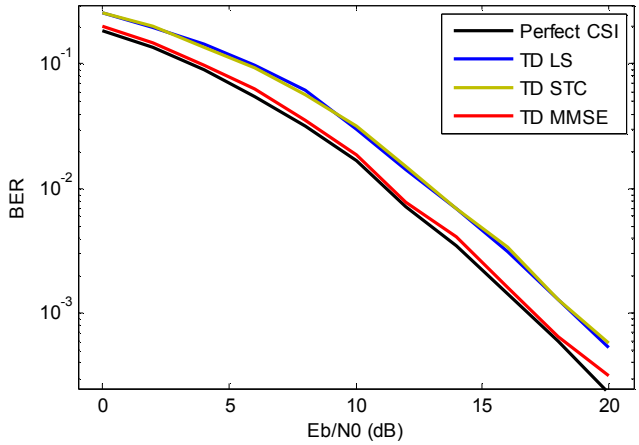

Figure 5.12. System BER performance (BRAN-E indoor channel).

5.5. Conclusions

In this chapter we have analyzed the three common pilot arrangements found in OFDM systems with multiple transmit antennas. We have designed pilot sequences that we advocate grant the receiver the ability to extract the CIRs for the different channels from the received symbols carrying pilots and data when the transmission is performed over Rayleigh fading multipath channels. Also, we have defined the conditions under which the CIR estimates are free of co-channel interference.

We have concluded that the proposed channel estimation schemes are able to estimate the different CIRs involved in the transmission process immediately from the TD received samples, eliminating the need to move from TD to FD and back to TD, commonly found in other transform-based methods. The addressed pilot schemes yield the same channel estimation MSE for the same overall pilot overhead and pilot power. The STC and TD MMSE algorithms were introduced in the estimation scheme, providing considerable performance improvements.

The channel estimation algorithms associated with the three pilot arrangement present very low computational load. Simulation results show that the investigated algorithms present a considerable performance improvement when compared to same of the reference methods that can be found in the literature [Li99], [Li02]. In the more demanding outdoor environment, the TD MMSE channel estimation algorithm shows the ability of maintaining the performance, despite the increased channel delay spread.

5.6. References

[802.11g] IEEE Std. 802.11g-2003, "Local and metropolitan area networks – Specific requirements – Part 11: Wireless LAN medium access control (MAC) and physical layer (PHY) specifications – Amendment 4: Further higher data rate extension in the 2.4 GHz band," June 2003.

[802.16] IEEE Std. 802.16-2009, "Local and metropolitan area networks – Part 16: Air interface for broadband wireless access systems," May 2009.

[802.16d] IEEE Std. 802.16-2004, "Local and metropolitan area networks – Part 16: Air interface for fixed broadband wireless access systems," Oct. 2004.

[Ala98] S. Alamouti, "A Simple Transmit Diversity Technique for Wireless Communications," *IEEE Journal on Selected Areas in Communications*, vol. 16, no. 8, pp. 1451 – 1458, October 1998.

[Aue03] G. Auer, "Channel estimation in two dimensions for OFDM systems with multiple transmit antennas," in *Proc. IEEE Global Telecommunications Conference*, vol. 1, pp. 322 – 326, San Francisco, USA, December 2003.

[Bar03] I. Barhumi, G. Leus, M. Moonen, "Optimal training design for MIMO OFDM systems in mobile wireless channels," *IEEE Transactions on Signal Processing*, vol. 51, no. 6, pp. 1615 – 1624, June 2003.

[BRAN] ETSI Project Broadband Radio Access Networks (BRAN), "HIPERLAN Type 2, Technical specification; Physical layer," October 1999.

[Dou03] A. Doufexi, A. Miguelez, A. Armour, A. Nix, M. Beach, "Use of space time block codes and spatial multiplexing using TDLS channel estimation to enhance the throughput of OFDM based WLANs," in Proc. IEEE Vehicular Technology Conference, vol. 1, pp. 704 – 708, Jejou, South Korea, April 2003.

[Dow02] A. Dowler, A. Doufexi, A. Nix, "Performance Evaluation of Channel Estimation Techniques for a Mobile Fourth Generation Wide Area OFDM System," in *Proc. IEEE Vehicular Technology Conference*, vol. 4, pp. 2036 – 2040, Vancouver, Canada, September 2002.

[Dow03] A. Dowler, A. Nix, "Performance Evaluation of Channel Estimation Techniques in a Multiple Antenna OFDM System," in *Proc. IEEE Vehicular Technology Conference*, vol. 2, pp. 1214 – 1218, Orlando, USA, October 2003.

[Edf96] O. Edfors, M. Sandell, J.-J. van de Beek, S. Wilson, P. Borjesson, "Analysis of DFT-based channel estimators for OFDM," Research Report TULEA 1996:17, Div. of Signal Processing, Lulea University of Technology, Sweden, September 1996.

[Fos96] G. Foschini, "Layered Space-Time Architecture for Wireless Communications in a Fading Environment when using Multi-Elements Antennas," *Bell Labs Technical Journal*, vol. 1, pp. 41 – 59, Autumn 1996.

[Jeo00] W. Jeon, K. Paik, Y. Cho, "An Efficient Channel Estimation Technique for OFDM Systems with Transmitter Diversity," in *Proc. IEEE International Symposium on Personal, Indoor and Mobile Radio Communications*, vol. 2, pp. 1246 – 1250, London, UK, September 2000.

[Lei02] S. Lei, S. Roy, "A rate-one non-orthogonal space-time coded OFDM system with estimation for frequency selective channels," in *Proc. IEEE Global Telecommunications Conference*, vol. 1, pp. 676 – 680, November 2002.

[Li02] Y. Li, "Simplified channel estimation for OFDM systems with multiple transmit antennas," *IEEE Transactions on Wireless Communications*, vol. 1, pp. 67 – 75, January 2002.

[Li99] Y. Li, N. Seshadri, S. Ariyavisitakul, "Channel estimation for OFDM systems with transmitter diversity in mobile wireless channels," *IEEE Journal on Selected Areas in Communications*, vol. 17, no. 3, pp. 461 – 471, March 1999.

[LTE] ETSI Technical Specification TS 136 201 v8.3.0, "LTE; Evolved universal terrestrial radio access (E-UTRA); Long Term Evolution (LTE) physical layer; General description," April 2009.

[Min02] H. Minn, K. Dong, V. Bhargava, "A reduced complexity channel estimation for OFDM systems with transmit diversity in mobile wireless channels," *IEEE Transactions on Communications*, vol. 50, no. 5, pp. 799 – 807, May 2002.

[Min06] H. Minn, N. Al-Dhahir, "Optimal training signals for MIMO OFDM channel estimation," *IEEE Transactions on Wireless Communications*, vol. 5, no. 5, pp. 1158 – 1168, May 2006.

[Nee00] R. Nee, R. Prasad, *OFDM for Wireless Multimedia Communications*, 1st ed. Artech House, 2000.

[Pau04] A. Paulraj, D. Gore, R. Nabar, H. Bolcskei, "An overview of MIMO communications - a key to gigabit wireless," *Proceedings of the IEEE*, vol. 92, no. 2, pp. 198 – 218, February 2004.

[Sam02] H. Sampath, S. Talwar, J. Tellado, V. Erceg, A. Paulraj, "A fourth-generation MIMO-OFDM broadband wireless system: design, performance, and field trial results," *IEEE Communications Magazine*, vol. 40, no. 9, pp. 143 – 149, September 2002.

[Shi04] M. Shin, H. Lee, C. Lee, "Enhanced channel-estimation technique for MIMO-OFDM systems," *IEEE Transactions on Vehicular Technology*, vol. 53, no. 1, pp. 261 – 265, January 2004.

[Ste05] M. Sternad, D. Aronsson, "Channel estimation and prediction for adaptive OFDMA/TDMA uplinks, based on overlapping pilots," in *Proc. IEEE International Conference on Acoustics, Speech, and Signal Processing*, vol. 3, pp. 861 – 864, Philadelphia, USA, March 2005.

[Stu04] G. Stuber, J. Barry, S. McLaughlin, Y. Li, M. Ingram, T. Pratt, "Broadband MIMO-OFDM wireless communications," *Proceedings of the IEEE*, vol. 92, no. 2, pp. 271 – 294, February 2004.

[Suh03] C. Suh, C. Hwang, H. Choi, "Preamble Design for Channel Estimation in MIMO-OFDM Systems," in *Proc. IEEE Global Telecommunications Conference*, vol. 1, pp. 317 – 321, San Francisco, USA, December 2003.

[Tar99] V. Tarokh, H. Jafarkhani, A. Calderbank, "Space-Time Block Codes from Orthogonal Designs," *IEEE Transactions on Information Theory*, vol. 45, no. 5, pp. 1456 – 1467, July 1999.

[Wol98] P. Wolniansky, G. Foschini, G. Golden, R. Valenzuela, "V-BLAST: An Architecture for Realizing Very High Data Rates Over the Rich-Scattering Wireless Channel," *URSI International Symposium on Signals, Systems, and Electronics*, pp. 295 – 300, Pisa, Italy, September 1998.

[Zam07] H. Zamiri-Jafarian, S. Pasupathy, "Robust and improved channel estimation algorithm for MIMO-OFDM systems," *IEEE Transactions on Wireless Communications*, vol. 6, no. 6, pp. 2106 – 2113, June 2007.

[Zha05] H. Zhang, Y. Li, A. Reid, J. Terry, "Channel estimation for MIMO-OFDM in correlated fading channels," in *Proc. IEEE International Conference on Communications*, vol. 4, pp. 2626 – 2630, Seoul, Korea, May 2005.

CHAPTER 6

ESTIMATION OF CFO AND CHANNELS IN PHASE-SHIFT ORTHOGONAL PILOT-AIDED OFDM SYSTEMS WITH TRANSMITTER DIVERSITY

In this chapter we present a CFO estimation algorithm and an associated channel estimation method for broadband OFDM systems with transmitter diversity. The CFO estimation algorithm explores the TD structure of the transmitted symbols carrying pilots and data, relying solely on the data component present on the symbols to estimate the CFO, thus avoiding additional overhead like training symbols or null sub-carriers. An intermediate output of the CFO algorithm provides an easy-to-get initial CIR estimate that will be improved with the utilization of a TD LMMSE filter. The feasibility of the investigated methods is substantiated by system simulation using indoor and outdoor broadband wireless channel models. Simulation results show that the joint algorithms provide a near optimal system's performance.

6.1. Introduction

The issue of synchronization is of great importance in all digital communications systems. Accurate synchronization is indispensable to suppress the negative impact of the synchronization errors in the communication systems no matter if it is a single carrier or a multicarrier system, whether it operates in continuous or packet mode transmission systems.

The long symbol duration makes OFDM-based systems especially sensitive to CFOs that always exist between the BS and the MT. The presence of CFO destroys the orthogonality among sub-carriers leading to ICI and causing severe degradation of the system's BER. The transmission over severe channel conditions of multipath fading and the mobility-induced Doppler shift significantly contribute to make a bad problem worse.

The sensitivity of OFDM systems to synchronization errors and the need for very accurate estimation and compensation of this malefic effect is well know and documented in several published works [Moo94], [Pol95], [Sat01], [Wan03], [Rug05]. Even a small trace of residual CFO introduces considerable degradation of the system's performance when using high order modulations like 64-QAM [Pol95].

The adoption of MIMO techniques requiring multiple transmit antennas along with OFDM-based modulations in recent broadband wireless systems [802.16], [LTE] and its most likely continued adoption in the near future standards [LTEadv], justifies the recent rush for new algorithms that can solve the challenges posed by the new specifications.

MIMO-OFDM receivers have to deal with the multi-antenna interference (MAI) caused by the simultaneous arrival of signals coming from the multiple transmit antennas. The MAI poses an additional challenge to the CFO estimation, forcing a careful design of the training sequences to decouple the MAI.

The CFO estimation algorithms can be classified into three categories:

- Blind methods – the algorithms explore the received signal statistics to get the estimate [Tur98], [Bol99], [Tur00], [Lui02], [Yao05];
- Non-Data Aided (NDA) methods – the algorithms use the OFDM symbol structure (usually the CP) to get the estimate [San96], [Bee97], [Las00], [Mor01];
- Data Aided (DA) methods – the algorithms use training symbols or pilots to get the estimate [Moo94], [Sch97], [Mor99], [Mod01], [Bes03], [Sch03], [Zha04], [Ma05], [Hua06a], [Hua06b], [Sim06], [Jia08a], [Jia08b].

The issue of CFO estimation for SISO-OFDM systems is well documented [Moo94], [Bee97], [Mor99], [Tur00], [Lui02], [Zha04], [Hua06a] and references therein, but only in the last few years has the MIMO-OFDM CFO estimation issue been tackled and a limited number of works on CFO estimation for MIMO-OFDM has appeared in the literature. A blind method CFO estimator for MIMO-OFDM that used a kurtosis-type criterion was investigated in [Yao05]. Some of the initial investigation on DA CFO estimation methods for MIMO-OFDM can be found in [Mod01], [Bes03], [Sch03], [Ma05].

The estimator proposed in [Mod01] uses training symbols to get the CFO estimate but the output of the algorithm is not very accurate. The ML-based estimation scheme investigated in [Bes03] uses training sequences to estimate the CFO and the channel gains. In [Sch03], the different transmit antennas send their training sequences in disjoint time intervals. The training overhead grows linearly with the number of transmit antennas, resulting in decreased efficiency. The presence of hopping null sub-carriers is exploited in [Ma05] to get CFO estimates. Similarly to the method proposed in [Bes03], the calculation of the CFO estimate requires large size DFT operations and a computationally demanding time consuming line search over a large frequency interval. This limitation was tackled in [Sim06], [Jia08a] and [Jia08b] where lower complexity algorithms were investigated.

The CFO estimator investigated in [Sim06] reduces the complexity of the previous methods using an iterative training-based ML CFO estimator. Like the algorithm in [Bes03], this estimator is only applied to flat-fading MIMO channels, what limits is usage. Via polynomial rooting of the CFO cost function, the estimator proposed in [Jia08a] is search-free and its complexity is reduced when compared to the previous methods. This algorithm is further simplified in [Jia08b] where the polynomial rooting is replaced by a simpler factor decomposition of the derivative of the CFO cost function.

This paper contains a proposal for a CFO estimation algorithm and associated channel estimation method for OFDM systems with transmitter diversity that exploits a standardized transmission format, where FD pilot symbols are regularly spread in the OFDM symbols. The proposed algorithms do not perform both operations jointly like [Kim06], [Ngu07], [Che08], [Ngu09], but the channel estimator profits from the processing done the CFO estimator, to reduce its complexity. The CFO estimator generates an initial channel estimate, and the channel estimator aims at improving this initial estimate.

To minimize the pilot overhead, the pilot sub-carriers are shared among all transmit antennas. To mitigate the resulting co-channel interference, the system adopts phase-shifted pilot sequences per transmit antenna [Li02], similarly to those considered in the previous chapter. By exploring the TD properties of the received symbols, the proposed algorithms are able to estimate and remove the CFO, separate each of the CIRs and generate the final channel estimate, without requiring any additional overhead (training symbols or null sub-

carriers). By performing most of the operations on the TD received symbols and by sharing operations, the overall computational load required to implement both algorithms is affordable for real time implementations.

The chapter is organized as follows. Next Section gives a brief introduction to the wireless multipath channel and the OFDM baseband model. In Section 6.3, the investigated CFO and channel estimation algorithms are developed. The feasibility of the developed method is substantiated by simulation results presented in Section 6.4. Finally, conclusions are drawn in Section 6.5.

6.2. OFDM in Mobile Wireless Channels

Before introducing the investigated method, we will briefly overview the mobile wireless multipath channel and the considered OFDM baseband model.

6.2.1 The wireless multipath channel

Let's consider that the system transmits over multipath Rayleigh fading wireless channels, modelled by the discrete-time CIR

$$\tilde{h}[n] = \sum_{l=0}^{L_p-1} \alpha_l \delta[n-\tau_l], \tag{6.1}$$

where L_p is the number of channel paths, α_l and τ_l are the complex value and delay of path l, respectively. The paths are assumed to be statistically independent, with normalized average power, $\sum_{l=0}^{L_p-1} \sigma_h^2[l] = 1$, where $\sigma_h^2[l]$ is the average power of path l. The channel is time-variant due to the motion of the MT, but we will assume that the CIR is constant during one OFDM symbol. The time dependence of the CIR is not present in the notation for simplicity. Assuming that the insertion of a long enough CP in the transmitter assures that the orthogonality of the sub-carriers is maintained after transmission, the CFR can be expressed as

$$h[k] = \sum_{l=0}^{L_p-1} \alpha_l \exp\left(-j\frac{2\pi}{N_C} k\tau_l\right), \tag{6.2}$$

where N_C is the total number of sub-carriers of the OFDM system.

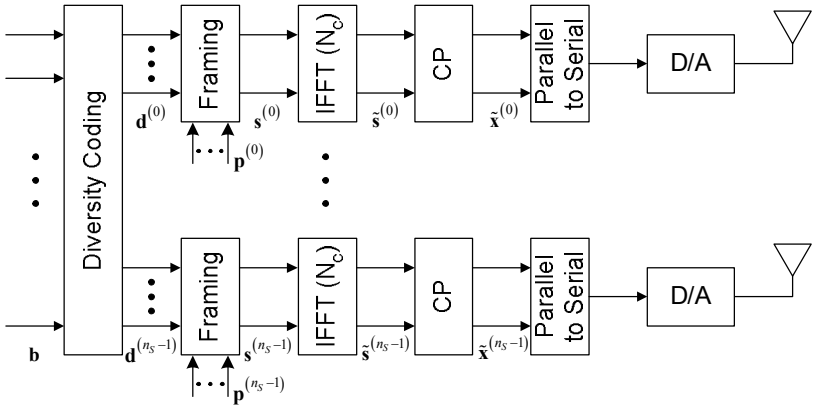

Figure 6.1. Pilot-aided MIMO-OFDM baseband transmitter model.

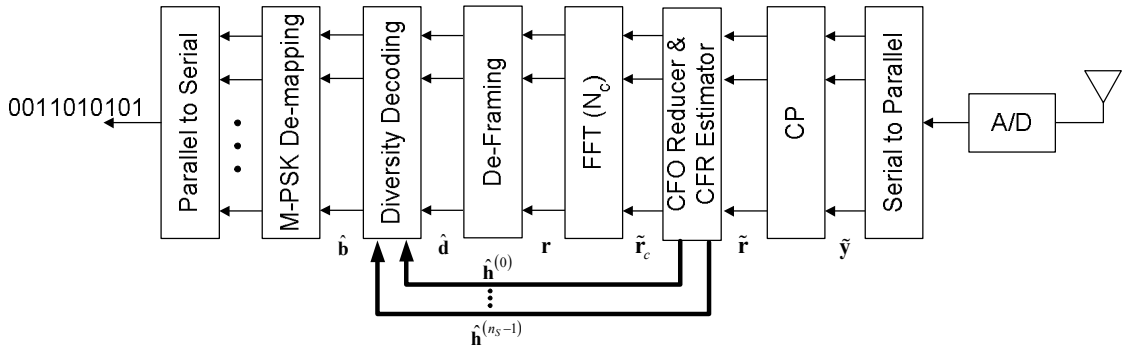

Figure 6.2. Pilot-aided MIMO-OFDM baseband receiver model.

6.2.2 OFDM baseband model

Consider the OFDM baseband system with n_S transmit antennas depicted in Figure 6.1 and Figure 6.2. The n_S vectors $\mathbf{d}^{(s)}$ hold the M-ary PSK or QAM coded data to be transmitted.

To assist in the channel estimation process, pilot symbols are added in each transmit antenna path. The n_S vectors $\mathbf{p}^{(s)}$ hold the pilot values for each path. The pilots are transmitted in dedicated sub-carries (vectors $\mathbf{p}^{(s)}$ and $\mathbf{d}^{(s)}$ contain non-zero values in disjoint positions). The resulting FD signal transmitted by antenna s is $\mathbf{s}^{(s)} = \mathbf{d}^{(s)} + \mathbf{p}^{(s)}$. All transmit antennas use the common set of sub-carriers $\wp$ to convey the overlapping pilot sequences. The pilots are regularly spread every N_f sub-carriers. The pilot separation can range from 1

(particular case where all sub-carriers in the OFDM symbol are dedicated to transmit pilots – training symbol) to N_C, fulfilling the condition $\frac{N_C}{N_f n_S} \in \mathbb{N}$.

The system uses distinct phase-shifted pilot sequences in each transmit antenna to allow the separation of the sequences in the receiver. The *k*-th element of the vector $\mathbf{p}^{(s)}$ is defined by,

$$p^{(s)}[k] = \sum_{m=0}^{N_t-1} \delta\left[k - k_{ini} - mN_f\right] \exp\left(-j2\pi \frac{s}{n_S} m\right), \tag{6.3}$$

where $N_t = \frac{N_C}{N_f}$ and $k_{ini} \in \{0, \cdots, N_f - 1\}$ is the first pilot sub-carrier.

The IDFT block present in each antenna path transforms the input vector into the TD vector $\tilde{\mathbf{s}}^{(s)}$, using an efficient N_C-points inverse FFT (IFFT) algorithm.

An L samples long guard interval, in the form of CP, is prefixed to vector $\tilde{\mathbf{s}}^{(s)}$, resulting in the TD transmitted vector

$$\tilde{\mathbf{x}}^{(s)} = \mathbf{A}_{CP}\mathbf{F}^H\mathbf{s}^{(s)} = \mathbf{A}_{CP}\left(\tilde{\mathbf{d}}^{(s)} + \tilde{\mathbf{p}}^{(s)}\right), \tag{6.4}$$

where $\mathbf{F} \triangleq N_C^{-1/2} \exp\left(-j\frac{2\pi}{N_C}kn\right)_{k,n=0,0}^{N_C-1,N_C-1}$ is the $N_C \times N_C$ DFT matrix and $\mathbf{A}_{CP} = \left[\mathbf{I}_{N_C,L} \;\; \mathbf{I}_{N_C}\right]^T$ is the matrix that adds the CP, with $\mathbf{I}_{N_C}$ denoting the $N_C \times N_C$ identity matrix and $\mathbf{I}_{N_C,L}$ denoting the last L columns of $\mathbf{I}_{N_C}$. The TD vectors $\tilde{\mathbf{d}}^{(s)}$ and $\tilde{\mathbf{p}}^{(s)}$ collect, respectively, the components of the data symbols and pilot symbols present in $\tilde{\mathbf{s}}^{(s)}$. The n_S vectors $\tilde{\mathbf{s}}^{(s)}$ are simultaneously transmitted to the receiver's antenna.

Let $w_o = 2\pi f_o \Delta t$ be the normalized angular CFO, where f_o is the frequency offset due to the frequency mismatch of the oscillators of the transmitter and the receiver, and Δt is the sampling interval.

The *n*-th received signal sample of the *i*-th symbol can be expressed as

$$\tilde{y}_i[n] = \exp\left[jw_o\left[i\left(N_C + L\right) + n\right]\right] \sum_{s=0}^{n_S-1} \sum_{l=0}^{L-1} \tilde{h}_i^{(s)}[l]\tilde{x}_i^{(s)}[n-l] + \overline{\tilde{n}}_i[n], \tag{6.5}$$

where $\bar{\bar{n}}_i[n]$ is a sample of *iid* zero mean AWGN with variance σ_n^2. Collecting the (N_C+L) samples of the symbol,

$$\tilde{\mathbf{y}}_i = \exp\left[jw_o i\left(N_C+L\right)\right]\mathbf{C}_{(N_C+L)}\left(w_o\right)\sum_{s=0}^{n_S-1}\tilde{\mathbf{H}}_{i,lin}^{(s)}\tilde{\mathbf{x}}_i^{(s)} + \tilde{\mathbf{z}}_i + \bar{\bar{\mathbf{n}}}_i, \tag{6.6}$$

where the vector $\bar{\bar{\mathbf{n}}}_i$ collects the noise samples that affect the *i*-th symbol, the vector $\tilde{\mathbf{z}}_i$ represents the ISI caused by the channel dispersion and the matrix $\tilde{\mathbf{H}}_{i,lin}^{(s)}$ is the $(N_C+L)\times(N_C+L)$ lower triangular Toeplitz channel convolution matrix with first column $\tilde{\mathbf{h}}_i^{(s)}$ (column N_C-vector with the discrete-time CIR ; its elements are defined by (6.1)) padded with zeros. The $(N_C+L)\times(N_C+L)$ diagonal matrix that holds the phase rotation that affects each symbol sample is

$$\mathbf{C}_{(N_C+L)}\left(w_o\right) = diag\left(\left[1 \;\; \exp\left(jw_o\right) \;\cdots\; \exp\left[jw_o\left(N_C+L-1\right)\right]\right]\right). \tag{6.7}$$

The receiver starts by removing the CP from the received symbol. Dropping the symbol index, the resulting vector is

$$\begin{aligned}\tilde{\mathbf{r}} = \mathbf{R}_{CP}\tilde{\mathbf{y}} &= \exp\left[jw_o i\left(N_C+L\right)\right]\mathbf{R}_{CP}\mathbf{C}_{(N_C+L)}\left(w_o\right)\sum_{s=0}^{n_S-1}\tilde{\mathbf{H}}_{lin}^{(s)}\tilde{\mathbf{x}}^{(s)} + \mathbf{R}_{CP}\tilde{\mathbf{z}} + \tilde{\mathbf{n}} \\ &= \theta_{imi}\mathbf{C}_{N_C}\left(w_o\right)\sum_{s=0}^{n_S-1}\mathbf{R}_{CP}\tilde{\mathbf{H}}_{lin}^{(s)}\mathbf{A}_{CP}\tilde{\mathbf{s}}^{(s)} + \mathbf{R}_{CP}\tilde{\mathbf{z}} + \tilde{\mathbf{n}}\end{aligned}, \tag{6.8}$$

where $\mathbf{R}_{CP} = \left[\mathbf{0}_{N_C\times L} \;\; \mathbf{I}_{N_C}\right]$ is the matrix that removes the CP with $\mathbf{0}_{N_C\times L}$ representing the $(N_C\times L)$ null matrix, $\tilde{\mathbf{n}} = \mathbf{R}_{CP}\bar{\bar{\mathbf{n}}}$ is the resulting TD noise column N_C-vector and $\theta_{imi} = \exp\left[jw_o\left[i\left(N_C+L\right)+L\right]\right]$ is the common phase that affects all samples of the *i*-th symbol.

The last step in (6.8) was possible considering the structure of the matrices involved,

$$\mathbf{R}_{CP}\mathbf{C}_{(N_C+L)}\left(w_o\right) = \exp\left(jw_o L\right)\mathbf{C}_{N_C}\left(w_o\right)\mathbf{R}_{CP}. \tag{6.9}$$

With the assumption that the length of the CP is larger than the duration of CIR, the ISI is completely removed and equation (6.8) can be written as

$$\begin{aligned}\tilde{\mathbf{r}} &= \theta_{ini}\mathbf{C}_{N_C}\left(\nu_o\right)\sum_{s=0}^{n_S-1}\tilde{\mathbf{H}}_{circ}^{(s)}\tilde{\mathbf{s}}^{(s)}+\tilde{\mathbf{n}} \\ &= \theta_{ini}\mathbf{C}_{N_C}\left(\nu_o\right)\sum_{s=0}^{n_S-1}\mathbf{F}^H\mathbf{Q}^{(s)}\mathbf{s}^{(s)}+\tilde{\mathbf{n}}\end{aligned}, \tag{6.10}$$

where $\tilde{\mathbf{H}}_{circ}^{(s)}=\mathbf{R}_{CP}\tilde{\mathbf{H}}_{lin}^{(s)}\mathbf{A}_{CP}$ is the $\left(N_C\times N_C\right)$ circulant matrix with circulant vector $\tilde{\mathbf{h}}^{(s)}$ and, due to the properties of the DFT, $\mathbf{Q}^{(s)}=\mathbf{F}\tilde{\mathbf{H}}_{circ}^{(s)}\mathbf{F}^H=diag\left(\mathbf{h}^{(s)}\right)$, with the elements of $\mathbf{h}^{(s)}$ defined by (6.2).

The CFO and channel estimation block is responsible for estimating both the CFO that affects the received samples and the n_S channels that disturbed the transmission process. Both estimation algorithms will be introduced in the next Section. Moreover, this block is also responsible for reducing the CFO, using the estimated CFO value $\hat{\nu}_o$. This operation can be described by

$$\tilde{\mathbf{r}}_c=\theta_{ini}\mathbf{C}_{N_C}^H\left(\hat{\nu}_o\right)\mathbf{C}_{N_C}\left(\nu_o\right)\sum_{s=0}^{n_S-1}\mathbf{F}^H\mathbf{Q}^{(s)}\mathbf{s}^{(s)}+\mathbf{C}_{N_C}^H\left(\hat{\nu}_o\right)\tilde{\mathbf{n}}\,. \tag{6.11}$$

It is clear that if $\hat{\nu}_o=\nu_o$, $\mathbf{C}_{N_C}^H\left(\hat{\nu}_o\right)\mathbf{C}_{N_C}\left(\nu_o\right)=\mathbf{I}_{N_C}$ and the CFO is completely removed. As it will be demonstrated in the next Section, the CFO ambiguity remaining after this block is an integer multiple of the pilot sub-carrier separation $N_f\Delta f$, where Δf is the sub-carrier separation. This acquisition range should be sufficient for current OFDM systems, however coarse CFO estimation techniques [Mor00] can be used to tackle this limitation, if proven necessary.

The DFT block transforms the vector $\tilde{\mathbf{r}}_c$ to FD with an efficient FFT operation. Assuming that the CFO is completely eliminated, the resulting FD column N_C-vector can be expressed as

$$\mathbf{r}=\mathbf{F}\tilde{\mathbf{r}}_c=\theta_{ini}\sum_{s=0}^{n_S-1}\mathbf{Q}^{(s)}\mathbf{s}^{(s)}+\mathbf{n}\,, \tag{6.12}$$

where $\mathbf{n}=\mathbf{F}\mathbf{C}_{N_C}^H\left(\hat{\nu}_o\right)\tilde{\mathbf{n}}$ is the resulting FD noise vector. The remaining phase-rotation θ_{ini} is naturally removed in the channel estimation process, assuming that the pilot-aided scheme calculates the LS estimates.

The de-framing block separates the signals in the sub-carriers conveying pilots and data symbols. The values in the data sub-carriers are collected in vector $\hat{\mathbf{d}}$ and fed to the decoding block. Together with the channels' estimate $\hat{\mathbf{h}}^{(s)}$, this block is now able to decode the received

symbols, according to some decision rule, and generate the estimate of the transmitted data symbols $\hat{\mathbf{b}}$.

6.3. CFO and Channel Estimations by Exploring the TD properties of Phase-Shifted Pilot Sequences

The algorithms implemented in this block estimate both the n_S channels over which the transmission occurred and the CFO that affects the received signal. The inputs to the CFO estimation algorithm are the TD symbols carrying both pilots and data, according to the model defined in the previous Section. The channel estimation algorithm reuses an intermediate output of the previous operation to attain an initial CIR estimate with minimal computational load.

6.3.1 Analysis of the TD symbol's structure

From (6.10), each element of the TD received symbols (carrying pilots and data), after CP extraction, can be expressed by

$$\tilde{r}[n] = \theta_{imi} \exp(jw_o n) \sum_{s=0}^{n_S-1} \sum_{l=0}^{L-1} \tilde{h}^{(s)}[l] \left(\tilde{d}^{(s)}[n-l] + \tilde{p}^{(s)}[n-l] \right) + \tilde{n}[n], \tag{6.13}$$

where the elements of the TD data vector $\tilde{\mathbf{d}}^{(s)}$ are

$$\tilde{d}^{(s)}[n] = N_C^{-1/2} \sum_{\substack{k=0 \\ k \notin \wp}}^{N_C-1} d^{(s)}[k] \exp\left(j \frac{2\pi}{N_C} kn \right), \tag{6.14}$$

where $d^{(s)}[k]$ is the k-th element of $\mathbf{d}^{(s)}$ (complex data symbol conveyed by the k-th sub-carrier of the s transmit antenna path), and the elements of the TD pilot vector $\tilde{\mathbf{p}}^{(s)}$ are

$$\begin{aligned} \tilde{p}^{(s)}[n] &= N_C^{-1/2} \sum_{k=0}^{N_C-1} \sum_{m=0}^{N_t-1} \delta\left[k - k_{imi} - mN_f \right] \exp\left(-j2\pi \frac{s}{n_S} m \right) \exp\left(j \frac{2\pi}{N_C} kn \right) \\ &= N_C^{1/2} N_f^{-1} \exp\left(j \frac{2\pi}{N_C} k_{imi} n \right) \sum_{m=0}^{N_f-1} \delta\left[n - \frac{s}{n_S} N_t - mN_t \right] \end{aligned}. \tag{6.15}$$

Replacing (6.14) and (6.15) in (6.13),

$$\begin{aligned}\tilde{r}[n] &= \theta_{ini} N_C^{-1/2} \exp(jw_o n) \sum_{s=0}^{n_S-1} \sum_{l=0}^{L-1} \sum_{\substack{k=0 \\ k\notin\wp}}^{N_C-1} \tilde{h}^{(s)}[l] d^{(s)}[k] \exp\left[j \frac{2\pi}{N_C} k (n-l) \right] + \tilde{n}[n] \\ &+ \theta_{ini} N_C^{1/2} N_f^{-1} \exp(jw_o n) \sum_{s=0}^{n_S-1} \sum_{l=0}^{L-1} \sum_{m=0}^{N_f-1} \tilde{h}^{(s)}[l] \exp\left[j \frac{2\pi}{N_C} k_{ini} (n-l) \right] \delta\left[n-l-\frac{s}{n_S} N_t - mN_t \right], \\ &= \tilde{r}_d[n] + \tilde{r}_p[n] + \tilde{n}[n]\end{aligned} \quad (6.16)$$

where $\tilde{\mathbf{r}}_d$ and $\tilde{\mathbf{r}}_p$ hold the data-dependent and pilot-dependent components in $\tilde{\mathbf{r}}$, respectively.

Expanding the pilot-dependent vector $\tilde{\mathbf{r}}_p$,

$$\begin{aligned}\tilde{r}_p[n] &= \theta_{ini} N_C^{1/2} N_f^{-1} \exp(jw_o n) \sum_{s=0}^{n_S-1} \sum_{m=0}^{N_f-1} \exp\left[j \frac{2\pi}{N_C} k_{ini} \left(mN_t + \frac{s}{n_S} N_t \right) \right] \tilde{h}^{(s)}\left[n - \frac{s}{n_S} N_t - mN_t \right] \\ &= \theta_{ini} N_C^{1/2} N_f^{-1} \exp(jw_o n) \sum_{m=0}^{N_f-1} \exp\left(j \frac{2\pi}{N_C} k_{ini} mN_t \right) \tilde{h}^{(0)}[n - mN_t] + \cdots \\ &+ \theta_{ini} N_C^{1/2} N_f^{-1} \exp(jw_o n) \sum_{m=0}^{N_f-1} \exp\left[j \frac{2\pi}{N_C} k_{ini} \left(mN_t + \frac{n_S-1}{n_S} N_t \right) \right] \tilde{h}^{(n_S-1)}\left[n - \frac{n_S-1}{n_S} N_t - mN_t \right]\end{aligned} \quad (6.17)$$

it becomes clear that it is made-up of N_f frequency-shifted and scaled replicas of each of the n_S CIR. Moreover, the replicas of each CIR are separated by N_t samples and transmit antenna s CIR replicas are time-shifted $\frac{s}{n_S} N_t$ samples from the reference position mN_t, $m \in \{0, \cdots, N_f - 1\}$.

6.3.2 CFO estimation

The CFO estimation method introduced in the following uses the pilot structures, introduced primarily for channel estimation purposes, to estimate the CFO present in the received samples. Therefore, it is absolutely bandwidth efficient, as it does not require any additional specific overhead. The algorithm exhibits a fast acquisition, being able to output an estimate with low deviation from a single OFDM frame. It proves adequate for burst mode transmission where the frequency offset varies from frame to frame.

The algorithm requires a search within the acquisition range to find the minimum value of the cost function. An initial candidate angular frequency offset $\hat{w}$ is applied to the input signal $\tilde{\mathbf{r}}_i$, together with the TD equivalent of the FD multi-band filter that selects the pilot sub-carriers [Rib07] (phase-shifted sum of the samples in the same relative position in all N_f segments of N_t samples). This operation can be described by

$$\tilde{\mathbf{g}} = \mathbf{T}\,diag\left(\left[\begin{array}{ccc} 1 & \exp\left(-j\frac{2\pi}{N_C}k_{ini}\right) & \cdots \exp\left[-j\frac{2\pi}{N_C}k_{ini}\left(N_C-1\right)\right]\end{array}\right]\right)\mathbf{C}_{N_C}^{H}\left(\hat{w}\right)\tilde{\mathbf{r}} = \tilde{\mathbf{g}}_d + \tilde{\mathbf{g}}_p + \tilde{\mathbf{v}}\,, \quad (6.18)$$

where the $N_t \times N_C$ matrix $\mathbf{T} = \left[\mathbf{I}_{N_t} \;\cdots\; \mathbf{I}_{N_t}\right]$, the column N_t-vectors $\tilde{\mathbf{g}}_d$ and $\tilde{\mathbf{g}}_p$ hold the data-dependent and pilot-dependent components in $\tilde{\mathbf{g}}$, respectively, and $\tilde{\mathbf{v}}$ is the resulting noise vector. The elements of $\tilde{\mathbf{g}}_p$ can be expressed by

$$\begin{aligned}\tilde{g}_p[n] &= \sum_{m=0}^{N_f-1}\exp\left(-j2\pi k_{ini}\frac{n+mN_t}{N_C}\right)\exp\left[-j\hat{w}\left(n+mN_t\right)\right]\tilde{r}_p\left[n+mN_t\right] \\ &= \theta_{ini}N_C^{1/2}N_f^{-1}\exp\left[j\left(w_o-\hat{w}\right)n\right] \\ &\times\sum_{s=0}^{n_S-1}\sum_{m=0}^{N_f-1}\sum_{q=0}^{N_f-1}\left[\begin{array}{l}\exp\left[-j\frac{2\pi}{N_C}k_{ini}\left(n+\left(m-q\right)N_t-\frac{s}{n_S}N_t\right)\right]\times \\ \exp\left[j\left(w_o-\hat{w}\right)mN_t\right]\tilde{h}^{(s)}\left[n-\frac{s}{n_S}N_t+\left(m-q\right)N_t\right]\end{array}\right]\end{aligned}. \quad (6.19)$$

If channel s maximum delay $\tau_{\max}^{(s)}$ (normalized to the system's sampling interval Δt) is short enough so that the adjacent CIR replicas in replicas in (6.19) to not overlap (fulfils the sampling theorem),

$$\tau_{\max}^{(s)} \le \frac{N_C}{N_f n_S}, \quad (6.20)$$

equation (6.19) can be further simplified to

$$\tilde{g}_p[n] = \theta_{ini}N_C^{1/2}N_f^{-1}\exp\left[j\left(w_o-\hat{w}\right)n\right]\sum_{s=0}^{n_S-1}\left[\begin{array}{l}\exp\left[-j\frac{2\pi}{Nc}k_{ini}\left(n-\frac{s}{n_S}N_t\right)\right]\tilde{h}^{(s)}\left[n-\frac{s}{n_S}N_t\right] \\ \times\sum_{m=0}^{N_f-1}\exp\left[j\left(w_o-\hat{w}\right)mN_t\right]\end{array}\right], \quad (6.21)$$

that clearly shows that the pilot-dependent samples are limited to the n_s sets of samples $\left\{L_p\right\}$ (with L_p elements) where the corresponding phase-shifted CIRs have energy. The remaining samples will depend only on the transmitted data and noise.

The elements of $\tilde{\mathbf{g}}_d$ can be expressed by

$$\begin{aligned}\tilde{g}_d[n] &= \sum_{m=0}^{N_f-1}\exp\left(-j2\pi k_{ini}\frac{n+mN_t}{N_C}\right)\exp\left[-j\hat{w}\left(n+mN_t\right)\right]\tilde{r}_d[n+mN_t] \\ &= \theta_{ini}N_C^{-1/2}\sum_{m=0}^{N_f-1}\left(\begin{array}{l}\exp\left(-j2\pi k_{ini}\dfrac{n+mN_t}{N_C}\right)\exp\left[j\left(w_o-\hat{w}\right)\left(n+mN_t\right)\right] \\ \times\sum_{s=0}^{n_S-1}\sum_{l=0}^{L-1}\sum_{\substack{k=0\\k\notin\wp}}^{N_C-1}\tilde{h}^{(s)}[l]d^{(s)}[k]\exp\left[j\dfrac{2\pi}{N_C}k\left(n-l+mN_t\right)\right]\end{array}\right), \\ &= \theta_{ini}N_C^{-1/2}\exp\left[j\left(w_o-\hat{w}\right)n\right]\exp\left(-j2\pi k_{ini}\frac{n}{N_C}\right)\sum_{s=0}^{n_S-1}\sum_{l=0}^{L-1}\tilde{h}^{(s)}[l]\Psi\end{aligned} \quad (6.22)$$

where

$$\begin{aligned}\Psi &= \sum_{\substack{k=0\\k\notin\wp}}^{N_C-1}d^{(s)}[k]\exp\left[j\frac{2\pi}{N_C}k\left(n-l\right)\right]\sum_{m=0}^{N_f-1}\exp\left[j\left(w_o-\hat{w}\right)mN_t\right]\exp\left[j\frac{2\pi}{N_f}\left(k-k_{ini}\right)m\right] \\ &= \sum_{\substack{k=0\\k\notin\wp}}^{N_C-1}d^{(s)}[k]\exp\left[j\frac{2\pi}{N_C}k\left(n-l\right)\right]\sum_{m=0}^{N_f-1}\exp\left[j\frac{2\pi m}{N_f}\left[\left(f_o-\hat{f}\right)N_C\Delta t+\left(k-k_{ini}\right)\right]\right]\end{aligned} \quad (6.23)$$

where $\hat{f}$ is the initial candidate frequency offset.

The elements of the noise vector $\tilde{\mathbf{v}}$ can be expressed by

$$\tilde{v}[n] = \sum_{m=0}^{N_f-1}\exp\left(-j2\pi k_{ini}\frac{n+mN_t}{N_C}\right)\exp\left[-j\hat{w}\left(n+mN_t\right)\right]\tilde{n}[n+mN_t]. \quad (6.24)$$

Figure 6.3 depicts an example of the constitution of vector $\tilde{\mathbf{g}}$ for a system with 2 transmission antennas, $N_C = 1024$ sub-carriers and pilot separation $N_f = 4$ $\left(N_t = 256\right)$. The plots put in evidence that the CIRs energy is limited to 2 sets of samples and the data-dependent component spans the entire symbol duration.

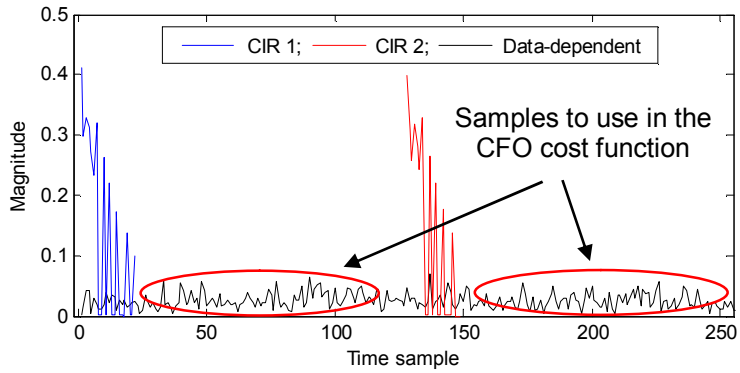

Figure 6.3. Example of the constitution of vector $\tilde{\mathbf{g}}$.

A careful inspection of (6.23) reveals that the factor Ψ (and the data-dependent component) is zero for

$$\left\{\phi = \left(f_o - \hat{f}\right) N_C \Delta t + \left(k - k_{imi}\right) : \phi \in \mathbb{Z} \wedge \phi \neq mN_f, m \in \mathbb{Z}\right\}, \tag{6.25}$$

independently of the considered sample. Keeping in mind that $k \notin \wp$ and $\left(k - k_{imi}\right) \neq mN_f, m \in \mathbb{Z}$, the solution for (6.25) is

$$\left(f_o - \hat{f}\right) N_C \Delta t = mN_f \Leftrightarrow \left(f_o - \hat{f}\right) = \frac{mN_f}{N_C \Delta t} = mN_f \Delta f, m \in \mathbb{Z}, \tag{6.26}$$

where Δf is the sub-carrier separation. It should be noted that the solution in (6.26) presents a periodicity $N_f \Delta f$ and includes the condition when the CFO is completely eliminated, $\left(f_o - \hat{f} = 0\right)$. A similar analysis reveals that the factor Ψ has maximum magnitude for

$$\left\{\gamma = \left(f_o - \hat{f}\right) N_C \Delta t : \gamma \in \mathbb{Z} \wedge \gamma \neq mN_f, m \in \mathbb{Z}\right\} \Rightarrow \left(f_o - \hat{f}\right) = \frac{l}{N_C \Delta t} = l\Delta f, l \in \mathbb{Z} \wedge l \neq mN_f. \tag{6.27}$$

We can conclude that Ψ has minimum values spread $N_f \Delta f$ Hz, with $\left(N_f - 1\right)$ maximum magnitude values in-between, separated by Δf Hz.

Let's define the column $\left(N_t - n_S L_p\right)$-vector $\mathbf{j}$ that collects the samples of $\tilde{\mathbf{g}}$ with no CIRs energy (only data-dependent and noise; example depicted in Figure 6.4) and the cost function $J\left(\hat{w}\right)$ as the energy in $\mathbf{j}$,

$$J\left(\hat{w}\right) = \mathbf{j}^H \mathbf{j}. \tag{6.28}$$

The definition of the cost function guarantees that, if within the acquisition range, its minimum value will converge to the true estimate as the number of elements in $\mathbf{j}$ increases (and the noise term tends to a floor in $J\left(\hat{w}\right)$). The elements in $\mathbf{j}$ may be obtained from one OFDM symbol or a set of symbols (with data and pilots) if higher accuracy on the estimate is required. From the previous analysis of the factor Ψ, it is clear that the acquisition range of our cost function is $\left]-N_f \Delta f / 2, N_f \Delta f / 2\right[$. The CFO estimate can be found by a line search within the acquisition range to find the minimum value of the cost function,

$$\hat{w}_o = \arg\left\{\min_{\hat{w}} J\left(\hat{w}\right)\right\}, \tag{6.29}$$

where $\hat{w}_0$ is the estimated CFO value. The exhaustive line search is computationally demanding, depending on the search's granularity. Hence, there is a trade-off between complexity and estimate's variance.

The cost function has a closed form expression and its behaviour is perfectly described: in the acquisition range there are N_f maximum values; in the interval limited by the maximum values that surround the perfect estimate, $J(\hat{w})$ presents a smooth shape with a single minimum. Using the knowledge we possess of the cost function, we propose a 2 step approach to find its minimum value. The initial step performs a coarse line search to locate the global minimum interval. Testing N_f candidate CFO values evenly spaced by Δf Hz should suffice. The candidate CFO will be the one with the lowest cost. If the number of elements in **j** is small and *SNR* is very low, the probability of wrong identification may not be negligible and the number of candidate CFO values can be increased thus decreasing the wrong identification probability. In the final step we use the gradient descent method [Boy04] to find the global minimum.

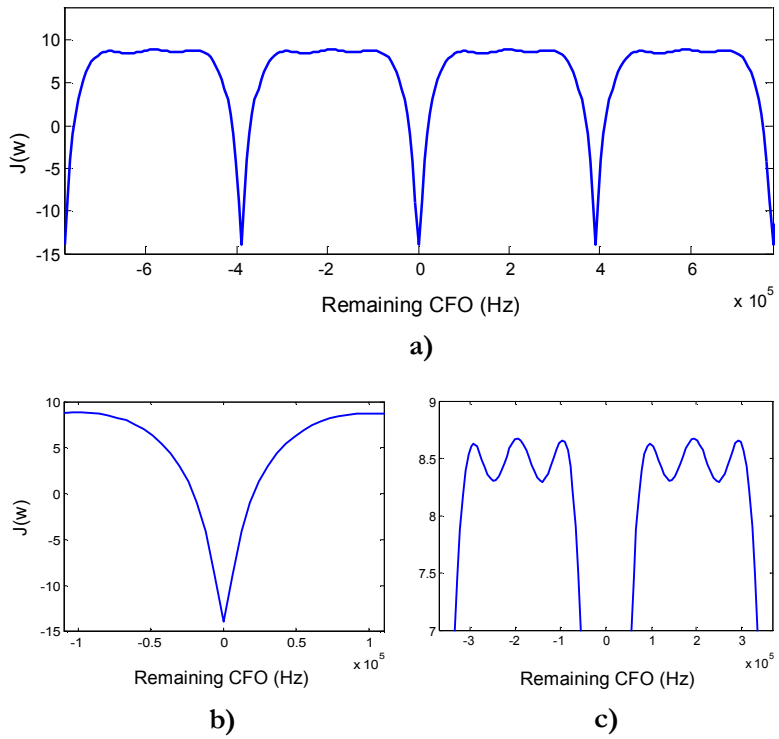

Figure 6.4. The cost function $J(w)$.

Figure 6.4 depicts an example of the cost function for a 2×1 Alamouti OFDM system with $N_C = 1024$ sub-carriers, sampling interval $\Delta t = 10ns$ and pilot separation $N_f = 4$. The values in the plot were acquired using an $SNR = 20dB$. In Figure 6.4-a) is visible the

separation of $\approx 390kHz$ between consecutives minimum values. Figure 6.4-b) shows in detail the interval around $\left(w_o - \hat{w}\right) = 0$. It is clear that it has a unique global minimum that is easy to find (no problem with local minimum values). In Figure 6.4-c), the $N_f - 1$ maximum values between consecutive minimum values are clearly visible. It also shows in detail that the separation of the maximum values around $\left(w_o - \hat{w}\right) = 0$ is $\approx 195kHz$.

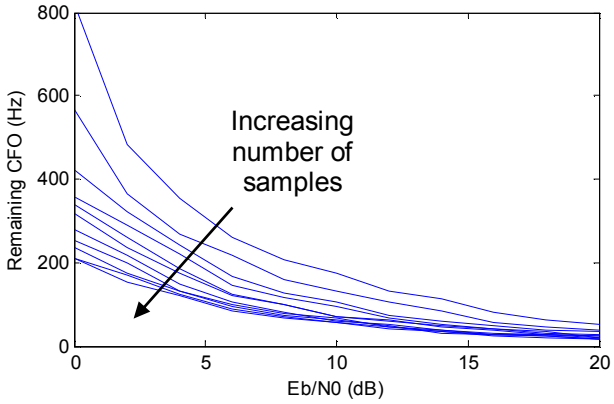

Figure 6.5. Estimated CFO standard deviation vs. number of samples in $J(w)$.

Figure 6.5 shows the evolution of the estimated CFO standard deviation with the number of samples used in estimation algorithm (elements of $\mathbf{j}$). The plots depict the standard deviation when the number of samples goes from 200 to 2000, in steps of 200 samples.

6.3.3 Channel estimation

Assuming that the CFO is completely eliminated, the output of the initial operation of the CFO algorithm is made-up of the pilot-dependent component and noise, $\tilde{\mathbf{g}} = \tilde{\mathbf{g}}_p + \tilde{\mathbf{v}}$. The data-dependent component was eliminated from this vector, opening way to easily obtain an initial CIR estimate.

The channel estimation algorithm starts by isolating each of the n_S phase-shifted CIRs from $\tilde{\mathbf{g}}$ and removing the modulating exponential factor. The elements of the resulting vectors $\hat{\tilde{\mathbf{h}}}_{LS}^{(s)}$ can be expressed by

$$\begin{aligned}\hat{\tilde{h}}_{LS}^{(s)}[n] &= \exp\left[j\frac{2\pi}{N_C}k_i n\right]\sum_{m=0}^{N_t-1}\delta\left[n+\frac{s}{n_S}N_t - m\right]\tilde{g}[n] \\ &= \theta_i \tilde{h}^{(s)}[n] + \exp\left[j\frac{2\pi}{N_C}k_i n\right]\tilde{v}_i\left[n+\frac{s}{n_S}N_t\right]\end{aligned} . \tag{6.30}$$

In [Rib07] it was demonstrated that for a single transmitting antenna OFDM system with perfect synchronization, (6.30) is the TD counterpart of FD LS estimate. By using phase-shifted pilot sequences that allow the separation of the different CIRs, the same result holds in the present model.

This initial estimate can be significantly improved by incorporating a TD LMMSE filter $\tilde{\mathbf{W}}_{MMSE}^{(s)}$ to reduce the estimate's error, taking advantage of the CIR energy concentration. The improvements provided by this filter are especially significant for low values of SNR.

The LMMSE filter can be expressed by [Bee95],

$$\tilde{\mathbf{W}}_{MMSE}^{(s)} = diag\left(\frac{\sigma_{h^{(s)}}^2[0]}{\sigma_{h^{(s)}}^2[0] + N_t^{-1}\sigma_{\mathbf{n}}^2}, \cdots, \frac{\sigma_{h^{(s)}}^2[L_p - 1]}{\sigma_{h^{(s)}}^2[L_p - 1] + N_t^{-1}\sigma_{\mathbf{n}}^2}, 0, \cdots, 0 \right). \tag{6.31}$$

The resulting CIR and CFR estimates are, respectively, $\hat{\tilde{\mathbf{h}}}^{(s)} = \tilde{\mathbf{W}}_{MMSE}^{(s)} \hat{\tilde{\mathbf{h}}}_{LS}^{(s)}$ and $\hat{\mathbf{h}}^{(s)} = \mathbf{F}\hat{\tilde{\mathbf{h}}}^{(s)}$.

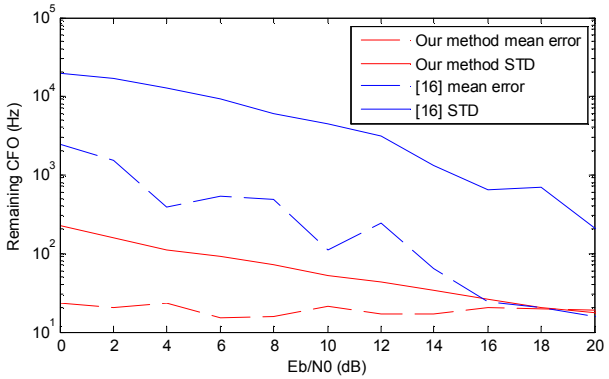

Figure 6.6. Remaining CFO.

6.4. Simulation Results

A simulation scenario was implemented using an Alamouti 2×1 OFDM system with $N_C = 1024$ modulated sub-carriers, sampling interval $\Delta t = 50ns$ and a CP with 100 samples. The transmitted OFDM symbols carried pilots and data, with a pilot separation $N_f = 8$. The OFDM frame consists of 16 symbols. The CFO value was randomly generated in each frame with a value inside the acquisition range $\left]-N_f\Delta f/2, N_f\Delta f/2\right[$. The CFO estimation and removal was performed on a frame basis. Two channel models with exponentially decaying PDP were used to simulate indoor ($50ns$ *rms* delay spread) and outdoor environments

(250*ns rms* delay spread). To validate the proposed method several simulations were performed using Eb/No values in the range of *0dB* to *20dB*.

Figure 6.6 shows the remaining CFO at the output of the CFO mitigate block when using the indoor channel model. The dashed lines represent the average remaining CFO. The solid lines represent the standard deviation of the CFO estimate. In our method, the gradient descent was stopped for a step of $10Hz$. For the method in [Ma05], one null sub-carrier was added to each OFDM symbol and an exhaustive search was performed with a $10Hz$ step. The results show that our method is unbiased for the all range of Eb/No values. The algorithm generates estimates with small deviation from the true value using a limited number of symbols (16). The estimate deviation is $\sim 1\%$ of that of [Ma05] for low values of *SNR*. The method in [Ma05] requires a large number of symbols and/or more receive antennas to generate accurate estimates. This result shows that the investigated method is quite adequate for burst systems.

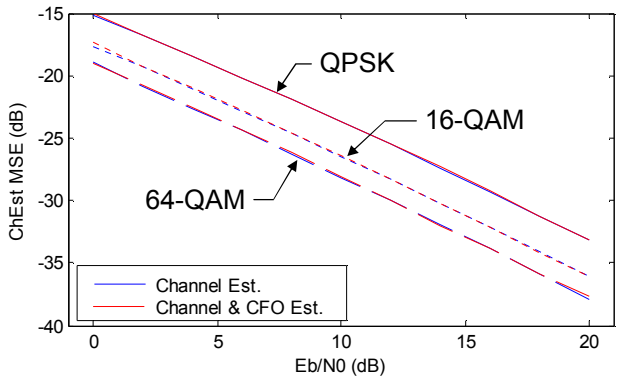

Figure 6.7. Joint Channel and CFO estimation MSE (indoor channel).

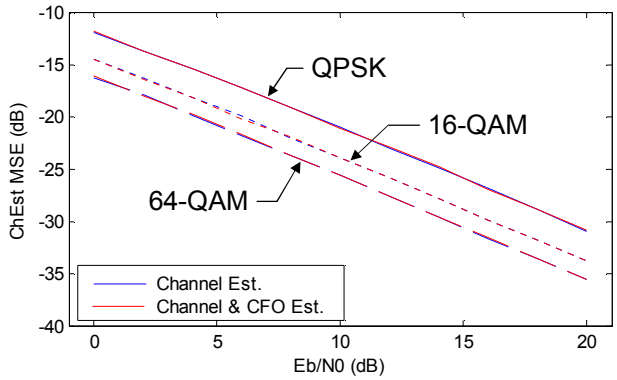

Figure 6.8. Joint Channel and CFO estimation MSE (outdoor channel).

Figure 6.7 and Figure 6.8 depict the MSE of the channel estimation algorithm (blue plots) when the system has perfect synchronization and the MSE of the joint CFO and channel estimation process (red plots), when using QPSK, 16-QAM and 64-QAM

modulations. Figure 6.7 presents the results for the indoor channel and Figure 6.8 for the outdoor channel.

Figure 6.9 and Figure 6.10 depict the system BER for 3 scenarios: the ideal situation where the receiver has perfect CSI (with no pilot overhead) and the CFO is absent (green plots); the situation when the receiver must estimate the channel from the received samples (blue plots) and the more realistic scenario where the receiver needs to estimate both the CFO and channel (red plots). Simulations results were obtained also for QPSK, 16-QAM and 64-QAM modulations as identified in the figures. Figure 6.9 presents the results for the indoor channel and Figure 6.10 for the outdoor channel.

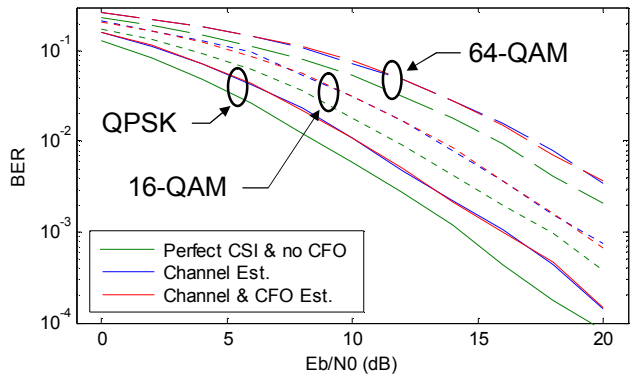

Figure 6.9. System BER performance (indoor channel).

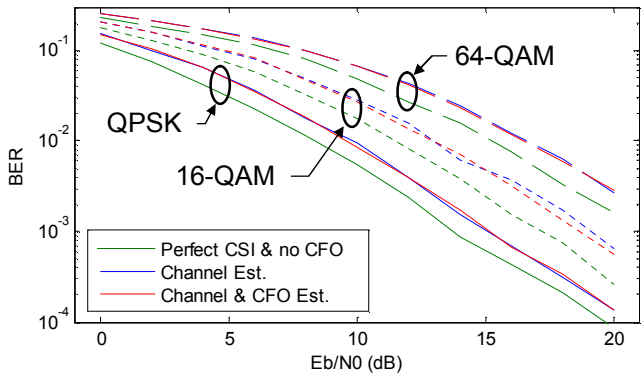

Figure 6.10. System BER performance(outdoor channel).

The channel estimation MSE improvement that can be observed for higher order modulations is due to the fact that the ratio between the powers in the pilot symbols and data symbols is kept constant in all simulations. The large increase of delay spread between both channels is the origin of the $\sim 3dB$ MSE degradation when moving from the indoor channel to the outdoor channel plots. This acceptable degradation shows the ability of the estimator to deal with the increasing channel delay spread by always weighing the energy of channel taps

vs. noise variance. The channel estimation BER plots present a degradation of $\sim 1,2dB$ that can be largely attributed to the 12,5% pilot overhead.

The joint CFO and channel estimation MSE is an effective measure of the degradation caused by both algorithms. In these plots the estimated channel was compared against the true channel affected by the same CFO that distorted the received signal (according to (6.10)). The results plotted in Figure 6.7 to Figure 6.10 show that the performance degradation of the joint process is marginal when compared with channel estimation only, substantiating the performance of the proposed algorithms.

6.5. Conclusions

We have investigated a CFO estimation algorithm and an associated channel estimation block for OFDM with transmitter diversity that explores the TD structure of transmitted symbols carrying pilots and data, avoiding additional overhead like training symbols or null sub-carriers.

The simulations results enable us to conclude that the proposed block can perform both operations in TD with a reduced degradation of the system's performance when compared with the ideal scenario. The residual CFO has a minimal impact in the system's performance, confirming that the CFO estimates have minimal deviation from the true value. The definition and shape of the cost function determine a very low complexity scheme, making this algorithm suitable for real-time applications. An intermediate output of the CFO algorithm provides an easy-to-get initial CIR estimate, minimizing the overall complexity. Similarly to the previous chapter, a TD LMMSE filter can be incorporated and proves to be effective in improving the accuracy of the channel estimate, even in the presence of the residual CFO coming from the previous operation.

6.6. References

[802.16] IEEE Std. 802.16-2009, "Local and metropolitan area networks – Part 16: Air interface for broadband wireless access systems," May 2009.

[Bee95] J.-J. van de Beek, O. Edfors, M. Sandell, S. Wilson, P. Börjesson, "On channel estimation in OFDM systems," in *Proc. IEEE Vehicular Technology Conference*, pp. 815 – 819, Chicago, USA, July 1995.

[Bee97] J.-J. Beek, M. Sandell, P. Börjesson, "ML estimation of time and frequency offset in OFDM systems," *IEEE Transactions on Signal Processing*, vol. 45, pp. 1800 – 1805, July 1997.

[Bes03] O. Besson, P. Stoica, "On parameter estimation of MIMO flat-fading channels with frequency offsets," *IEEE Transactions on Signal Processing*, vol. 51, no. 3, pp. 602 – 613, March 2003.

[Bol99] H. Bölcskei, "Blind high-resolution uplink synchronization of OFDM-based multiple access schemes," in *Proc. IEEE Workshop Signal Processing Advances in Wireless Communications*, pp. 166 – 169, Annapolis, USA, May 1999.

[Boy04] S. Boyd, L. Vandenberghe, *Convex Optimization*, Cambridge University Press, 2004.

[Che08] J. Chen, Y. Wu, S. Ma, T. Ng, "Joint CFO and channel estimation for multiuser MIMO-OFDM systems with optimal training sequences" *IEEE Transactions on Signal Processing*, vol. 56, no. 8, part 2, pp. 4008 – 4019, August 2008.

[Hua06a] D. Huang, K. Letaief, "Carrier frequency offset estimation for OFDM systems using subcarriers," *IEEE Transactions on Communications*, vol. 54, no. 5, pp. 813 – 823, May 2006.

[Hua06b] D. Huang, K. Letaief, "Enhanced carrier frequency offset estimation for OFDM using channel side information," *IEEE Transactions on Wireless Communications*, vol. 5, no. 10, pp. 2784 – 2793, October 2006.

[Jia08a] Y. Jiang, H. Minn, X. Gao, X. You, Y. Li, "Frequency offset estimation and training sequence design for MIMO OFDM," *IEEE Transactions on Wireless Communications*, vol. 7, no. 4, pp. 1244 – 1254, April 2008.

[Jia08b] Y. Jiang, H. Minn, X. You, X. Gao, "Simplified Frequency Offset Estimation for MIMO OFDM Systems," *IEEE Transactions on Vehicular Technology*, vol. 57, no. 5, pp. 3246 – 3251, September 2008.

[Kim06] K. Kim, R. Iltis, "Frequency offset synchronization and channel estimation for the MIMO-OFDM system using Rao-Blackwellized Gauss-Hermite filter," in *Proc. IEEE Wireless Communications and Networking Conference*, vol. 2, pp. 860 – 865, Las Vegas, USA, April 2006.

[Las00] N. Lashkarian, S. Kiaei, "Class of cyclic-based estimators for frequency-offset estimation of OFDM systems," *IEEE Transactions on Communications*, vol. 48, pp. 2139 – 2149, December 2000.

[Li02] Y. Li, "Simplified channel estimation for OFDM systems with multiple transmit antennas," *IEEE Transactions on Wireless Communications*, vol. 1, pp. 67 – 75, January 2002.

[LTE] ETSI Technical Specification TS 136 201 v8.3.0, "LTE; Evolved universal terrestrial radio access (E-UTRA); Long Term Evolution (LTE) physical layer; General description," April 2009.

[LTEadv] ETSI Technical Report 136 913 V8.0.1, "LTE; Requirements for further advancements for Evolved Universal Terrestrial Radio Access (E-UTRA) (LTE-Advanced)," April 2009.

[Lui02] M. Luise, M. Marselli, R. Reggiannini, "Low-complexity blind carrier frequency recovery for OFDM signals over frequency-selective radio channels," *IEEE Transactions on Communications*, vol. 50, no. 7, pp. 1182 – 1188, July 2002.

[Ma05] X. Ma, M.-K. Oh, G. Giannakis, D.-J. Park, "Hopping pilots for estimation of frequency-offset and multiantenna channels in MIMO-OFDM," *IEEE Transactions on Communications*, vol. 53, pp. 162 – 172, January 2005.

[Mod01] A. Mody, G. Stuber, "Synchronization for MIMO OFDM systems," in *Proc. IEEE Global Telecommunications Conference*, vol. 1, pp. 509 – 513, San Antonio, USA, November 2001.

[Moo94] P. Moose, "A technique for orthogonal frequency division multiplexing frequency offset correction," *IEEE Transactions on Communications*, vol. 42, no. 10, pp. 2908 – 2914, October 1994.

[Mor00] M. Morelli, A. D'Andrea, U. Mengali, "Frequency ambiguity resolution in OFDM systems," *IEEE Communications Letters*, vol. 4, pp. 134 – 136, April 2000.

[Mor01] M. Morelli, A. Andrea, U. Mengali, "Feedback frequency synchronization for OFDM applications," *IEEE Communications Letters*, vol. 5, no. 1, pp. 28–30, January 2001.

[Mor99] M. Morelli, U. Mengali, "An improved frequency offset estimator for OFDM applications," *IEEE Communication Letters*, vol. 3, pp. 75 – 77, March 1999.

[Ngu07] H. Nguyen-Le, T. Le-Ngoc, C. Ko, "Vector RLS-based joint estimation of channel response and frequency offsets for MIMO-OFDM," in *Proc. IEEE Global Telecommunications Conference*, pp. 2801 – 2805, Washington DC, USA, November 2007.

[Ngu09] H. Nguyen-Le, T. Le-Ngoc, C. Ko, "Turbo Processing for Joint Channel Estimation, Synchronization, and Decoding in Coded MIMO-OFDM Systems," *EURASIP Journal on Wireless Communications and Networking*, vol. 2009, pp. 1 – 12, 2009.

[Pol95] T. Pollet, M. Bladel, M. Moeneclaey, "BER sensitivity of OFDM systems to carrier frequency offset and Wiener phase noise," *IEEE Transactions on Communications*, vol. 43, pp. 191 – 193, February-March-April 1995.

[Rib07] C. Ribeiro, A. Gameiro, "Direct time-domain channel impulse response estimation for OFDM-based systems," in *Proc. IEEE Vehicular Technology Conference*, pp. 1082 – 1086, Baltimore, USA, October 2007.

[Rug05] L. Rugini, P. Banelli, "BER of OFDM systems impaired by carrier frequency offset in multipath fading channels," *IEEE Transactions on Wireless Communications*, vol. 4, no. 5, pp. 2279 – 2288, September 2005.

[San96] M. Sandell, "Design and Analysis of Estimators for Multicarrier Modulation and Ultrasonic Imaging," Lulea University, Sweden, 1996.

[Sat01] K. Sathananthan, C. Tellambura, "Probability of error calculation of OFDM systems with frequency offset," *IEEE Transactions on Communications*, vol. 49, no. 11, pp. 1884 – 1888, November 2001.

[Sch03] T. Schenk, A. Zelst, "Frequency synchronization for MIMO OFDM wireless LAN systems," in *Proc. IEEE Vehicular Technology Conference*, vol. 2, pp. 781 – 785, Orlando, USA, October 2003.

[Sch97] T. Schmidl, D. Cox, "Robust frequency and timing synchronization for OFDM," *IEEE Transactions on Communications*, vol. 45, no. 12, pp. 1613 – 1621, December 1997.

[Sim06] F. Simoens, M. Moeneclaey, "Reduced complexity data-aided and code-aided frequency offset estimation for flat-fading MIMO channels," *IEEE Transactions on Wireless Communications*, vol. 5, no. 6, pp. 1558 – 1567, June 2006.

[Tur00] U. Tureli, H. Liu, M. Zoltowski, "OFDM blind carrier offset estimation: ESPRIT," *IEEE Transactions on Communications*, vol. 48, no. 9, pp. 1459 – 1461, Sept. 2000.

[Tur98] U. Tureli, H. Liu, "Blind carrier synchronization and channel identification for OFDM communications," in *Proc. IEEE International Conference on Acoustics, Speech, and Signal Processing*, vol. 6, pp. 3509 – 3512, Seattle, USA, May 1998.

[Wan03] X. Wang, T. Tjhung, Y. Wu, B. Caron, "SER performance evaluation and optimization of OFDM system with residual frequency and timing offsets from imperfect synchronization," *IEEE Transactions on Broadcasting*, vol. 49, no. 2, pp. 170 – 177, June 2003.

[Yao05] Y. Yao, G. Giannakis, "Blind carrier frequency offset estimation in SISO, MIMO and multiuser OFDM systems," *IEEE Transactions on Communications*, vol. 53, no. 1, pp. 173 – 183, January 2005.

[Zha04] Z. Zhang, K. Long, Y. Liu, "Complex efficient carrier frequency offset estimation algorithm in OFDM systems," *IEEE Transactions on Broadcasting*, vol. 50, no. 2, pp. 159 – 164, June 2004.

CHAPTER 7

CONCLUSIONS

In this chapter we give a brief introduction to the demands that the future cellular wireless systems will have to fulfil to fully support the 4G requirements. The success of OFDM modulation is recent wireless standards turns it into a strong candidate as the modulation technique for future 4G systems. We introduce some of the most challenging issues affecting these systems and identify the topics of research addressed in this thesis. We draw the main conclusions that come out of this work and relate them to the major contributions resulting from this thesis. Finally, we identify some of the directions for future research work on the addressed topics.

7.1. Conclusions

The birth of wireless communications in the 19th century constitutes a turning point in our world by giving hope that our need to communicate would by fulfilled. The 20th century witnessed the dramatic evolution of wireless communications. The 21st century is witnessing the proliferation of wireless LANs [802.11], [802.11g], wireless MANs [802.16], wireless Personal Area Networks (PAN) [802.15.3], [Blu09] and wireless sensor networks [802.15.4]. The 4G cellular systems are expected to follow the path of co-existence and integration with heterogeneous networks, offering multiple services with mobility and a full IP network for Internet ubiquity. Building on the success of recent standards [802.11], [802.11g], [802.16], [DAB], [DVB-T], [LTE], OFDM is a strong candidate as the modulation technique that will help the future 4G wireless cellular systems to meet the extensive list of demands to fully support the 4G requirements [ITU1645].

The use of high order modulations and extended service coverage, thus forcing the receivers to operate at very low SNR regimes, will surely be unavoidable in future 4G systems. To explore its full potential, the system needs to mitigate the severe impact of the transmission over multipath wireless channels, noise, interference and systems imperfections.

The use of multiple sub-carriers makes OFDM systems highly sensitive to synchronization errors and its mitigation is of paramount importance for the system's performance. Thus, the synchronization algorithms must achieve a near perfect performance. The effect of the transmission channel on the received signal must be accurately estimated as this estimate will be used throughout the system for coherent detection, AMC, MIMO techniques, pre-equalization, interference cancellation, MT positioning and cross-layer design. These operations must exhibit a near perfect performance while keeping the complexity to a minimum so that the MT size and cost are kept low and battery life is maximized.

This thesis is within the scope of signal processing techniques for multicarrier systems and has contributed with original low complexity algorithms for channel estimation and CFO estimation of pilot-aided OFDM-based wireless systems. The investigated algorithms considered systems with multiple antenna configurations at both ends of the link, thus contemplating the different applications and scenarios in real life applications. The results presented throughout this thesis show that the performance of the investigated algorithms is adequate for present and future wireless cellular standards.

The main conclusions that come out of this work can be summarized in the following:

- Embedding of scattered pilot symbols in the OFDM frame is of major importance to the design of high performance channel estimation algorithms when transmitting over time-variant multipath wireless channels, but its presence decreases the system's power efficiency. It is however possible to optimize the pilot symbols' density and distribution to maximize the performance of the channel estimation algorithm for a given power efficiency
- Though there is a general tendency to design FD channel estimation algorithms, TD channel estimation algorithms can take advantage of the simpler TD channel model, where the CIR energy is limited to a reduced number of samples, to generate accurate estimates; The MMSE estimation is implemented with a diagonal matrix with a limited number of non-zero elements, which leads to a significant complexity reduction when compared with its FD counterpart;
- The performance of TD channel estimation algorithms greatly benefits from the use of a pilot distance, N_f, that is harmonically related to the DFT size, N_C, and the exploitation of the DFT properties, to separate the pilot-dependent component from the data-dependent component;
- The use of phase-shift orthogonal pilots sequences originates considerable gains in the accuracy of the channels estimates by reducing or eliminating the co-channel interference, when considering OFDM systems with transmitter diversity;
- The majority of the CFO estimation schemes uses training symbols with special properties to estimate the CFO in the TD and is unable to track the CFO along the remainder of the OFDM frame. A CFO estimation algorithm for OFDM systems with transmitter diversity was investigated that outputs a very accurate estimate exploring the presence of the pilot-carrying symbols with the same pilot placement and pilot sequence design of the channel estimation scheme. Moreover, the CFO estimate takes advantage of all pilot-carrying symbols within the OFDM frame to track the CFO. The accuracy of outputted CFO estimate and the short acquisition time make this algorithm adequate for the mitigation of CFO of the highly sensitive burst-type OFDM systems;
- Exploiting of the signal processing commonalities between CFO estimation and channel estimation, allows the identification of common modules that can

be shared, without compromising the systems performance and leading to the reduction of the overall complexity.

At this point, the major contributions of this thesis will be identified and related to the main conclusions that were previously presented.

Regarding the loss of power efficiency resulting from the embedding of pilot symbols in the OFDM frame, the impact of the pilot density in the performance of the channel estimation is investigated in Chapter 3. The analytical formulation of the channel estimation MSE for the single-user downlink scenario with a generic channel estimation algorithm is given. The contributions from this investigation can be summarized as:

- It was shown that the channel estimation MSE is very sensitive to the fulfilment of the sampling frequency in the symbol axis, due to Doppler spectrum energy being concentrated near the Doppler frequency. A conservative symbol-axis pilot distance should be used when designing the OFDM frame if mobility is to be considered, to avoid undersampling the channel.
- The typical multipath wireless channels in real scenarios present an approximately exponentially decaying PDP, with most of the energy concentrated in a small set of initial samples and the remaining energy scattered in the longer CIR tail. It was shown that the use of an excessive frequency-axis pilot distance, leading to the undersampling of the channel, is not as severe as in the previous axis. When undersampling starts to occur, the distortion (aliasing) on the CIR estimate is not severe because the tails of the CIR replicas have little energy.

Regarding the advantage of TD channel estimation algorithms in generating accurate estimates with reduced complexity, due to fact that the CIR energy is limited to a reduced number of samples, the method investigated in Chapter 4 demonstrates that:

- A simple linear operation outputs an initial CIR estimate from the TD received samples of symbols carrying both data and pilots. The conditions for the use of this operation are identified;
- A simplified TD MMSE estimator generates final estimates with greatly improved accuracy; Due to the fact that the channel correlation matrix is diagonal, the MMSE filter is implemented with a diagonal matrix, avoiding the

processing demanding matrix inversion of its FD counterpart, leading to a large reducing in computational load;

- Using the knowledge that the CIR energy is limit to a reduced set of samples, the estimation of the MMSE filter parameters is easier when compared with its FD counterpart. A simple, yet efficient, method of estimating these required filter parameters is proposed.

Regarding the performance benefits of TD channel estimation algorithms from the careful placement of the pilot symbols in the OFDM frame to separate the pilot-dependent component from the data-dependent component, the investigation presented in Chapters 4 and 5 lead to the following contributions:

- By constraining the initial position and separation of the pilot sequences in the FD and using this knowledge on the receiver's channel estimator, the investigated schemes decouple the pilot-dependent components arriving from different transmit antennas from the data-dependent components and generate CIR estimates for all channels involved in the transmission process.
- The proposed channel estimation methods generate the estimates without using DFT/IDFT operations, resulting in algorithms with an undemanding structure and very low computational load, adequate for portable, low-consumption, low-processing power real-time devices;

Regarding the design of the pilot sequences when using OFDM systems with transmitter diversity, the results in Chapter 5 demonstrate the gains in the accuracy of the channels estimates resulting from the careful design of the sequences. The main outcomes can be summarized in the following:

- The use of phase-shift orthogonal pilot sequences simplifies the separation of the signals arriving from the different transmit antennas in the TD, significantly reducing the co-channel interference present in the combined signal;
- Under the assumption that channels involved in the transmission process have limited impulse response, an exact condition is given for the complete elimination of the co-channel interference;
- The phase-shift orthogonal pilot sequences have the ability to concentrate the energy of the TD CIR replicas in a small number of samples. This allows a

significant noise reduction when using the STC or MMSE estimation algorithms, leading to significant improvements in the estimates.

- The concentration of the different CIR replicas' energy identified in the previous point also eases the estimate of the channels' correlations and noise variance required by the MMSE filter.

Regarding the investigation of a CFO estimation algorithm for OFDM systems with transmitter diversity that explores the presence of the symbols carrying data and pilots within the OFDM frame, the investigation in Chapter 6 shows that:

- The proposed algorithm explored the presence of the symbols carrying data and pilots within the OFDM frame to estimate the CFO present in the received signal;
- The proposed algorithm is able to estimate the CFO from the TD received samples in the presence of co-channel interference;
- All pilot-carrying symbols are used by the CFO algorithm, unlike the common training-based algorithms found in the literature that use the frame preamble to get the CFO estimate;
- The same pilot structure utilized by the channel estimator investigated in Chapter 5 is used to generate a CFO estimate;
- There is no need for additional overheads (like training symbols or null sub-carriers) to get an accurate CFO estimate.
- The generated estimate is very accurate when compared with other methods in the literature and the residual CFO has a minimal impact in the system's performance, confirming that the CFO estimates have minimal deviation from the true value, thus making the proposed algorithm suitable for the mitigation of CFO in the highly sensitive OFDM systems;
- The ability of the investigated algorithm to generate accurate estimates with a limited number of OFDM symbols makes its use appropriate for burst-type OFDM cellular systems;

Regarding the exploitation of the CFO and channel estimators' commonalities to yield an overall low complexity joint block, the contributions arising from the results attained in Chapter 6 are:

- An intermediate output of the proposed CFO estimation algorithm is used to get an initial channel estimate;
- The initial estimate is improved with the use of the STC or MMSE algorithms;
- The joint CFO and channel estimation block exhibits low computational load with no performance trade-off;
- By using the scattered pilots for both operations, the required overhead is reduced and the efficiency of the transmission system is increased.

7.2. Future Work

In a work such as this where multiple topics are addressed, some subjects are left open for future research. Relative to the channel estimation, the following open issues were identified and call for future work.

- The channel estimation methods proposed in this thesis only take advantage of the independence of the channel taps to improve the estimate. Exploring the correlation of the OFDM symbols in the time domain may lead to an improvement in the accuracy of the estimate. Assuming a band-limited Doppler spectrum, common to all channels involved in the transmission process, a single MMSE filter could be used to reduce the noise variance in the estimate of all channels. Furthermore, because the initial estimate is performed in TD, the design of the new MMSE filter comes greatly simplified as the estimate of the common Doppler spectrum can use the methods in the literature [Yuc05], without the additional computational load of having to move between transform domains;
- The use of MIMO-OFDM systems brings another dimension into play that can be explored to improve the accuracy of the estimate, similarly to the frequency and time dimensions: the spatial dimension. Under the assumption of uncorrelated channel taps, the correlation between the same indices TD taps or FD sub-carriers of different antennas is the spatial correlation between the different antennas [Zha05]. The use of this new dimension was investigated in different published works [Kie03], [Zha05], where the use of MMSE or ML filtering was proven to improve the channels' estimates. The investigation on the use of a MMSE filter that explored the correlation of the same indices TD taps of different antennas would most likely bring added improvement to

channel estimator, without compromising the low computational load of the proposed methods;

- The major downside of using phase-shift orthogonal sequences is the resulting moderate to high PAPR. The PAPR value will depend on the energy used for pilot transmission and pilot separation. Though in current systems this does not pose a serious issue, further investigation on pilot sequences that allow the control of PAPR would be beneficial and contribute to adoption of the investigated method in real systems.

Relative to the CFO estimation, the following open issues were identified and call for future work.

- The investigated CFO method presents a CFO ambiguity of an integer multiple of the FD pilot sub-carrier separation; Though this separation is adequate for the current standards [LTE], [802.16], it would be desirable to further extended the acquisition range with the use of a coarse estimation algorithm. This algorithm would be responsible for identifying the possible CFO ambiguity remaining after the first stage and it would only be needed in the CFO acquisition phase, where the CFO can be considerable.
- The results in Chapter 6 show that the proposed algorithm is very accurate in estimating the CFO present in the received signal. A theoretical bound on the performance of the investigated method would answer the question on the possibility of existence of a more accurate algorithm;
- The evolution of the proposed CFO estimation algorithm for OFDM systems with multiple receive antennas was not addressed. It is a reasonable assumption that following a path similar to the trends of recent works on preamble-base CFO estimators for MIMO-OFDM [Jia08a], [Jia08b] would lead to further improvements in the performance of the estimator.

7.3. References

[802.11] IEEE Std. 802.11, second edition, "Local and metropolitan area networks – Specific requirements – Part 11: Wireless LAN Medium Access Control (MAC) and Physical Layer (PHY) Specifications," August 2005.

[802.11g] IEEE Std. 802.11g-2003, "Local and metropolitan area networks – Specific requirements – Part 11: Wireless LAN medium access control (MAC) and physical layer (PHY) specifications – Amendment 4: Further higher data rate extension in the 2.4 GHz band," June 2003.

[802.15.3] IEEE Std. 802.15.3-2003, "Local and metropolitan area networks – Specific requirements – Part 15.3: Wireless Medium Access Control (MAC) and Physical Layer (PHY) Specifications for High Rate Wireless Personal Area Networks (WPANs)," September 2003.

[802.15.4] IEEE Std. 802.15.4-2006, "Local and metropolitan area networks – Specific requirements – Part 15.4: Wireless Medium Access Control (MAC) and Physical Layer (PHY) Specifications for Low-Rate Wireless Personal Area Networks (WPANs)," September 2006.

[802.16] IEEE Std. 802.16-2009, "Local and metropolitan area networks – Specific requirements – Part 16: Air interface for broadband wireless access systems," May 2009.

[Blu09] Bluetooth Special Interest Group, "Bluetooth Specification Version 3.0 + HS," April 2009.

[DAB] ETSI Std. ETS 300 401 v1.4.1, "Radio broadcasting systems; Digital audio broadcasting (DAB) to mobile, portable and fixed receivers," June 2006.

[DVB-T] ETSI Std. ETS 300 744 v1.6.1, "Digital video broadcasting (DVB); Framing structure, channel coding and modulation for digital terrestrial television," January 2009.

[ITU1645] ITU-R Recommendation M.1645, "Framework and overall objectives of the future development of IMT-2000 and systems beyond IMT-2000," June 2003.

[Jia08a] Y. Jiang, H. Minn, X. Gao, X. You, Y. Li, "Frequency offset estimation and training sequence design for MIMO OFDM," *IEEE Transactions on Wireless Communications*, vol. 7, no. 4, pp. 1244 – 1254, April 2008.

[Jia08b] Y. Jiang, H. Minn, X. You, X. Gao, "Simplified Frequency Offset Estimation for MIMO OFDM Systems," *IEEE Transactions on Vehicular Technology*, vol. 57, no. 5, pp. 3246 – 3251, September 2008.

[Kie03] M. Kiessling, J. Speidel, I. Viering, M. Reinhardt, "Statistical prefiltering for MMSE and ML receivers with correlated MIMO channels," in *Proc. IEEE Wireless Communications and Networking Conference*, vol. 2, pp. 919 – 924, New Orleans, USA, March 2003.

[LTE] ETSI Technical Specification TS 136 201 v8.3.0, "LTE; Evolved universal terrestrial radio access (E-UTRA); Long Term Evolution (LTE) physical layer; General description," April 2009.

[Yuc05] T. Yucek, R. Tannious, H. Arslan, "Doppler Spread Estimation for Wireless OFDM Systems," in *Proc. IEEE Symposium on Advances in Wired and Wireless Communication*, pp. 233 – 236, April 2005.

[Zha05] H. Zhang, Y. Li, A. Reid, J. Terry, "Channel estimation for MIMO OFDM in correlated fading channels," in *Proc. IEEE International Conference on Communications*, vol. 4, pp. 2626 – 2630, Seoul, Korea, May 2005.